Wind-evaporation feedback, angular momentum conservation, and the abrupt onset of monsoons

by

William Ronald Boos

M.S. Geosystems
Massachusetts Institute of Technology, 2002
B.S. Physics and B.A. Mathematics
Binghamton University, 1997

Submitted to the Department of Earth, Atmospheric and Planetary Sciences
in partial fulfillment of the requirements for the degree of

Doctor of Philosophy in Atmospheric Science

at the

MASSACHUSETTS INSTITUTE OF TECHNOLOGY

February 2008

Author .....
Department of Earth, Atmospheric and Planetary Sciences
December 17, 2007

Certified by .....
Kerry A. Emanuel
Breene M. Kerr Professor of Atmospheric Science
Thesis Supervisor

Accepted by .....
Maria T. Zuber
E. A. Griswold Professor of Geophysics
Head, Department of Earth, Atmospheric and Planetary Sciences

Wind-evaporation feedback, angular momentum conservation, and the abrupt onset of monsoons

by

William Ronald Boos

Submitted to the Department of Earth, Atmospheric and Planetary Sciences
on December 17, 2007,
in partial fulfillment of the requirements for the degree of
Doctor of Philosophy in Atmospheric Science

Abstract

This thesis examines the mechanisms responsible for the abrupt onset of monsoon circulations, focusing on the role played by wind-evaporation feedback and its interaction with angular momentum conserving flow.

The first half of the thesis examines the effect of wind induced surface heat exchange (WISHE) on nonlinear, axisymmetric Hadley circulations in a convective quasi-equilibrium framework. For thermal forcings localized off the equator, WISHE is found to reduce the critical forcing amplitude needed to produce angular momentum conserving flow. For forcings that are subcritical even with the effects of WISHE, the combination of WISHE and momentum advection is shown to nonlinearly enhance the circulation strength for all but the weakest forcings. These results hold for the time-dependent response to seasonally varying forcings: for forcings of intermediate strength, WISHE produces an abrupt onset of solsticial flow when only a linear response would otherwise occur, while for strong forcings WISHE shifts the abrupt onset to an earlier time in the seasonal cycle.

The second half of the thesis examines the consistency of these idealized results with the onset of the South Asian monsoon in both observations and a detailed three-dimensional model. Observational composites of monsoon onset are consistent with a wind-evaporation feedback in that the increase in baroclinic flow during onset is accompanied by a large increase in surface enthalpy flux over the off-equatorial ocean. This increase in surface enthalpy flux is collocated with the peak increase in deep tropospheric ascent. Results from the three-dimensional numerical model were less conclusive in that this model did not successfully simulate an abrupt monsoon onset even with WISHE, although WISHE did strongly control the intensity and spatial structure of the model's mean summer circulation. In particular, a version of the model integrated without WISHE failed to produce a strong, angular momentum conserving monsoon circulation. Combined with the axisymmetric model results from the first half of the thesis, this suggests that the thermal forcing of the South Asian land mass may not be sufficiently strong in the absence of WISHE to produce angular momentum conserving monsoon flow.

Thesis Supervisor: Kerry A. Emanuel
Title: Breene M. Kerr Professor of Atmospheric Science

Acknowledgments

Am I no longer young, and still not half-perfect? Let me
keep my mind on what matters,
which is my work,

which is mostly standing still and learning to be
astonished.

– Mary Oliver, *Thirst*

While some amount of long hours and rote effort is necessary for the creation of a graduate thesis, it is probably smaller than many think. I did my best work when I was well-rested, clear-headed, and able to maintain some sense of awe for the vast, swirling fluid envelopes of Earth and other planets. Of course such a state was not frequent, but when it did occur was due almost entirely to the good company of colleagues, friends, and family.

I could not have written this thesis without the guidance, support, and creativity of my advisor, Kerry Emanuel. I greatly appreciate his willingness to start me off on a path, let me wander fairly independently, and patiently rein in my excursions and digressions. Reading through this thesis, I noticed that most of the interesting methods and ideas came either directly from Kerry or from one of our discussions.

Discussions with the other members of my thesis committee were invaluable. Richard Lindzen helped me to ask meaningful questions about the monsoon, and to examine some basic assumptions prevalent in the literature. Alan Plumb provided practical, clear advice that helped me to understand the mechanisms operating in some of my numerical models. And Steve Sherwood helped me to realize that there was more to the monsoon than was dreamt of in my simple models. I appreciate their patience and attention in listening to my presentations and reading my writings.

I would not have finished graduate school without the support and encouragement of Stefan, my parents, and my sister Amy. They made finishing possible, and the life that happened in the meantime worthwhile. I thank Andrea Graham for our many writing sessions, as well as the good company and friendship. I imagine that all of these people are happier than I that this thesis is finally complete.

Numerous interactions with colleagues and friends over the past five years provided essential support for both this thesis and my general eduation. I particularly wish to thank

Nikki Privé, Arnaud Czaja, and Andrea Molod for both crucial assistance with numerical models as well as more general discussions. Valuable feedback on both the work in this thesis and broader issues of tropical dynamics was provided by Olivier Pauluis, Tapio Schneider, Adam Sobel, George Kiladis, and Zhiming Kuang. Sandrine Bony graciously hosted a summer stay at the Laboratoire de Météorologie Dynamique. I thank Masahiro Sugiyama for useful conversations on convection and two-mode models, and both Peter Molnar and Katherine Dayem for discussions about the Tibetan Plateau. Jeff Scott, Brian Tang, Mike Ring, Roberto Rondanelli, and Jon Moskaitis sat through many of my practice talks and provided informed and helpful criticism. Rob Korty and Greg Lawson were good colleagues and friends who graduated all too early in my time at MIT. Angela Zalucha proved to be an excellent person with whom to share an office. Many people not named individually here were an important part of my graduate education, including the faculty, administrative staff, and fellow students at MIT. All of these people helped me to not only get through graduate school, but to enjoy the process.

Contents

Chapter 1

Introduction: The abrupt onset of monsoons

The Earth's climate is forced by the absorption of insolation and the loss of energy to space by radiative cooling, and the variation with latitude of the rates at which these processes occur drives a thermally direct circulation in the atmosphere (e.g. Peixoto and Oort, 1992). As the distribution of insolation varies in a seasonal cycle, the latitude at which the ascent branch of this circulation is centered oscillates from one hemisphere to the other. The associated horizontal flow varies concomitantly, conserving angular momentum in the rotating atmosphere. This pattern of seasonally varying flow is complicated by the fact that water changes phase in the atmosphere, condensing and precipitating primarily in ascending regions of the thermally direct circulation, and evaporating from land and ocean surfaces at a rate that depends in part on the circulation itself. This thesis examines the role played by these phase changes of water in the seasonal cycle of angular momentum conserving atmospheric flow.

1.1 The phenomenon

The global distribution of tropospheric ascent, deep convection, and precipitation on Earth is concentrated in monsoon regions during the few months surrounding each solstice. This can be seen in a climatology of outgoing longwave radiation (OLR) for 1979-2004, as estimated by satellites of the National Oceanic and Atmospheric Administration (NOAA) and interpolated to a global grid (Liebmann and Smith, 1996). OLR, which is often used as a

proxy for deep convection because it is strongly reduced by the presence of cold cloud tops (e.g. Liou, 2002), exhibits tropical minima clearly located over or near continents in the summer hemisphere (Fig. 1-1). During austral summer, tropical OLR minima of roughly equal magnitude are centered over South America, southern Africa, and Indonesia. During boreal summer, a large and intense OLR minimum is centered over the coastal regions of South Asia, with secondary maxima just north of the equator in Africa and the East Pacific. Although not shown here, similar features are seen in climatologies of free-tropospheric vertical velocity from the Reanalysis of the National Centers for Environmental Prediction/National Center for Atmospheric Research (NCEP/NCAR, Kalnay et al., 1996). With the exception of the Pacific, these regions of tropical OLR minima are the sites of summer monsoons, where the term monsoon is used in the fairly broad sense of a thermally direct large-scale circulation produced by a seasonally reversing thermal forcing. While this forcing is typically taken to result from insolation falling on an off-equatorial land surface, the seasonal cycle in sea surface temperature (SST) can also play a role in monsoon circulations, particularly over the northern Indian Ocean where the meridional SST gradient changes sign seasonally (Webster and Fasullo, 2003; Lestari and Iwasaki, 2006).

The study of the seasonal cycle of the tropical tropospheric circulation is thus largely a study of the transition between the summer monsoons of one hemisphere and those of the other. Numerous authors have shown that the various regional monsoons begin abruptly (see below), by which we mean they evolve faster than can be explained by a linear response to the insolation forcing. Such behavior is interesting because, by definition, an abrupt onset would not occur if monsoons could be represented simply as large-scale sea breeze circulations in which the dynamics respond directly to the insolation forcing. Most introductory-level textbooks discuss monsoons in the context of sea-breeze dynamics, although many also posit that a positive feedback between large-scale ascent and latent heating strengthens monsoon circulations (e.g. Holton, 2004; Ahrens, 2000), in notable violation of statistical equilibrium views of moist convection (Emanuel et al., 1994).

More precisely, we define an abrupt event as having a time series that projects onto frequencies higher than those of the first three Fourier harmonics of Earth's annual cycle[1]. Murakami et al. (1986) found that the OLR signals associated with the onset of both

[1]This is a common definition of the seasonal cycle (e.g. Wheeler and Kiladis, 1999) and is a fairly generous definition of the forcing for a monsoon circulation, because the first two harmonics account for more than 99 percent of the insolation variance (Weickmann and Chervin, 1988) and more than 95 percent of the sea

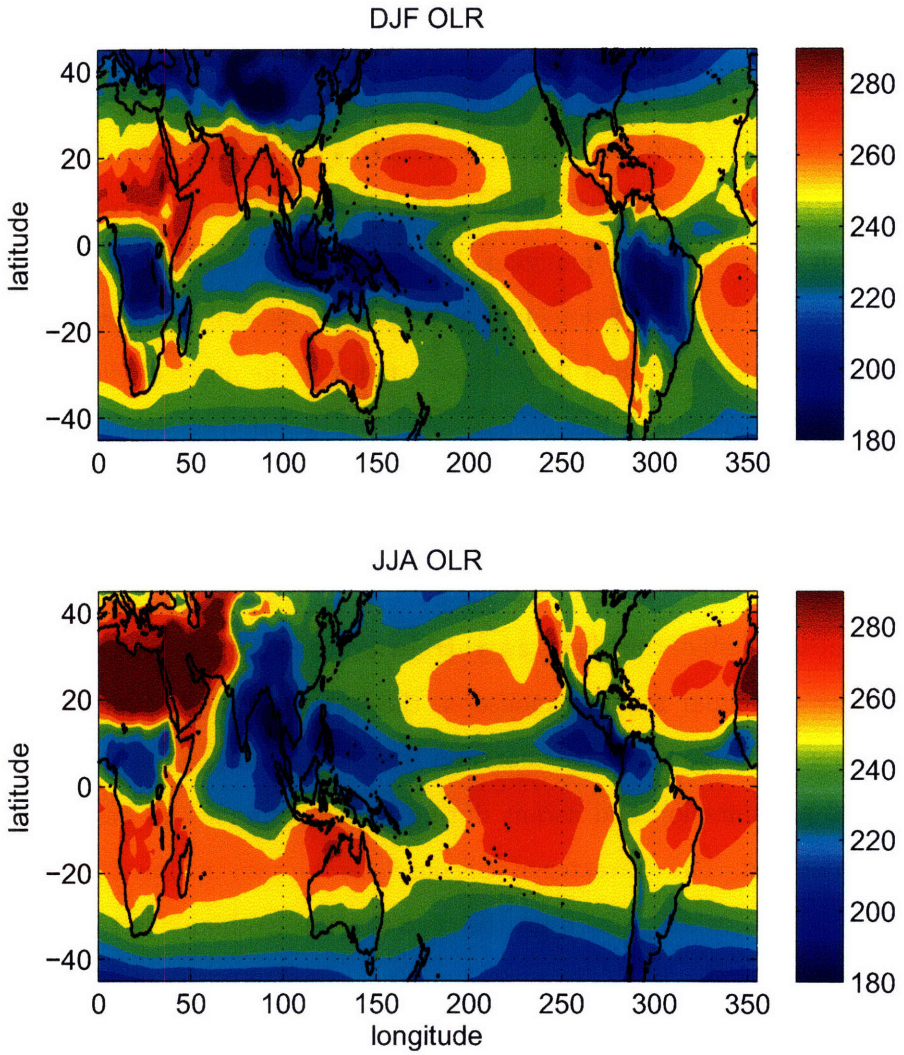

Figure 1-1: Climatological NOAA OLR (1979-2004) for December-January (top) and June-August (bottom). Contour interval is 10 W m^{-2}.

the South Asian and Australian monsoons had an abrupt component, according to this definition, that was comparable in amplitude to the component projecting onto the three seasonal harmonics. Webster et al. (1998) showed that low-level winds over the western Indian Ocean typically change from weak northerlies to strong southerlies within a single week in early June, which easily qualifies as abrupt, and that a similarly rapid increase in low-level westerlies occurs over the northern Indian Ocean. The onset of the Australian monsoon at Darwin occurs anywhere from early December to mid-January, and is characterized by a change in the direction of low-level zonal wind and an increase in precipitation from near zero to over 7 mm day^{-1}, both occurring within about five days (Wheeler and McBride, 2005). Some authors have also presented evidence for an abrupt poleward shift of the precipitation maximum accompanying the onset of the West African monsoon (Sultan and Janicot, 2000), but this phenomenon is not nearly as well documented as the onset of the South Asian and Australian monsoons. Studies of the onset of the South American monsoon have been performed, but no assessment of its rapidity seems to exist, perhaps because the onset there seems to be more highly variable and possesses classical monsoon characteristics, such as a reversal in the direction of low-level wind, only when a strong annual mean circulation is removed (Marengo et al., 2001; Zhou and Lau, 1998).

Although the first half of this thesis uses highly idealized theory and models not intended to represent any particular regional monsoon, the latter half focuses on the South Asian summer monsoon. The South Asian monsoon is chosen because it is associated with the bulk of tropical precipitation and ascent during boreal summer and has an onset that is fairly well documented. The character of this onset can be seen in climatological daily OLR averaged over 60-90°E, which runs from the center of the Arabian Sea to the center of the Bay of Bengal and includes India. In early June (near day 160), the minimum OLR in this region migrates poleward from the equator to about 15°N while simultaneously intensifying and expanding meridionally (Fig. 1-2). After removing the best linear fit of the first three seasonal harmonics from this limited zonal mean of OLR, an abrupt component is clearly evident, consisting of a poleward propagating anomaly in early June (Fig. 1-3). The fact that this abrupt component has an amplitude just as large as the seasonal component (30 W

surface temperature (SST) variance (Boyer et al., 2005). We retain the third harmonic because we are primarily concerned with atmospheric dynamics in this thesis, and SST in the northern Arabian Sea does project onto this mode. Even there, however, the amplitude of the third harmonic is only about 0.3 K (see note in Mapes et al., 2005).

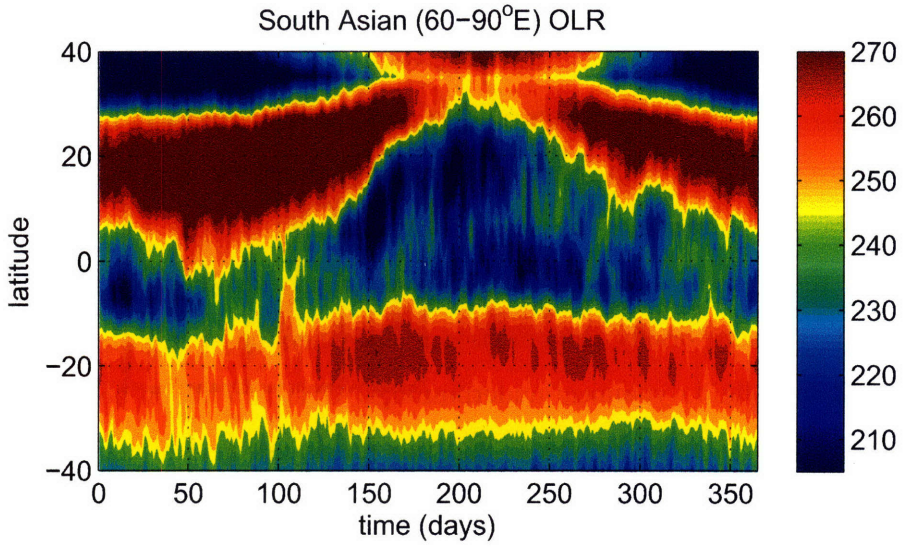

Figure 1-2: Climatological daily NOAA OLR, mean for 60-90°E. Contour interval is 5 W m^{-2}.

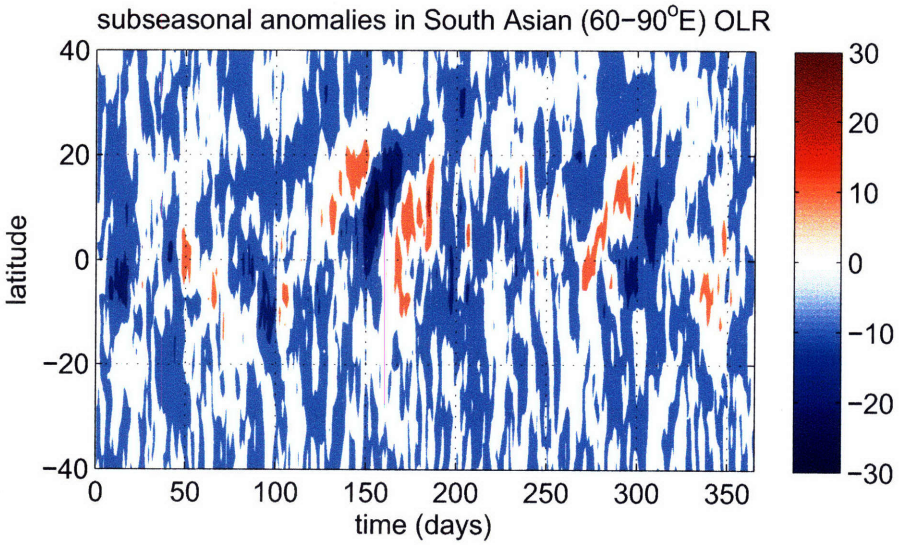

Figure 1-3: As in the previous figure, but after removing the component projecting onto the first three seasonal harmonics. Contour interval is 10 W m^{-2} with negative anomalies in blue and positive in red.

m^{-2}) in a calendar-based climatology is a testament to the regularity and intensity of South Asian monsoon onset. We examined a limited zonal mean here in order to exclude convective variability over the Pacific, which is organized into off-equatorial, zonally elongated bands with highest amplitudes on the east and west sides of the basin. The Pacific distribution projects strongly onto the zonal mean, and is associated with discontinuous shifts of the zonal mean convective maximum across the equator that are not representative of behavior in any particular monsoon region, as shown in Appendix A.

While this thesis focuses entirely on the mechanisms involved in the nonlinearity of monsoon onset, we note briefly that monsoons and their onset are of interest for many reasons beyond their fluid dynamical underpinnings. Over two billion people in Asia alone rely on monsoon precipitation for water, and this precipitation exhibits intraseasonal and interannual variability that influence agricultural and economic activity and are poorly forecast by dynamical models (e.g. Webster et al., 1998; Webster and Hoyos, 2004). For the particular example of India, agricultural output has been shown to be directly related to the total summer monsoon rainfall, with negative rainfall anomalies of 10 percent (which correspond to drought conditions) typically associated with reductions in agricultural gross domestic product (GDP) of about 5 percent (Gadgil and Kumar, 2006). Even when the total summer rainfall is not deficient relative to the climatological mean, a substantial delay in the onset of monsoon rains can ruin the initial rice crop, which must be planted about one month before the start of summer precipitation. This occurred in 2003, when a late onset of monsoon rains that was not forecast by any model led to the abandonment of the initial rice crop in Andhra Pradesh, one of India's main rice exporting states (Gadgil and Kumar, 2006). This occurred despite the fact that the total summer rain was 2 percent above climatology that year, and that a large fraction of rice in Andhra Pradesh is irrigated, rather than rain fed. The hope is that a better fundamental understanding of the processes involved in the seasonal cycle of monsoons, including onset, will lead to better representation and prediction of monsoons in both dynamical and statistical models. This is clearly needed, since the major droughts that occurred in India in 2002 and 2004, with country-wide summer rainfall deficits of 19 and 13 percent, respectively, were not forecast by the empirical models of India's meteorological department or the dynamical models of international meteorology centers (Gadgil et al., 2005).

1.2 Previous theories

Numerous hypotheses have been proposed to explain the nonlinear response of monsoon onset to the insolation forcing, and it would be difficult, at best, to review them thoroughly here. Several categories of mechanisms are prominent in the literature: those in which dynamics or thermodynamics internal to the atmosphere respond nonlinearly to an applied forcing, those in which the nonlinearity is produced by changes in enthalpy fluxes from the land or ocean surface, and those in which the nonlinearity is an artifact of the superposition of a linear response with some independently existing, higher frequency phenomenon. Examples from these categories are discussed briefly here, with the understanding that they need not operate exclusively.

Several theories exist in which atmospheric dynamics alone have been shown to produce circulations that strengthen nonlinearly with an imposed thermal forcing. Theoretical solutions for angular momentum conserving axisymmetric flow on a sphere will prove to be particularly relevant to the hypothesis explored in this thesis (which is explicitly stated in the next section). Lindzen and Hou (1988) showed that the strength and meridional extent of such axisymmetric flow are highly sensitive to small displacements of the peak thermal forcing off the equator. Plumb and Hou (1992) showed that the strength of steady, axisymmetric meridional flow increases nonlinearly as the magnitude of a thermal forcing localized off the equator is enhanced beyond a threshold value. They suggested that this threshold behavior might be relevant to the seasonal onset of monsoons, but noted that the effect of zonal asymmetries and time-dependence needed to be assessed. Walker and Schneider (2006) found that momentum transports by zonally asymmetric eddies played an important role in setting the strength of the Hadley circulation in a series of general circulation models (GCMs) with thermal forcings having maxima centered on the equator. An abrupt transition between this eddy-controlled equinoctal regime and a solsticial regime in which momentum transports by the zonal mean circulation dominate was proposed by Schneider and Bordoni (2007, in press) to be responsible for the sudden onset of monsoons. We give no reason here to doubt the relevance of any of the above theories to monsoon onset, but note that none of them explicitly consider the effect of phase changes of water on the dynamics, which is the task undertaken in this thesis. Part of this thesis essentially expands on the theory of Plumb and Hou (1992).

Some authors have proposed that the abrupt onset of monsoons results from a hydrodynamic instability of the atmosphere. Krishnakumar and Lau (1997, 1998) found that the onset of the South Asian monsoon in a general circulation model (GCM) was accompanied by flow having locally anticyclonic potential vorticity (PV), thereby satisfying a necessary condition for symmetric instability. However, the use of symmetric instability to explain the abrupt nature of monsoon onset typically involves invoking the release of a large amount of convective available potential energy (CAPE) to amplify the instability, as will be discussed in Chapter 4. Similar reasoning underlies the idea that abrupt onset is caused by a positive feedback between convective latent heating and the convergence of water vapor by the circulation driven by that heating (e.g. Webster and Fasullo, 2003); such a hypothesis implicitly assumes that the kinetic energy of the thermally direct circulation is extracted from a reservoir of available potential energy (APE). These ideas are at odds with statistical equilibrium views of moist convection, in which convection maintains an equilibrium state against the destabilizing effects of surface entropy fluxes and free-tropospheric radiative cooling (e.g. Arakawa and Schubert, 1974). While this alone is not a reason for rejecting theories requiring a large change in APE during monsoon onset, Emanuel et al. (1994) discussed how convective closures that are based on moisture convergence encourage an active exchange between APE and the kinetic energy of the circulation with no regard for the fact that disturbance growth requires a positive correlation between heating and temperature. Thus, while theories of convective quasi-equilibrium have not been incontrovertibly verified in observations, there are some theoretical reasons for questioning theories for abrupt onset that are based on feedbacks involving moisture convergence (e.g. Krishnakumar and Lau, 1997; Webster and Fasullo, 2003).

Thus far we have not addressed the fact that only a small fraction of insolation heats the atmosphere directly, with most shortwave radiation being absorbed by the land or ocean surface and energy transfer to the atmosphere occurring via surface fluxes of latent and sensible heat. The net surface enthalpy flux varies with the properties of both the surface and the near-surface air, providing several ways in which a nonlinear response to the insolation forcing could be achieved without nonlinear atmospheric dynamics. The central hypothesis of this thesis, which will be stated more precisely in the next section, is that the wind dependence of ocean surface evaporation plays an important role in the abrupt onset of monsoons. This idea was previously proposed by Numaguti (1995) to explain the

abrupt poleward shift of a precipitation maximum in a GCM. His work, although a valuable contribution on the subject, did not examine the angular momentum conserving dynamics of the associated meridional flow or the consistency with observations, which are tasks taken up in this thesis. Furthermore, the thermal forcing used by Numaguti (1995) was never localized in the subtropics, and such localization was suggested by Plumb and Hou (1992) to possibly be important for producing an abrupt monsoon onset. This issue is also explored in this thesis.

For time scales longer than a few days, the wind-dependence of surface enthalpy fluxes is typically important only over oceans because of the much smaller heat capacity of land surfaces. Variations in land surface properties might still play a role in monsoon onset, however. For example, the albedo of the land surface is sensitive to soil moisture, snow cover, and vegetative cover, so that the amount of shortwave radiation absorbed by the surface will generally increase as snow melts and precipitation falls over land. Such land-atmosphere feedbacks have been examined in the context of the timing of monsoon onset (e.g. Mapes et al., 2005), and in the intensity and structure of the seasonal mean monsoon (e.g. Meehl, 1994; Ferranti et al., 1999), but we know of no study that examines whether changes in land surface properties alone can explain the abrupt nature of monsoon onset. Studies of land-atmosphere feedbacks in monsoon onset have typically emphasized the effect of changes in the ratio of sensible and latent heat fluxes (i.e. the Bowen ratio) on the transition from dry to deep moist convection over the continent. One example of this is the numerical modeling study of Xie and Saiki (1999), who found that monsoon onset was delayed weeks past the establishment of a poleward temperature gradient in the lower troposphere. A shallow, thermally-direct circulation existed in this pre-onset state, with a low-level zonal jet in thermal wind balance with the temperature gradient. An equatorward temperature gradient persisted in the tropical upper troposphere until a baroclinic disturbance propagated through the region concurrent with the initiation of deep convection and full-tropospheric ascent. This is a classic example of a paradigm in which the seasonal reversal of the meridional free-tropospheric temperature gradient is delayed due to the formation of a thick boundary layer over a dry, hot land surface (see also Kawamura et al., 2002). Even here, though, the role of land surface feedbacks is unclear because it is not known whether monsoon onset would have been any less abrupt in their model if the soil was specified to be moist throughout the year. It is worth noting in the context of

these land surface feedbacks that the peak convective activity in the South Asian summer monsoon occurs over ocean and, as will be shown in Chapter 4, that the peak convective signal associated with the abrupt onset of the South Asian monsoon is also centered over ocean.

Finally, we note that the onset of various monsoons has been associated with horizontally propagating convective anomalies of particular intraseasonal frequencies. The onset of the Indian monsoon is generally coincident with the first of several poleward migrations of a zonally elongated convective maximum that, in the time mean, are responsible for a considerable fraction of summer monsoon precipitation (Yasunari, 1979; Sikka and Gadgil, 1980). The poleward propagating OLR anomaly seen near day 160 in Fig. 1-3 might be a climatological signal of this phenomenon. The convective phase of the eastward propagating Madden Julian Oscillation (MJO, Madden and Julian, 1972) often occurs together with these poleward propagating anomalies, although there are numerous instances where poleward migration occurs without eastward migration (Wang and Rui, 1990; Lawrence and Webster, 2002). Poleward migrating convective anomalies do not seem to occur in the Australian monsoon. There, monsoon onset is associated with the convective phase of the MJO, although this association is only of moderate strength and the MJO seems to act mainly as one of several possible triggers for the abrupt onset (Hendon et al., 1989; Hung and Yanai, 2004; Wheeler and McBride, 2005). This suggests that the abrupt nature of Australian monsoon onset is not due entirely to the superposition of an independent intraseasonal mode with a monsoon circulation that responds linearly to the insolation forcing. It remains to be seen whether the onset of the South Asian monsoon can be similarly described as being phase locked with, but not necessarily caused by, the MJO and poleward propagating convective anomalies. Some theoretical support for a non-causative association is presented in chapters 2 and 3, which show that the onset of idealized monsoon circulations in axisymmetric models can occur abruptly without the existence of either zonally or meridionally propagating intraseasonal anomalies.

1.3 Proposed hypothesis

This thesis examines whether the wind-dependence of ocean surface enthalpy fluxes in a convective quasi-equilibrium framework (e.g. Emanuel et al., 1994) is responsible, at least

in part, for the abrupt onset of monsoon circulations. We are motivated by several aspects of the previous theories discussed above. First, many theories for onset consider only the dry dynamics of the atmosphere, with moist convection treated as an external heat source if it is accounted for at all. In particular, dry theories that treat the Hadley circulation as angular momentum conserving flow have met with some success at representing the solsticial circulation (Lindzen and Hou, 1988; Plumb and Hou, 1992; Schneider and Bordoni, 2007, in press), and we wish to determine how such theories behave in a seasonally-varying moist atmosphere with wind-dependent surface enthalpy fluxes. Our second motivation is that some existing theories for abrupt onset that do treat the atmosphere as a moist fluid require the release of a large amount of APE coincident with onset; while this in and of itself is not necessarily a defect, the convective closure assumed by such theories is almost always based on low-level moisture convergence rather than a physical measure of convective instability, as noted in the previous section. Convective quasi-equilibrium might provide a useful alternate framework in which to understand the processes responsible for monsoon onset. Finally, we are motivated by the fact that peak convective activity is centered over ocean, rather than over land, for the two monsoons known to have abrupt onsets (in South Asia and Australia). Over oceans the net flux of enthalpy into the boundary layer depends strongly on surface wind speed, making a wind-evaporation feedback potentially relevant. Such a mechanism would also be consistent with the fact that, near South Asia and Australia, the intraseasonal variance of OLR is even more strongly biased to occur over ocean than the seasonal mean OLR (see plots in Murakami et al., 1986; Wheeler and Kiladis, 1999).

The central hypothesis of this thesis is that the abrupt onset of monsoons occurs because of a positive feedback between wind-driven ocean surface enthalpy fluxes and the strength of the thermally direct circulation. Because surface evaporation accounts for the bulk of these enthalpy fluxes, this is often called wind-evaporation feedback (e.g. Neelin et al., 1987). Our hypothesis assumes a form of convective quasi-equilibrium in which deep convection does not provide a direct thermal forcing for the circulation, but maintains an equilibrium between changes in free-tropospheric temperature and boundary layer entropy (Emanuel et al., 1994). The wind-evaporation feedback is proposed to operate for solsticial circulations because strong off-equatorial surface winds and weak near-equatorial surface winds produce a poleward gradient of ocean evaporation, which acts to increase the poleward gradient of boundary layer entropy and thus of free-tropospheric temperature. An

enhanced meridional temperature gradient will then drive a stronger meridional circulation with larger surface wind speeds, providing a positive feedback on the meridional gradient of surface evaporation. This thesis examines this simple hypothesis in both observations and a hierarchy of numerical models.

1.4 Overview of chapters

This introductory chapter briefly reviewed the phenomenon of abrupt monsoon onset and some previous theories for its underlying mechanism. More detailed discussion of the theories most relevant to this thesis is presented in the ensuing chapters, together with additional observations of monsoon onset.

The next two chapters examine how the wind-dependence of surface enthalpy fluxes alters nonlinear axisymmetric theories of Hadley circulations. The first of these two chapters considers the effect of wind-evaporation feedback for forcings that are localized off the equator and have sufficiently weak amplitude so that an angular momentum conserving (AMC) response is not produced. Weak forcings are first considered as a separate case because, as will be shown in the second of these two chapters, a circulation in an AMC regime must satisfy dynamical constraints that complicate the effect of wind-evaporation feedback. The work in these two chapters is undertaken as an extension of the studies of Plumb and Hou (1992) and Lindzen and Hou (1988) to a moist framework with a seasonally varying forcing. Zheng (1998) did examine nonlinear axisymmetric theory in a moist model with a seasonally varying forcing, but did so without wind-dependent surface enthalpy fluxes. As noted above, Numaguti (1995) studied wind-evaporation feedback in a moist GCM with a seasonally varying forcing, but did not explore the detailed dynamics of AMC flow, and he also used a forcing that might not be appropriate for monsoon climates. The next two chapters can thus be seen as further development of these studies.

The fourth chapter attempts to determine whether the observed onset of the South Asian monsoon is consistent with the dynamics of the wind-evaporation feedback seen in the axisymmetric models of chapters 2 and 3. A dynamically based index of the monsooxn circulation is defined and used to create composites of the onset process. This is a necessary step because most detailed observational composites of monsoon onset have been based on either OLR or precipitation (e.g. Zhang et al., 2002; Fasullo and Webster, 2003), quantities

which could conceivably evolve nonlinearly even if the associated circulation exhibits a linear response to its forcing. Composites of onset using wind have generally done so only at one particular continental location (e.g. Wheeler and McBride, 2005), and one can imagine an abrupt onset occurring at a single point simply due to the slow, seasonal migration of a front in the velocity field. Chapter 4 uses observations to frame the onset of the South Asian monsoon as the seasonal transition of a large fraction (over half) of the zonal mean Hadley circulation, and examines this transition in a convective quasi-equilibrium paradigm.

The fifth chapter returns to the world of numerical models, but does so using a three-dimensional primitive equation model with realistic topography, a prescribed SST climatology, and detailed representations of subgrid scale physics. Model integrations with and without wind-dependent surface enthalpy fluxes are used to assess the effect of wind-evaporation feedback on the seasonal cycle of the South Asian monsoon. While we find that the control version of the model (with wind-dependent surface fluxes) does not simulate the abrupt onset of this monsoon, the results still prove useful in that wind-evaporation feedback exerts a strong control on the distribution of ascent and precipitation in the model's mean summer monsoon, consistent with results from the axisymmetric models of Chapter 3.

The thesis concludes with a short summary of the findings presented in the individual chapters and a discussion of how these results collectively alter our understanding of monsoons. Suggestions for future work are also included in this final chapter.

THIS PAGE INTENTIONALLY LEFT BLANK

Chapter 2

Wind-evaporation feedback and abrupt seasonal transitions of weak, axisymmetric Hadley circulations

Abstract

For an imposed thermal forcing localized off the equator, it is known that conservation of absolute angular momentum in axisymmetric flow produces a nonlinear response once the forcing exceeds a critical amplitude. It is shown here that, for a moist atmosphere in convective quasi-equilibrium, the wind-dependence of ocean surface enthalpy fluxes can provide a feedback that causes the meridional flow to evolve nonlinearly as a function of a periodic sea surface temperature (SST) forcing, even if an angular momentum conserving response is not achieved.

This wind-evaporation feedback is examined in both an axisymmetric primitive equation model and a simple model that retains only a barotropic and single baroclinic mode. Only SST forcings that do not produce an angular momentum conserving response are examined here. The wind-evaporation feedback is found to be inhibited in models with linear dynamics because the barotropic component of the Hadley circulation, which is coupled to the baroclinic circulation via surface drag, keeps surface winds small compared to upper level winds. In models with nonlinear dynamics, the convergence of zonal momentum into the ascending branch of the cross-equatorial Hadley cell can create barotropic westerlies that enhance the baroclinic wind at the surface, thereby eliminating the inhibition of the wind-evaporation feedback. The possible relevance of these results to the onset of monsoons is discussed.

2.1 Introduction

Steady-state, axisymmetric solutions for the circulation in a differentially heated fluid on a rotating sphere have been advanced over the past few decades as a means of understanding the Hadley circulation (e.g. Schneider, 1977; Held and Hou, 1980). The associated theory emphasizes conservation of absolute angular momentum in the free troposphere, which results in a nonlinear dependence of circulation strength and extent on the imposed thermal forcing.

Results of this theory have been used to explain certain aspects of the seasonal cycle of the Hadley circulation. Lindzen and Hou (1988) showed that the steady axisymmetric response to a heating having a peak displaced just a few degrees off the equator exhibits a strong asymmetry, consistent with observations, in the strength and meridional extent of the summer and winter Hadley cells. Plumb and Hou (1992) showed that the strength of steady, axisymmetric meridional flow increases nonlinearly as the magnitude of a thermal forcing localized off the equator is enhanced beyond a threshold value. They suggested that this threshold behavior might be relevant to the seasonal onset of monsoons, but noted that the roles of zonal asymmetries and time-dependence need to be assessed.

The effect of time-dependence on axisymmetric theory has only begun to be explored. Fang and Tung (1999) examined a version of the axisymmetric dry model used by Lindzen and Hou (1988) with a time-dependent forcing. They found that there was no abrupt change in the circulation as the maximum of the thermal forcing was moved meridionally in a seasonal cycle, primarily because the circulation did not achieve equilibrium with its forcing during the course of this cycle. The dry axisymmetric models used by Fang and Tung (1999) and Plumb and Hou (1992) equilibrate on time scales on the order of 100 days, which is longer than the time scale associated with the seasonal cycle of Earth's insolation forcing[1]. However, moist axisymmetric models with stratifications and rates of radiative cooling similar to those of th Earth's tropics will equilibrate much faster, an issue we discuss in Appendix B. Therefore, it is not reasonable to apply a time-varying forcing with a 365 day period to a dry axisymmetric model with an equilibration time scale on the order of 100 days and expect the results to be relevant to the seasonal cycle of Earth's Hadley circulation.

The fact that moist axisymmetric models equilibrate on a time scale shorter than that

[1] A sinusoid with a period of 365 days varies with a time scale $\tau = 58$ days, if τ is interpreted as the e-folding time.

of the Earth's seasonal cycle is illustrated by the results of Zheng (1998), who extended the results of Plumb and Hou (1992) using a moist axisymmetric model forced by an off-equatorial sea surface temperature (SST) anomaly. Zheng (1998) confirmed that the circulation entered an angular momentum conserving regime once the magnitude of the SST anomaly exceeded a certain threshold, and found that an abrupt, nonlinear onset of the summer circulation occurred when the SST forcing was varied in a seasonal cycle. It is of interest that Zheng (1998) did not use wind-dependent surface enthalpy fluxes in his model runs, because Numaguti (1995) found that wind-dependent ocean evaporation was needed to obtain an abrupt poleward shift in the peak precipitation as a prescribed SST maximum was gradually shifted poleward in a three-dimensional general circulation model (GCM). Based on the diagnostics presented by Numaguti (1995), it is difficult to judge whether the meridional flow in his model exhibited abrupt or nonlinear behavior similar to that found by Zheng (1998). The main goal of this and the next chapter is to examine the effect of wind-induced surface heat exchange (WISHE) on meridional flow in the context of previous studies of nonlinear axisymmetric theory.

Zonally asymmetric eddies may play an important role in Hadley circulation dynamics by transporting momentum meridionally; the zonal mean meridional circulation cannot conserve absolute angular momentum where these transports are important. For thermal forcings centered on the equator in a three-dimensional model with zonally symmetric boundary conditions, Walker and Schneider (2006) found that the strength of the Hadley circulation was directly related to the eddy momentum flux divergence, and that scalings based on the assumptions of axisymmetric angular momentum conservation did not hold. However, when the peak thermal forcing was displaced sufficiently far from the equator, their model produced cross-equatorial flow that nearly conserved absolute angular momentum, at least in its free-tropospheric ascending branch. Schneider and Bordoni (2007, in press) found that abrupt transitions between the eddy-controlled equinoctal regime and the angular momentum conserving solsticial regime occurred in a model with a seasonally-varying forcing, and discussed the similarity between the dynamics of this transition and the onset and end of monsoons. While eddy transports may thus play an important role in seasonal Hadley dynamics, we shall demonstrate that a wind-evaporation feedback may also play an important role, and that this feedback is sufficiently complex to merit initial examination in idealized two-dimensional models.

In this chapter we examine the seasonal cycle of the Hadley circulation in a series of axisymmetric (non-eddy resolving) models forced by thermal maxima localized off the equator. Results from a dry primitive equation model are presented first to show the importance of the model equilibration time scale, and to illustrate how in a time-dependent model, meridional flow generated by a transient, linear, thermal equilibration can be just as strong as that occurring in a nonlinear, angular momentum conserving (AMC) regime. Results from a moist primitive equation model are then used to show that a wind-evaporation feedback can produce a circulation that depends nonlinearly on the SST forcing, and that this feedback requires zonal momentum conservation even though the upper-level circulation is not near the AMC regime. An idealized two-mode model of tropospheric flow is introduced to explain this interaction between wind-evaporation feedback and zonal momentum advection. We conclude by discussing the relevance of these results to monsoons and some possible effects of processes omitted from the idealized models used here.

2.2 Primitive equation model

We examine the time-dependent behavior of Hadley circulations in dry and moist versions of the zonally symmetric (two-dimensional) GCM used by Pauluis and Emanuel (2004) and Pauluis (2004). The model dynamics are based on the MIT GCM (Marshall et al., 1997; Adcroft et al., 1999; Marshall et al., 2004), but a series of alternate parameterizations is used for subgrid scale physics. The model domain is a partial sphere extending between rigid walls at 64°N and 64°S, with 1° meridional resolution on a staggered spherical polar grid. There are 40 pressure levels with 25 hPa resolution, from 1000 hPa to a rigid lid at 0 hPa, and no representation of orography. Viscosity is represented by the vertical diffusion of momentum with a coefficient of 100 $Pa^2\ s^{-1}$. Frictional stresses in the planetary boundary layer are represented by vertically homogenizing horizontal velocities in the lowest 200 hPa of the atmosphere over a time scale of 20 minutes. An eighth-order Shapiro filter is used to reduce small-scale horizontal noise in the temperature, specific humidity, and horizontal wind fields.

Instead of diagnosing the spatial maximum of the overturning streamfunction as a metric for circulation intensity, we use the meridional flow integrated both vertically through the boundary layer (800-1000 hPa) and meridionally over all model latitudes, a quantity

hereafter called the PBL flow. The PBL flow has the advantage of being a single scalar that is continuously relevant during the transition from summer to winter, whereas the streamfunction extremum of the dominant Hadley cell changes sign between summer and winter. This will become relevant when the thermal forcing is prescribed to vary in a seasonal cycle. Because the PBL flow involves a meridional integral, it does not measure the equatorially antisymmetric component of the streamfunction. We purposely chose the fairly large dynamical boundary layer depth of 200 hPa in order to constrain most of the meridional mass flux in the lower branch of the Hadley circulation to move through the boundary layer (Pauluis, 2004).

2.2.1 Dry model

Although using a dry model may in some ways seem a digression from the primary task of assessing the effect of wind-evaporation feedback on Hadley circulations, it is done in order to reconcile the dry model results of Fang and Tung (1999) with the moist results of Zheng (1998). Furthermore, the dry results will prove to be a useful comparison for the subsequently presented moist results.

Dry model configuration

In a dry version of the axisymmetric MIT GCM, the circulation is forced by relaxation of temperature over a spatially uniform time scale of 10 days to a prescribed distribution T_{eq} similar to that used by Plumb and Hou (1992, hereafter PH92), which provides a thermal forcing centered at latitude ϕ_0:

$$T_{eq} = T_0 + T_{max}\frac{\pi}{2}\sin\left(\pi\frac{p_0 - p}{p_0}\right)\cos^2\left(\frac{\pi}{2}\frac{\phi - \phi_0}{\Delta\phi}\right) \tag{2.1}$$

This is used to specify T_{eq} only between $\phi_0 + \Delta\phi$ and $\phi_0 - \Delta\phi$; outside this range T_{eq} is set to T_0. Here p_0 is pressure at the lowest model level and we use $\phi_0 = 25°$N and $\Delta\phi = 15°$. This gives an equilibrium temperature with no meridional gradient outside the range 10°N - 40°N and an extremum centered at 25°N and 500 hPa.

Most integrations of the dry model use an isothermal background state with $T_0 = 200$ K. As discussed in Appendix B, the use of an isothermal background state will produce relatively weak meridional velocities and thus an equilibration time scale for absolute angular

momentum M of about 165 days, which is much longer than the time scale of the seasonal cycle of Earth's insolation forcing. One integration is also performed using a background state having near neutral stratification, with $\partial T_0/\partial z = 0.9g/c_p$. This reduces the time scale for M advection to about 15 days.

We examine the equilibrated response to steady forcings as well as the time-dependent response to a seasonally varying forcing. In all cases, the initial model state used was that of an atmosphere at rest with meridionally uniform temperature T_0. To avoid high-amplitude initial transients, the off-equatorial anomaly of equilibrium temperature was increased from zero for the steady forcings according to:

$$T_{max} = \theta_m(1 - e^{-t/\tau_i}) \tag{2.2}$$

with $\tau_i = 30$ days. Three separate integrations with steady forcings were performed, using $\theta_m = 5$ K, 10 K and 15 K. For the seasonal forcing, T_{max} in (2.1) was varied according to:

$$T_{max} = \theta_m \cos\left(2\pi \frac{t}{365 \text{ days}}\right) \tag{2.3}$$

where t is time in days and $\theta_m = 15$ K.

This model configuration is intended to represent, in a highly idealized fashion, the thermal forcing associated with an off-equatorial land mass in a monsoon climate. The meridional and vertical structures of equilibrium temperature, which are similar to those used by PH92, were chosen for conceptual simplicity. Our aim is not to simulate the zonal mean climate on Earth, but to illustrate the comparative time evolution of the meridional circulation and the M field in an axisymmetric framework.

Dry model results

As in PH92, the response to steady forcings took hundreds of days to achieve a steady state, at which time the equilibrated PBL flow depended nonlinearly on θ_m (Fig. 2-1). The model evolution can be understood in terms of the evolution of M. During the first 100 days of integration for $\theta_m = 15$ K, the M distribution is only slightly perturbed from its initial state of solid-body rotation, although the streamfunction and PBL flow reach amplitudes nearly as large as in equilibrium (Fig. 2-2, left panel). After equilibration, which takes more than 500 days, the M field has undergone considerable homogenization in the upper troposphere

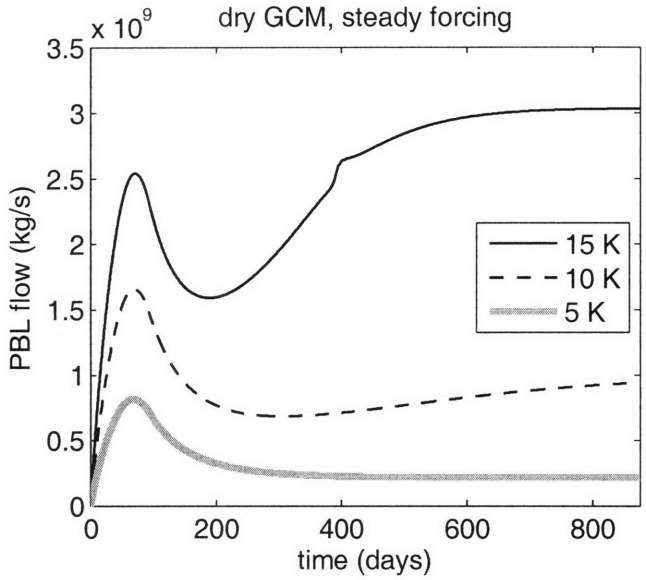

Figure 2-1: Time evolution of the PBL flow (defined as the meridional wind integrated vertically and meridionally in the boundary layer) for the dry GCM with steady forcing. The three curves correspond to forcings with different values of θ_m, which sets the magnitude of the off-equatorial equilibrium temperature anomaly.

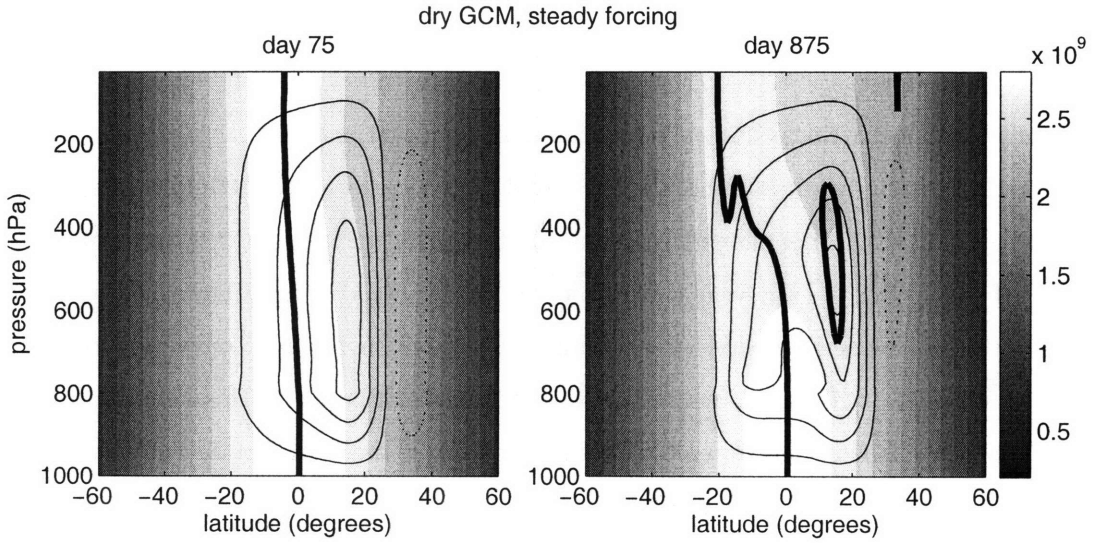

Figure 2-2: Absolute angular momentum (shading) and meridional streamfunction (thin contours) for the dry GCM with steady forcing and $\theta_m = 15$ K, at the initial transient peak (left panel) and after the model achieved a steady state (right panel). Thick solid line is the zero absolute vorticity contour. Streamfunction contour interval is 1×10^{10} kg s^{-1}, starting at 0.5×10^{10} kg s^{-1}, with negative contours (denoting clockwise rotation) dashed. Angular momentum contour interval is 0.2×10^9 m^2 s^{-1}.

with the zero contour of absolute vorticity displaced to about 20°S (Fig. 2-2, right panel). During both the initial transient peak and the final steady state, most of the lower branch of the meridional circulation flows through the boundary layer, peak ascent occurs slightly equatorward of ϕ_0, and a weak summer cell exists in the mid-latitude summer hemisphere. The streamfunction maximum is fairly low in the free troposphere, suggesting that these results are free of any amplification of the circulation due to the rigid lid upper boundary condition (Walker and Schneider, 2005).

Comparing the time series for different values of θ_m presented in Fig. 2-1, the time evolution seems to be a superposition of a relatively rapid and linear thermally-dominated adjustment followed by a slow, nonlinear adjustment dominated by M advection. Although this in many ways restates some results of PH92, we include this discussion to emphasize a particular point: changes in the thermal forcing can produce a linear response in the strength of the circulation within a few inertial periods (the initial transient peak occurs after 80 days because of the spin-up used for the forcing). If the thermal forcing is not externally specified but depends on the circulation itself, feedbacks could occur because of interactions between the circulation and the forcing. This chapter will examine the particular case of a wind-evaporation feedback, but coupling between the circulation and the thermal forcing could also occur via radiation or other processes. Depending on the nature of these interactions, such feedbacks could operate in a regime where the atmospheric dynamics are mostly linear and M advection is not important.

For the seasonally varying forcing, the circulation took less than 100 days to achieve a regular periodic cycle (not shown). After this initial adjustment period, the streamfunction and PBL flow peaked each year shortly before T_{eq} reached its maximum. We will refer to this time of peak PBL flow as the summer solstice, using the convention of boreal summer for $T_{max} > 0$. The streamfunction and M distribution at this summer solstice, shown in Fig. 2-3, closely resemble those seen during the initial transient peak of the runs with steady forcing, without the folding over of M surfaces seen in the equilibrated response to the steady forcing. Contours of M tilt very slightly against the flow in the upper troposphere of the winter hemisphere, suggestive of their deformation by flow during the previous solstice. Also, the meridional width of the M peak near the equator is slightly larger for the seasonally varying forcing than for the steady forcing, suggesting that some homogenization is accomplished by the seasonally reversing meridional winds.

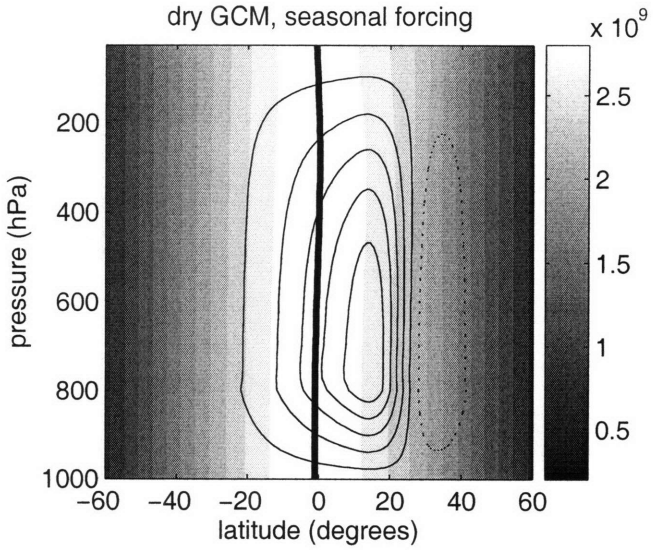

Figure 2-3: As in the previous figure, but for the dry GCM with seasonally varying forcing, at the time of largest PBL flow.

The PBL flow exhibits no abrupt transitions over time, although a slight nonlinearity is apparent between summer and winter seasons when the PBL flow is plotted against $T_{max}\pi/2$, which is the equilibrium temperature anomaly at 25°N (Fig. 2-4). This phase space trajectory would be a perfect ellipse if the PBL flow varied linearly with T_{max} with only a phase lag between the two quantities. The equilibrated PBL flow for the steady forcings, also plotted on this phase diagram, increases nonlinearly with T_{max}.

The PBL flow in the seasonally forced run leads T_{max}, as shown by the clockwise phase space trajectory. It is straightforward to show that this phase relationship is expected when the thermal relaxation time is short compared to the forcing period. If $T_{max} = \sin At$ and T is assumed to lag T_{max} by Δt but to have the same frequency A, then a trigonometric identity can be used to write the Newtonian cooling as:

$$Q = \frac{T_{max} - T}{\tau} = \frac{2}{\tau} \cos(At - \frac{A\Delta t}{2}) \sin \frac{A\Delta t}{2} \tag{2.4}$$

This shows that Q will lead T_{max} by $(\pi/2 - A\Delta t/2)$, which is slightly less than one-quarter cycle if Δt is much smaller than the forcing period. Linear theory for a sea breeze (Rotunno 1983), although formulated on an f-plane instead of a sphere, predicts that the circulation will be in phase with Q so long as f is larger than the frequency of the thermal forcing,

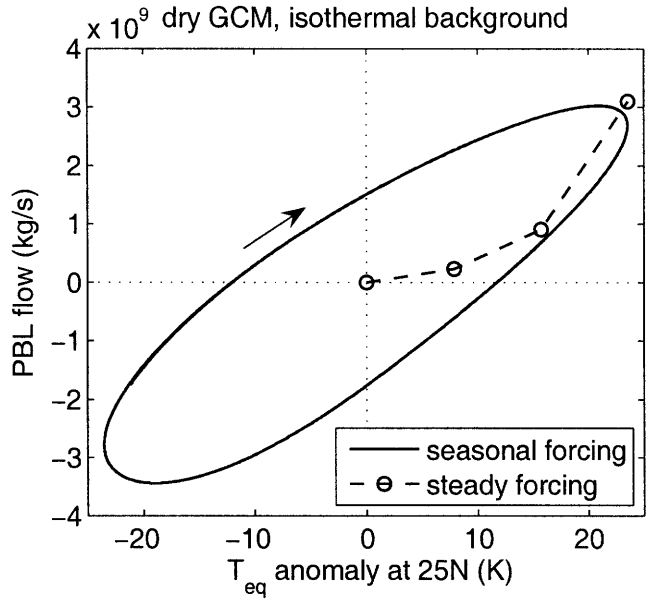

Figure 2-4: Phase diagram of the PBL flow and the spatial extremum of the equilibrium temperature anomaly for the dry GCM. Solid line is for the run with seasonally varying forcing, with time progressing in the direction of the arrow. The circles connected by the dashed line denote the equilibrated response to steady forcings.

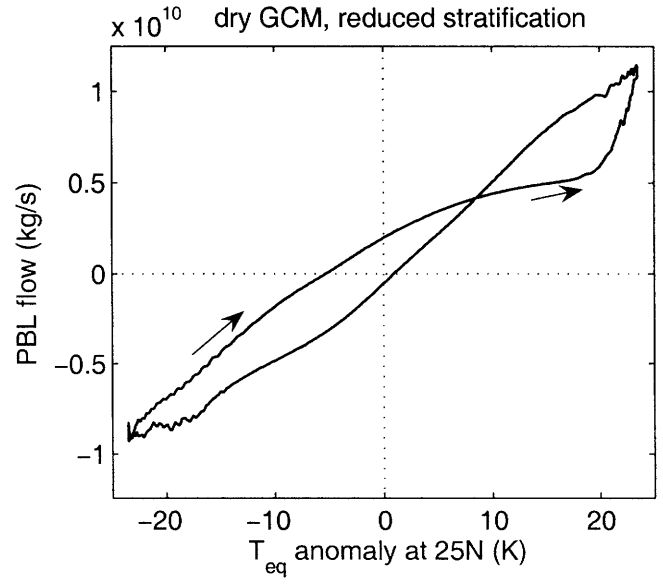

Figure 2-5: As in the previous figure, but the phase diagram for the dry GCM with a reduced background stratification ($\partial T_0 x/\partial z = 0.9\ \Gamma_d$) and a strong forcing ($\theta_m = 15$ K).

which is true for a forcing period of 365 days everywhere except within a tenth of a degree of the equator. Since M advection seems to be of minor importance for the evolution of the streamfunction for the seasonally varying forcing, the dynamics might be decently described by this linear theory, with Q in phase with the PBL flow and both leading T_{max} by one-quarter cycle. However, the PBL flow and T_{max} peak at nearly the same time, giving the major axis of the phase-space ellipse its positive slope and indicating that part of the circulation must be in phase with T_{max}. So it would seem that the phase lag between T_{max} and the PBL flow explains why the phase trajectory is an ellipse rather than a straight line, but that a significant part of the flow is also in phase with T_{max}. Similar phase relationships were obtained for an increased Newtonian cooling time scale of 30 days, as well as for a reduced viscosity of 10 $Pa^2\ s^{-1}$. This reduced viscosity was near the lowest value for which numerically stable solutions could be obtained. Integrations using smaller values of ϕ_0 and θ_m also produced circulations which evolved nearly linearly with T_{max}.

If the time scale of M advection is smaller than that of variations in T_{max}, then we expect the time evolution of a seasonally forced model to become nonlinear. This hypothesis is tested by using the reduced background stratification of $\partial T_0/\partial z = 0.9g/c_p$, for which M advection has an estimated time scale of around 15 days (see Appendix B). When this model is integrated using the same value of $\theta_m = 15$ K in (2.3), the phase diagram shows that the sensitivity of the PBL flow to T_{max} does increase suddenly shortly before the summer solstice (Fig. 2-5). This trajectory deviates considerably from the linear ellipse and loosely resembles the figure "8" expected for two time series where one evolves at twice the frequency of the other. At the time when the sensitivity of the PBL flow to T_{max} increases abruptly, the absolute vorticity near the model tropopause approached zero throughout much of the tropics (not shown), indicating that the abrupt transition is associated with the onset of M conserving flow at upper levels.

2.2.2 Moist model

Moist model configuration

In a moist version of the model, the circulation is forced by parameterized radiative cooling together with surface fluxes of latent and sensible heat which are vertically redistributed by

moist convection. Surface evaporation F_q is represented by a bulk formula:

$$F_q = \rho C_k |\mathbf{V}|(q^*(T_s) - q) \tag{2.5}$$

where ρ and q are the density and specific humidity of air at the lowest model level, C_k is a transfer coefficient set to 0.0012, and $q^*(T_s)$ is the saturation specific humidity at surface temperature T_s. The effective wind speed is:

$$|\mathbf{V}| = \sqrt{u^2 + v^2 + v_g^2} \tag{2.6}$$

where u and v are the horizontal winds at the lowest model level. Surface fluxes of sensible heat and momentum take a similar form, with the same nondimensional transfer coefficient. The parameter v_g is included to represent the effects of a range of subgrid scale variations in wind, from dry convective eddies to meso-scale convective systems, and in a more realistic treatment would vary with the local dynamic and thermodynamic state. Indeed, many surface flux formulae represent the effect of dry convective gustiness with a state-dependent convective velocity scale that typically has a value near 1 m s^{-1} (Stull, 1988), while schemes to parameterize gustiness in precipitating convection have predicted values that typically vary from 1 to 5 m s^{-1} (e.g. Williams, 2001). For simplicity, we set v_g to the constant value of 4 m s^{-1}. This somewhat large value was chosen to suppress the formation in the model of convective anomalies that propagate meridionally on intraseasonal time scales. Bellon and Sobel (2008, in press) have examined what seem to be similar poleward propagating anomalies in another axisymmetric model forced by steady SST, and proposed that they are relevant to the observed poleward migrations of the convective maximum associated with "active" and "break" episodes of the South Asian monsoon (e.g. Yasunari, 1979). These intraseasonal anomalies are purposely suppressed here in order to simplify the physics of the model's seasonal cycle, and we hope that future work will examine the interaction of such intraseasonal anomalies with seasonal transitions.

Radiation in the moist GCM is calculated by the longwave scheme of Morcrette (1991) and the shortwave scheme of Fouquart and Bonnel (1980). Insolation is independent of latitude and moves through a diurnal cycle, although the diurnal cycle has an effect only through atmospheric absorption of shortwave radiation because of the use of an entirely oceanic lower boundary with prescribed SST. Integrations are performed with no repre-

sentation of cloud radiative effects (i.e. clear-sky), and the specific humidity used for the radiative calculations is fixed at a reference profile that does not vary with latitude or time. While the radiative effects of variable moisture are expected to alter the solutions, they are neglected here in order to better isolate the physics involving wind-dependent surface fluxes. Moist convection is represented by the scheme of Emanuel and Zivkovic-Rothman (1999).

The lower boundary consists entirely of ocean with a specified SST given by the one-dimensional analogue of (2.1):

$$T_s = T_0 + T_{max} \frac{\pi}{2} \cos^2 \left(\frac{\pi}{2} \frac{\phi - \phi_0}{\Delta\phi} \right) \tag{2.7}$$

with $\phi_0 = 25°$N and $\Delta\phi = 15°$, as in the dry model, and $T_0 = 296$ K. This provides an SST anomaly centered at 25°N and confined between 10°N and 40°N, with no cross-equatorial SST gradient. The anomaly is prescribed to oscillate with the same seasonal cycle used for the dry model, given by (2.3).

Runs without WISHE

We first discuss model integrations with $|\mathbf{V}|$ in the surface flux formulae for latent and sensible heat fixed at 5 m s^{-1}, thereby eliminating any effects of WISHE. The results are consistent with the findings of Zheng (1998), in that an AMC circulation occurs only when the amplitude of the off-equatorial SST anomaly exceeds a certain threshold. For example, using $T_{max} = 15$ K produces a phase space trajectory resembling that obtained for the seasonally forced dry model with near-neutral stratification, in that the sensitivity of PBL flow to the amplitude of the SST anomaly changes abruptly as the anomaly nears its summer maximum (Fig. 2-6). Shortly after this increase in sensitivity (at a time indicated by the dot on the phase trajectory), M contours are strongly deformed from a resting state, with the zero contour of absolute vorticity η shifted to nearly 20°S near the tropopause (Fig. 2-7). The lower branch of the circulation crosses the equator well above the boundary layer, roughly following M contours in the free-troposphere. This cross-equatorial jumping behavior presumably has such high amplitude because of interactions with moist convection, as discussed by (Pauluis, 2004).

When a much weaker forcing is used, with $T_{max} = 1.0$ K and no WISHE, no abrupt

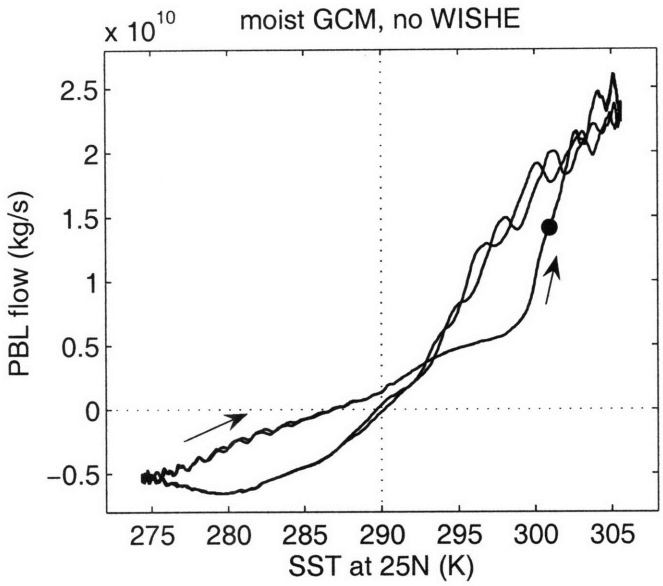

Figure 2-6: As in Fig. 2-4, but the phase diagram for the moist GCM with strong forcing (θ_m = 15 K) and wind-independent surface enthalpy fluxes. The dot denotes the model state for which M and ψ are shown in the next figure.

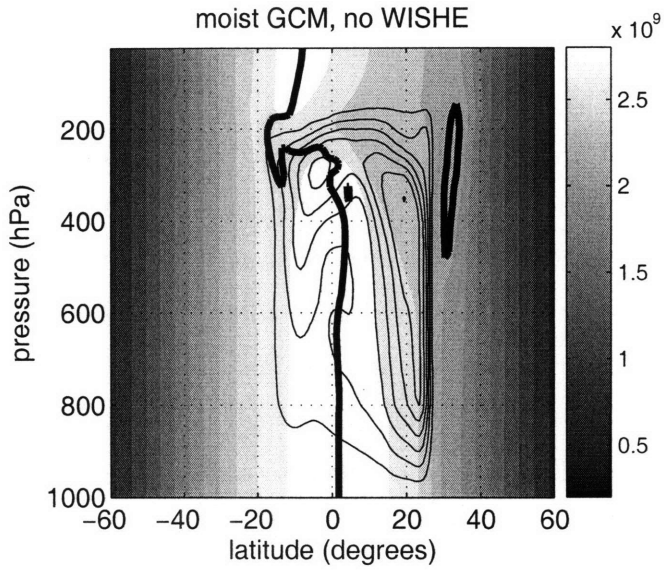

Figure 2-7: As in Fig. 2-2 but for the moist GCM with strong forcing (θ_m = 15 K) and wind-independent surface enthalpy fluxes, at the time represented by the dot in the previous figure. Streamfunction contour interval is 4×10^{10} kg s^{-1}, which is four times that used in Figs. 2-2 and 2-3.

intensification is seen (Fig. 2-8, grey line in left panel). The phase diagram closely resembles the ellipse obtained for the seasonally-forced dry model with an isothermal background state. The circulation near the time of peak SST is weak and confined entirely to the summer hemisphere, and M contours deviate only very slightly from the vertical in the upper troposphere (Fig. 2-9, right panel).

Runs with WISHE

Now we examine a series of model integrations with surface enthalpy fluxes that depend on wind speed according to (2.5) and (2.6). In this chapter, runs with WISHE will only be performed for weak forcings that do not produce an AMC response; stronger forcings are examined in the next chapter.

For a run with WISHE and $\theta_m = 1$ K, the circulation exhibits a rapid onset and withdrawal of the summer circulation, as seen by the sudden increase in the slope of the phase trajectory near the time of maximum SST (Fig. 2-8, black line in left panel). Halfway through the abrupt intensification of the summer circulation in the WISHE run, M contours are slightly deformed from a resting state (Fig. 2-9, left panel), although they are far from the near horizontal state characteristic of an AMC regime (compare with Fig. 2-7). The circulation at this time exists mostly in the summer hemisphere.

Given that the deformation of M contours is weak in the WISHE run, one might hypothesize that the abrupt intensification occurs because of a linear feedback between the strength of the Hadley circulation and the surface enthalpy flux. However, the abrupt onset of a strong solsticial circulation occurred only when both WISHE and nonlinear momentum advection were represented in the model. This was found by conducting a third model run with WISHE but without the advection of either zonal or meridional relative momentum. The phase trajectory of this run was nearly elliptical with a weak solsticial circulation and no abrupt transitions (Fig. 2-8, right panel). Eliminating both WISHE and momentum advection in a fourth model run also produced a nearly elliptical phase trajectory. The use of WISHE without momentum advection did make the summer circulation almost twice as strong as the winter circulation, but this occurred without any rapid change in the slope of the phase trajectory and was a weak effect compared to that produced by the combination of WISHE and momentum advection.

Omitting the advection of relative momentum from the model equations without also

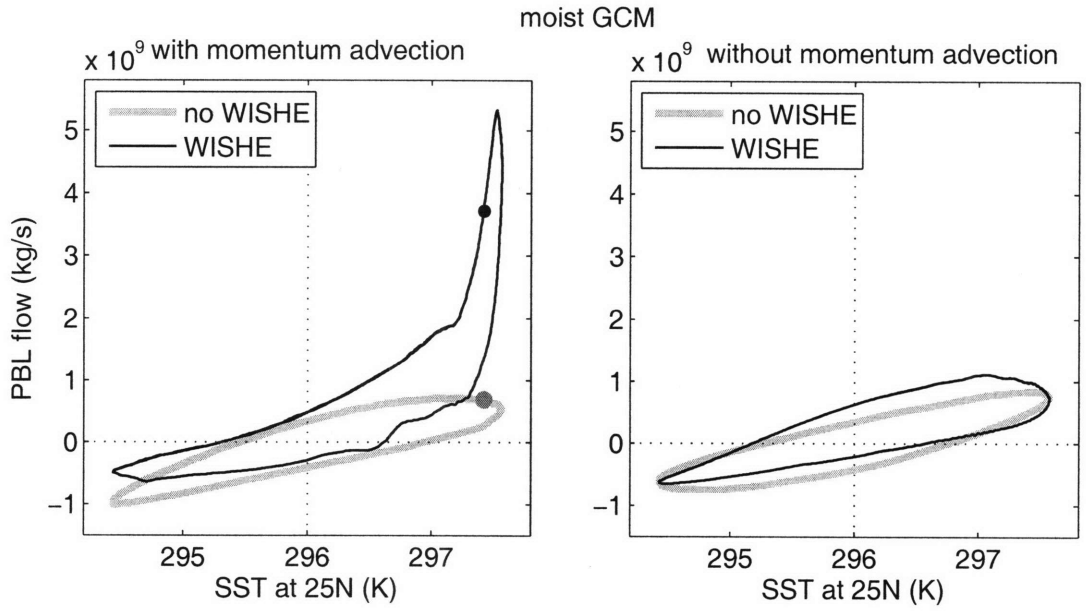

Figure 2-8: As in Fig. 2-4, but the phase diagram for the moist GCM with weak forcing (θ_m = 1.0 K). The left and right panels are for runs with and without nonlinear momentum advection, respectively. The black and grey lines are for runs with and without WISHE, respectively. Dots in the left panel denote the model states for which M and ψ are shown in the next figure.

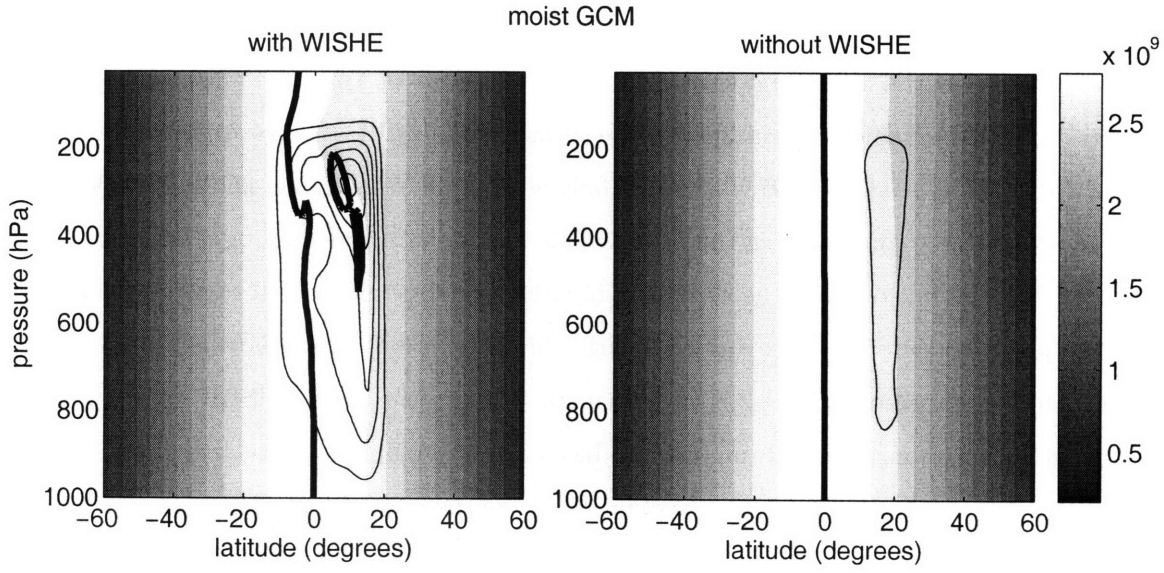

Figure 2-9: As in Fig. 2-7, but for the moist GCM with weak forcing (θ_m = 1.0 K), at times denoted by the dots in the previous figure. Left and right panels are for the runs with and without WISHE, respectively (both included nonlinear momentum advection).

omitting the advection of humidity and potential temperature results in nonconservation of total energy in the model. However, omitting all of these advection terms in an additional run produced a phase trajectory that differed only slightly from that of the run in which only relative momentum advection was omitted (not shown). This establishes that the combination of nonlinear advection and WISHE are both required for the abrupt intensification, and suggests that it is the nonlinear advection of relative momentum in particular that plays a central role in the feedback. An understanding of the interaction between WISHE and momentum advection will prove to be facilitated by use of an even simpler model, which is introduced in the next section.

2.3 Two-mode model

To better understand the nature of the abrupt intensification in the GCM run with WISHE, we use a different axisymmetric model in which the assumption of convective quasi-equilibrium is used to simplify the thermodynamics and in which only a barotropic mode and one baroclinic mode of the horizontal wind are represented.

2.3.1 Model formulation

General physics

This model is highly similar to the Quasi-Equilibrium Tropical Circulation Model (QTCM) of Neelin and Zeng (2000), but phrases the thermodynamics in terms of moist entropy instead of temperature and humidity. This is done for consistency with previous theoretical studies of purely baroclinic WISHE modes by Emanuel (1987) and Emanuel (1993); an overview of the thermodynamics is given here, and the reader is directed to those papers for a more detailed derivation.

Moist convection is assumed to keep variations in s^*, the saturation moist entropy of the free troposphere, constant with height. This allows variations in the geopotential Φ to be partitioned into a barotropic component, $\delta\Phi_0$, that is invariant with height, and a baroclinic component that can be written in terms of variations in s^*:

$$\frac{\partial}{\partial p}\delta\Phi = -\left(\frac{\partial T}{\partial p}\right)_{s^*}\delta s^* + \frac{\partial}{\partial p}\delta\Phi_0 \tag{2.8}$$

where the derivative of T is taken at constant s^*. In this particular model we assume no variations in surface pressure, so that the above can be integrated to obtain $\delta\Phi$:

$$\delta\Phi - \delta\Phi_b = (T_b - T)\delta s^* \tag{2.9}$$

where the b subscript denotes a property at the top of the subcloud layer, and T serves as a vertical coordinate. Using (2.9) together with the property that the vertical integral of purely baroclinic Φ perturbations must vanish gives

$$-\delta\Phi = (T - \overline{T})\delta s^* \tag{2.10}$$

where $\overline{T}$ is a mass-weighted vertical mean tropospheric temperature.

Conservation equations, phrased on a β-plane, for axisymmetric horizontal winds can then be written in terms of the fluctuating component of s^* (the δ symbol is henceforth omitted):

$$\begin{aligned} \frac{\partial u}{\partial t} + v\frac{\partial u}{\partial y} + w\frac{\partial u}{\partial z} - \beta y v &= F_u \\ \frac{\partial v}{\partial t} + v\frac{\partial v}{\partial y} + w\frac{\partial v}{\partial z} + \beta y u &= (T - \overline{T})\frac{\partial s^*}{\partial y} - \frac{\partial}{\partial y}\Phi_0 + F_v \end{aligned} \tag{2.11}$$

with the F terms representing both surface drag and diffusion.

Tendencies of s^* and subcloud-layer entropy s_b are:

$$\begin{aligned} \frac{\partial s^*}{\partial t} + v\frac{\partial s^*}{\partial y} &= -N^2(w - \epsilon M) - R + \kappa\frac{\partial^2 s^*}{\partial y^2} \\ H_b\left(\frac{\partial s_b}{\partial t} + v\frac{\partial s_b}{\partial y}\right) &= E + \mathrm{MIN}(0, (w_b - M))(s_b - s_m) + H_b\kappa\frac{\partial^2 s_b}{\partial y^2} \end{aligned} \tag{2.12}$$

where M is the net upward mass flux in convective clouds, H_b is the depth of the subcloud layer, w_b is the vertical velocity at the top of the subcloud layer averaged over clear and cloudy areas, ϵ is a bulk precipitation efficiency, and R is the rate of radiative cooling, which is fixed at 1 K day^{-1}. The second term on the right hand side of the s_b equation represents the downward advection of low entropy mid-tropospheric air into the boundary layer, with the difference between s_b and the mid-tropospheric entropy s_m hereafter assumed to be a constant, denoted χ. The MIN function is used to eliminate this term when the net mass

flux is upward. Horizontal diffusion is represented with a constant diffusivity κ. A dry static stability is defined

$$N^2 \equiv c_p \Delta T \frac{\Gamma_d}{\Gamma_m} \frac{\partial \ln \theta}{\partial z} \tag{2.13}$$

with Γ_d and Γ_m the dry and moist adiabatic temperature lapse rates, respectively. The surface entropy flux is given by a bulk transfer formula:

$$E = C_k |\mathbf{V}| (s_o^* - s_b) \tag{2.14}$$

where s_o^* is the saturation moist entropy at the temperature of the sea surface. Here $|\mathbf{V}|$ is given by (2.6) as for the primitive equation model, although the surface gustiness is increased to 6 m s^{-1} to suppress what seem to be meridionally propagating WISHE modes that are more intense in this model than in the moist GCM. Again, these transients may be relevant to actual monsoon circulations, and we hope to examine their interaction with the seasonal cycle in future work.

Subcloud-layer equilibrium is used to specify an equilibrium cloud-base mass flux:

$$M_{eq} = w + \frac{1}{\chi} \left[E + H_b \left(\kappa \frac{\partial^2 s_b}{\partial y^2} - v \frac{\partial s_b}{\partial y} \right) \right] \tag{2.15}$$

The actual convective mass flux is relaxed toward this equilibrium value over a time scale of 6 hours, and is constrained to be nonnegative. We also set $M = 0$ if $s_b < s^*$, so that there is no convection where the atmosphere is stable.

Modal decomposition

The horizontal wind is projected onto a barotropic mode $\mathbf{v}_0$, and a baroclinic mode $\mathbf{v}_1$ that uses temperature as a vertical coordinate:

$$\mathbf{v} \equiv \mathbf{v_0} + T' \mathbf{v_1} \tag{2.16}$$

where T' is the temperature anomaly normalized by $\Delta T \equiv T_s - \overline{T}$:

$$T' \equiv \frac{T - \overline{T}}{\Delta T} \tag{2.17}$$

The axisymmetric continuity equation

$$\frac{\partial w}{\partial z} + \frac{\partial v}{\partial y} = 0 \tag{2.18}$$

combined with the assumptions of no topography and constant surface pressure gives a nondivergent barotropic wind. Under the constraint that v vanishes at the meridional boundaries, the barotropic wind must be purely zonal so that $v \equiv T' v_1$. The horizontal wind is thus completely specified by u_0, u_1, and v_1, which depend on y and time only. No dynamical boundary layer is used in the momentum equations, and u_1 and v_1 can be taken to represent baroclinic winds at the surface.

With these assumptions, the vertical velocity must have a vertical structure independent of latitude and time:

$$w(y,z,t) \equiv \overline{w}(y,t)\Omega(z) \tag{2.19}$$

with the vertical structure obtained from the temperature profile:

$$\Omega(z) = \int_0^z T' dz \tag{2.20}$$

In the axisymmetric two-mode framework, continuity is then:

$$\overline{w} = -\frac{\partial v_1}{\partial y} \tag{2.21}$$

Prognostic equations for u_1 and v_1 are obtained by substituting (2.16) into (2.11), multiplying by T', and integrating from the surface to the tropopause:

$$\frac{\partial u_1}{\partial t} + v_1 \frac{\partial u_0}{\partial y} + \frac{\langle T'^3 \rangle}{\langle T'^2 \rangle} v_1 \frac{\partial u_1}{\partial y} - \frac{\langle \Omega T' \partial_p T' \rangle}{\langle T'^2 \rangle} \frac{\partial v_1}{\partial y} u_1 = \beta y v_1 - \frac{1}{\langle T'^2 \rangle} \left[\frac{C_D}{H} |\mathbf{V}| (u_0 + u_1) \right] + \kappa \frac{\partial^2 u_1}{\partial y^2} \tag{2.22}$$

$$\frac{\partial v_1}{\partial t} + \frac{\langle T'^3 \rangle}{\langle T'^2 \rangle} v_1 \frac{\partial v_1}{\partial y} - \frac{\langle \Omega T' \partial_p T' \rangle}{\langle T'^2 \rangle} \frac{\partial v_1}{\partial y} v_1 = \Delta T \frac{\partial s^*}{\partial y} - \beta y u_1 - \frac{1}{\langle T^2 \rangle} \left[\frac{C_D}{H} |\mathbf{V}| v_1 \right] + \kappa \frac{\partial^2 v_1}{\partial y^2}$$

where triangle brackets represent mass-weighted vertical integrals, which are represented in pressure coordinates for simplicity. Quantities on the left hand side are the time tendency and advective terms. Quantities on the right hand side are the Coriolis, drag, and horizontal diffusion terms, with the v_1 equation also containing a pressure gradient forcing phrased

in terms of s^*. Horizontal diffusion is used to represent some effects of eddies and to numerically stabilize the model. Vertical diffusion is neglected. The drag terms have been written using the same bulk flux formula for momentum as in the primitive equation model. The depth of the troposphere, H, is assumed constant.

A prognostic equation for the barotropic wind is calculated by integrating the zonal momentum equation in (2.11) in the vertical and taking the curl, to give a barotropic vorticity equation:

$$\frac{\partial \zeta_0}{\partial t} - \left\langle T'^2 \right\rangle \frac{\partial^2}{\partial y^2}(v_1 u_1) = \frac{\partial}{\partial y}\left[\frac{C_D}{H}|\mathbf{V}|(u_0 + u_1)\right] + \kappa \frac{\partial^2 \zeta_0}{\partial y^2} \tag{2.23}$$

The left hand side contains the time tendency term and the advective terms written in flux form. The right hand side contains the drag and horizontal diffusion terms, which use the same coefficients C_D and κ as for the baroclinic modes. The barotropic wind u_0 is obtained by inverting ζ_0.

The conservation equation for s^*, given in (2.12), must also be vertically integrated to eliminate the height-dependence of w and M:

$$\frac{\partial s^*}{\partial t} = -N^2 \langle \Omega \rangle (\overline{w} - \epsilon \overline{M}) - R + \kappa \frac{\partial^2 s^*}{\partial y^2} \tag{2.24}$$

where R is assumed to be a prescribed, vertically uniform constant. This is the fully nonlinear conservation equation for s^*, where the horizontal advection term has been eliminated by the assumption that s^* is constant with height. The conservation equation for s_b does not need to be modified, although care must be taken to use the values of w and M at the top of the subcloud layer and the mean value of v within that layer:

$$\left(H_b \frac{\partial s_b}{\partial t} + v_b \frac{\partial s_b}{\partial y}\right) = E + \mathrm{MIN}(0, (\overline{w} - \overline{M}))\Omega_b \chi + H_b \kappa \frac{\partial^2 s_b}{\partial y^2} \tag{2.25}$$

Here Ω_b denotes the value of Ω, given by (2.20), at the top of the subcloud layer. The mass-weighted meridional wind within the subcloud layer is denoted by v_b. The equilibrium mass flux then becomes:

$$\overline{M}_{eq} = \overline{w} + \frac{1}{\chi \Omega_b}\left[E + \left(H_b \kappa \frac{\partial^2 s_b}{\partial y^2} - v_1 \frac{\partial s_b}{\partial y}\Omega_b\right)\right] \tag{2.26}$$

Table 2.1: Parameters used in the two-mode model.

Parameter name	symbol	Value
Surface minus mean atmospheric temperature	ΔT	31 K
Mean boundary layer depth	H_b	450 m
Mean tropopause height	H	14 km
Dry static stability	N^2	0.8 J kg^{-1} m^{-1}
Normalized second moment of temperature	$\langle T'^2 \rangle$	0.64
Normalized third moment of temperature	$\langle T'^3 \rangle$	-0.47
Correlation function for vertical advection	$\langle \Omega T' \partial_p T' \rangle$	-0.23
Vertical mean structure function	$\langle \Omega \rangle$	1.9×10^4
Structure function at top of subcloud layer	Ω_b	420 m
Mean subcloud layer meridional wind	v_b	0.95 v_1
Horizontal diffusivity	κ	2.0×10^5 m^2 s^{-1}
Surface transfer coefficient for momentum	C_D	0.0012
Enthalpy exchange coefficient	C_k	0.0012
Surface gustiness	v_g	6.0 m s^{-1}
Radiative cooling rate	R	1 K day^{-1}
Bulk precipitation efficiency	ϵ	0.9
Entropy drop at top of subcloud layer	$\theta_{eb} - \theta_m$	5 K
Gradient of Coriolis parameter	β	2.28×10^{-11} m^{-1} s^{-1}
Specific heat of air at constant pressure	c_p	1010 J kg^{-1} K^{-1}
Convective response time	τ_c	6 hours

with $\overline{M}$ relaxed toward $\overline{M}_{eq}$ over a 6 hour time scale.

The model consists of (2.13), (2.14),(2.17), and (2.21) - (2.26), which include the time tendency equations for the prognostic variables s^*, s_b, u_1, v_1, and ζ_0. The parameters dependent on temperature were derived assuming a surface temperature of 296 K at 1000 hPa, a dry adiabat up to 950 hPa, and a moist pseudoadiabat from 950 hPa to 150 hPa. The values used for model parameters are listed in Table 2.1.

This model employs many simplifications even when compared to other reduced models of the tropical atmosphere, and because of this cannot represent a number of processes, including wave radiation into the stratosphere (Yano and Emanuel, 1991), dynamical boundary layer effects (Sobel and Neelin, 2006), moisture-radiation feedbacks, and some eddy transports. We do find, however, that it can represent the fundamental physics of the WISHE-induced abrupt seasonal transition found in the moist GCM.

2.3.2 Linear properties

The above system includes nonlinear advection terms which, because of the GCM results, we expect to be required for a WISHE feedback. It is of interest that Emanuel (1993) found purely baroclinic zonally symmetric circulations to be unstable to WISHE in a linearized version of the above system that employed no SST gradient and a basic state with easterly surface winds. While a basic state having a poleward SST gradient and westerly surface winds would be more relevant to the onset of the solsticial Hadley circulation, we discuss in the next section how the presence of a coupled barotropic circulation can stabilize WISHE modes in a linear system. Indeed, the Hadley circulation cannot be represented in terms of a purely baroclinic mode; a barotropic mode must be added to obtain zonal winds that are simultaneously strong at upper levels and weak at the surface, as discussed in detail by Burns et al. (2006). For this reason, a linear stability analysis of a purely baroclinic system is not presented here.

However, some insight can still be gained by examining such a highly simplified, purely baroclinic system with dynamics linearized about a resting state. We neglect horizontal diffusion, and represent surface drag as Rayleigh damping over a time scale $1/r$. For simplicity, we assume radiative cooling operates on the same time scale as this mechanical damping, so that R in (2.12) can be written as rs^*. We set the precipitation efficiency ϵ equal to unity, which corresponds to an atmosphere in which evaporatively-driven downdrafts do not occur and free-tropospheric temperatures are controlled by boundary layer processes (Emanuel, 1993). The system consisting of (2.11) and (2.12) can then be rewritten, assuming modal perturbations in u, v and s^* proportional to $e^{-i\omega t}$:

$$(r - i\omega)u = fv \tag{2.27}$$

$$(r - i\omega)v = (T - \overline{T})\frac{\partial s^*}{\partial y} - fu \tag{2.28}$$

$$(r - i\omega)s^* = \frac{N^2(T - \overline{T})}{\chi}E \tag{2.29}$$

These can be combined into a single expression:

$$v = \left(\frac{1}{(r - i\omega)^2 + f^2}\right)\frac{N^2(T - \overline{T})}{\chi}\frac{\partial E}{\partial y} \tag{2.30}$$

If the time scale of the damping is short compared to that of the forcing (i.e. $r \gg \omega$), then

the real part of (2.30) is well approximated by:

$$v \simeq \left(\frac{1}{r^2+f^2}\right)\frac{N^2(T-\overline{T})}{\chi}\frac{\partial E}{\partial y} \tag{2.31}$$

which is the same as the solution for the steady response to a time-invariant forcing. For ω corresponding to Earth's seasonal cycle of insolation, this limit will hold if viscous losses are dominated by the strong vertical mixing of momentum in the planetary boundary layer, so that $1/r$ is on the order of a few days. This result then shows that the meridional gradient of the surface entropy flux is the relevant forcing for meridional flow, and that the flow will be nearly in phase with this forcing. If the circulation is instead controlled by nearly-inviscid free-tropospheric dynamics, then such a linear axisymmetric treatment will not provide an appropriate description.

2.3.3 Numerical results

The fully nonlinear two-mode model is forced by the same time-varying SST used for the GCM, consisting of (2.3) and (2.7) with $\theta_m = 1.0$ K. The same set of integrations was performed as for the GCM: runs with and without WISHE, and with and without nonlinear momentum advection. The results exhibit phase space trajectories remarkably similar to those from the GCM, with an abrupt, high amplitude intensification of the summer circulation occurring only when both WISHE and nonlinear momentum advection are used (Fig. 2-10). This intensification in the two-mode model was even more abrupt than in the GCM, with the phase trajectory becoming near vertical when the SST reached its peak. Although no explicit dynamical boundary layer exists in the two-mode model, the PBL flow displayed in this phase trajectory was computed by integrating meridional flow through the lowest 200 hPa of the atmosphere, to ease comparison with the GCM results.

In the no-WISHE integrations of the two-mode model, the boundary layer flow peaked at least one-quarter cycle before the SST. This would seem to occur because of the relatively short phase lag between SST and subcloud layer entropy. The surface entropy flux relaxes the entropy of the boundary layer toward that of the sea surface over the time scale τ_E:

$$\frac{E}{H_b} = \frac{1}{\tau_E}(s_o^* - s_b) \tag{2.32}$$

with $\tau_E \equiv H_b/(C_k|\mathbf{V}|)$. For typical values of these parameters, τ_E is on the order of 10

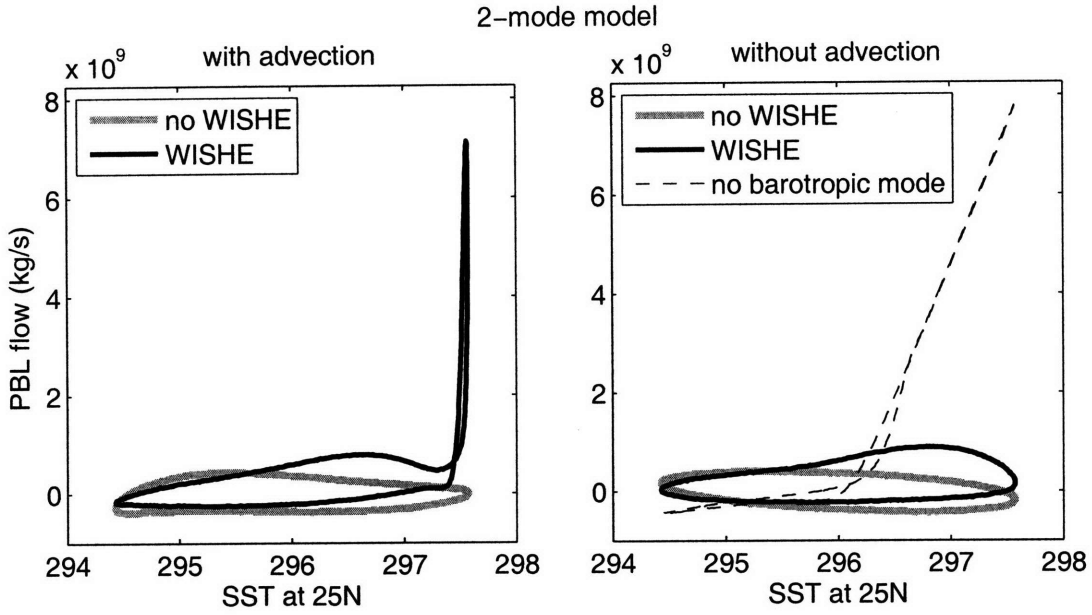

Figure 2-10: As in Fig. 2-8 but for the two-mode model. The dashed line in the right panel is for a run with no barotropic wind and no nonlinear momentum advection, but with WISHE.

days, so that the phase lag between s_b and s_o^* is expected to be small compared to the 365-day period of s_o^*. Thus, the relation of E to the prescribed s_o^* is analogous to the relation of Newtonian cooling to the prescribed equilibrium temperature in the dry model. By the same trigonometric relationships used for the dry model to derive (2.4), E should then lead s_o^* by slightly less than one-quarter cycle, and the meridional circulation should be in phase with E. In such a simple linear theory, the major axis of the phase space ellipse should be horizontal, as it nearly is for the two-mode model without WISHE. This contrasts with the GCM results where the major axis has a positive slope. In any case, the main differences between the two-mode model and the GCM seem to result from phase lags in a predominantly linear response, with both showing an abrupt intensification of solsticial flow due to the interaction of WISHE and nonlinear momentum advection.

2.4 Physics of the WISHE feedback

This section explains how the combination of WISHE and nonlinear momentum advection produces an abrupt intensification of the summer circulation in both the GCM and the

two-mode model.

In the GCM run using both WISHE and nonlinear momentum advection, the surface enthalpy flux peaks about 8° south of the SST maximum, and the enthalpy flux peak is meridionally sharper than the SST peak (Fig. 2-11, left panel). Given that the meridional gradient of the surface enthalpy flux is the relevant forcing in a linear regime, it seems natural to ask how linear the atmospheric response is when viewed as a function of this quantity[2]. We compute the mean value of $\partial_y E$ between 10°N and the latitude at which E peaks, and plot this quantity as a function of the SST at 25°Nfor the GCM runs with momentum advection and $\theta_m = 1.0$ K (Fig. 2-12). The resulting phase trajectories closely resembles the corresponding trajectories for meridional PBL flow in the moist GCM. Thus, the meridional circulation does not seem to be far from a linear response to $\partial_y E$, even though nonlinear dynamics are needed to achieve the positive feedback. This is an important point, because WISHE could be viewed simply as a way to reduce the critical SST gradient needed to obtain a nonlinear intensification from M advection, so that the same physics explored by PH92 and Zheng (1998) would apply at a lower SST threshold. The near linear relationship between $\partial_y E$ and PBL flow is one piece of evidence that WISHE actually provides a separate mechanism for a nonlinear response of the PBL flow to the SST. Another piece of evidence is the small deformation of M contours in the GCM run with WISHE; in this run the $\eta = 0$ contour is displaced 8° off the equator at the tropopause, compared to a 5° displacement for the near-linear initial transient peak of the dry model with $\theta_m = 15$ K and a 20° displacement for this dry model in its equilibrated nonlinear state. The transition to an AMC regime for models integrated with WISHE will be shown in the next chapter.

If the net meridional mass flux exhibits a near-linear response to the surface enthalpy flux, why does WISHE not produce an abrupt onset when momentum advection is omitted from the model? The reason for this was briefly mentioned above in discussion of the linear properties of the two-mode model. Emanuel (1993) showed that zonally symmetric, purely baroclinic circulations can be unstable to WISHE. The Hadley circulation, however, projects strongly onto a barotropic mode, with surface winds that are generally weak compared to upper tropospheric winds. Since WISHE instabilities arise from enthalpy flux anomalies driven by surface winds, a reduction in the magnitude of surface winds by the partial

[2]At the SSTs used here, the enthalpy flux is very close to a constant linear multiple of the entropy flux, so we use the two somewhat interchangeably in this section.

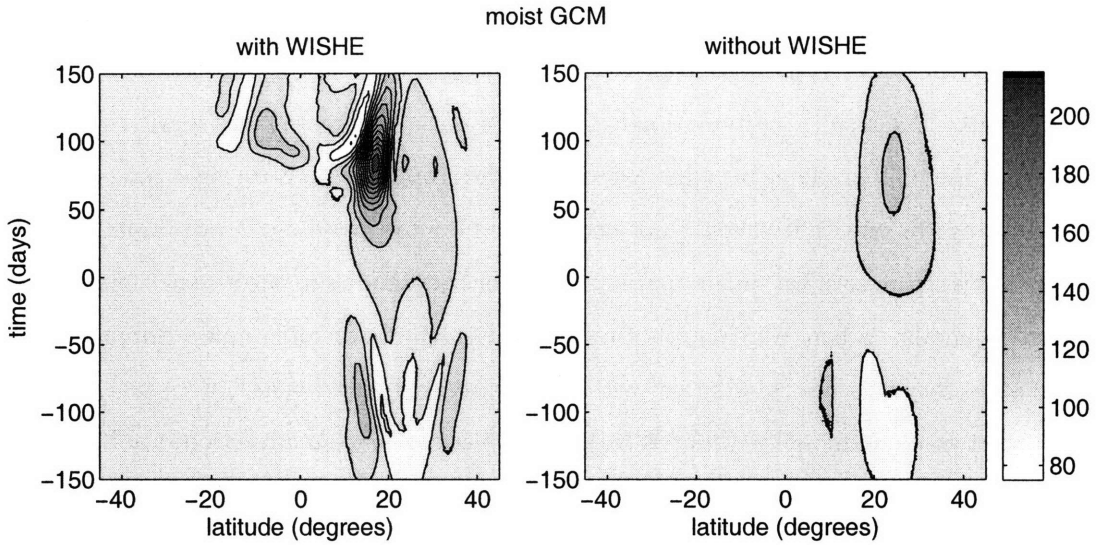

Figure 2-11: Surface enthalpy flux for the moist GCM with weak forcing ($\theta_m = 1.0$ K). Left and right panels are for the runs with and without WISHE, respectively. Time is the number of days after SST has zero gradient, with maximum SST occurring at day 91 and 25°N.

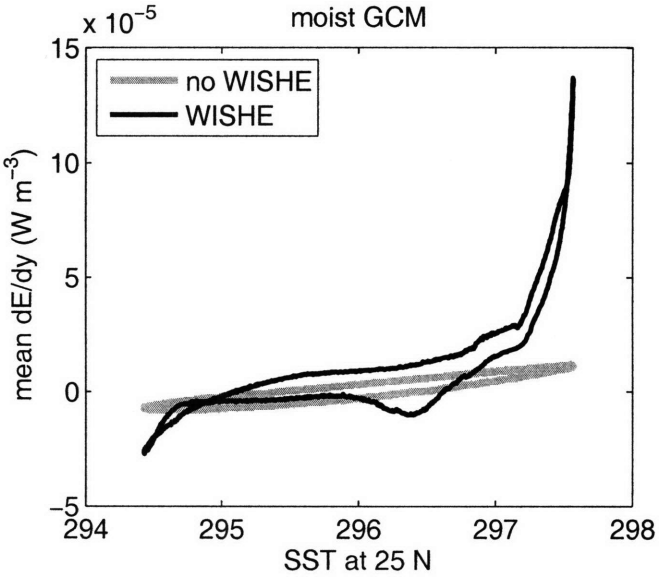

Figure 2-12: Phase diagram, for the moist GCM with weak forcing ($\theta_m = 1.0$ K), of the meridional mean meridional gradient of surface enthalpy fluxes, with the mean taken between the enthalpy flux peak and 10°N, plotted against the SST at 25°N. The black and grey lines are for runs with and without WISHE, respectively, both with nonlinear momentum advection.

cancellation of the baroclinic and barotropic components of zonal wind at the surface would be expected to reduce or even eliminate any instability. This hypothesis was tested by eliminating the barotropic mode from a version of the two-mode model linearized about a resting state. The resulting circulation exhibited an abrupt increase in its sensitivity to SST as soon as the SST gradient became poleward in the tropics (Fig. 2-10, right panel). While such a change in sensitivity should not necessarily be interpreted as an instability, WISHE clearly has a stronger effect on circulations with linear dynamics in the absence of a coupled barotropic mode. When WISHE was turned off with the barotropic mode eliminated, the phase trajectory was nearly elliptical with a much weaker meridional flow (not shown).

In the two-mode model without WISHE but with momentum advection, the barotropic zonal wind does, in general, nearly cancel the low-level baroclinic wind everywhere (Fig. 2-13, right column). In the upper troposphere, the two modes must then add to produce strong easterlies south of the SST maximum during "summer" conditions. In the two-mode model with both WISHE and momentum advection, the barotropic wind opposes the surface baroclinic wind in most places except just south of the SST maximum during peak summer, during the time when the rapid intensification occurs (Fig. 2-13, left column). In this region, the two modes add to produce strong surface westerlies, which are in turn associated with strong surface enthalpy fluxes. The conservation equation for barotropic zonal wind, (2.23), shows that, in a region of baroclinic surface westerlies, the only process that can increase barotropic westerlies is convergence of the meridional flux of zonal momentum.

Similar dynamics seem to occur in the moist GCM. A barotropic wind was defined as the mass-weighted vertical mean of the zonal wind between the surface and the tropopause, with the tropopause defined as the level at which the static stability increased sharply to stratospheric values. Instead of a particular baroclinic mode, we examine the residual obtained by subtracting the barotropic wind from the total zonal wind field. In the run conducted without WISHE but with momentum advection, the barotropic zonal wind and this baroclinic residual nearly cancel at low levels (Fig. 2-14, right column). In the run with both WISHE and momentum advection, the meridional structure of these modes is similar to that seen in the two-mode model: the barotropic wind adds to the baroclinic residual only near the ascent branch of the circulation just south of the SST maximum (Fig. 2-14, left column).

In both the two-mode model and the GCM, then, a positive feedback seems to occur

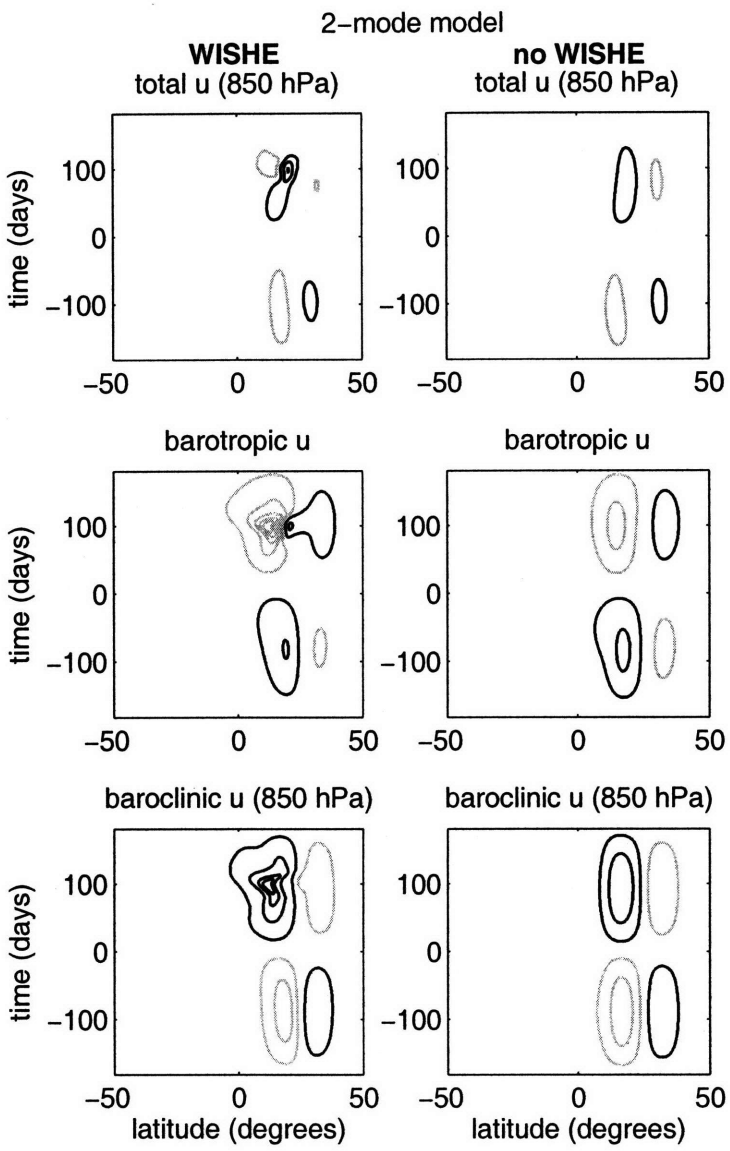

Figure 2-13: Decomposition of the low-level zonal wind in the two-mode model. Left and right columns are for the runs with and without WISHE, respectively. Both of these runs included nonlinear momentum advection. Top row is the total zonal wind at 850 hPa, middle row the barotropic component, and bottom row the baroclinic component at 850 hPa. Black lines denote westerlies and grey lines easterlies, with a contour interval of 5 m s^{-1} starting at 2.5 m s^{-1}. Time is the number of days after the SST has zero gradient, with maximum SST occurring at day 91 and 25°N.

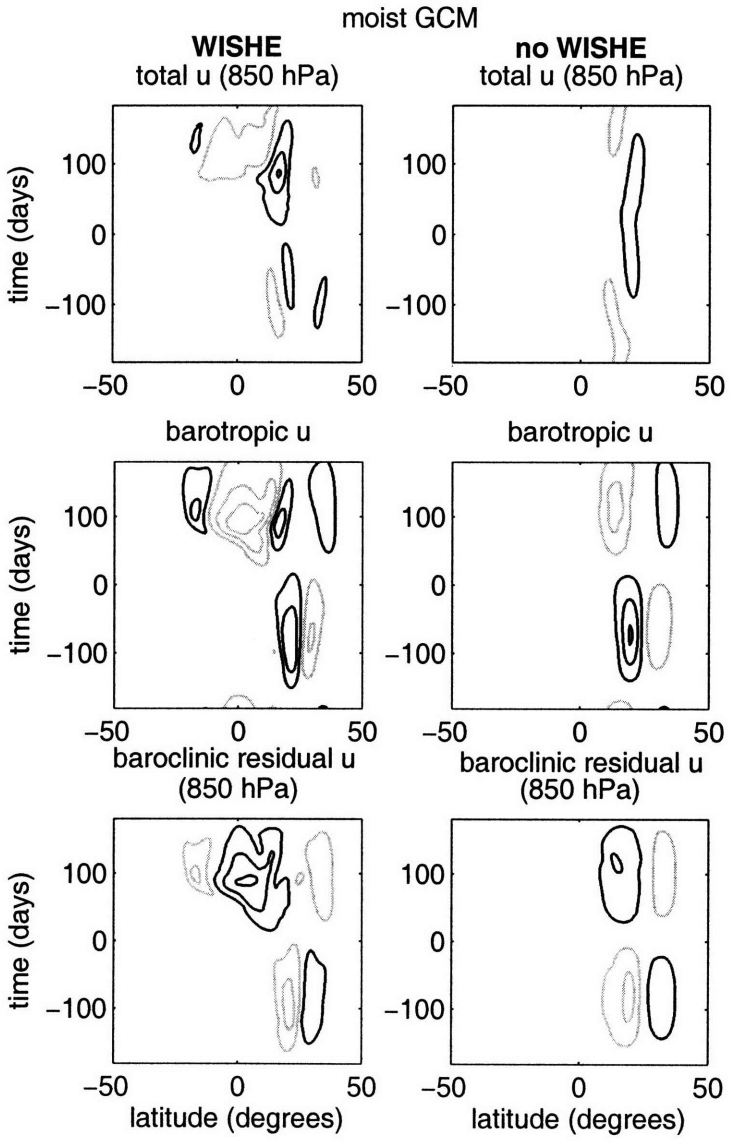

Figure 2-14: As in the previous figure, but for the moist GCM with weak forcing ($\theta_m = 1.0$ K). The barotropic component is a vertical tropospheric mean, and the baroclinic residual was obtained by subtracting this barotropic component from the total zonal wind.

when the convergence of the meridional flux of zonal momentum becomes sufficiently strong to produce a barotropic wind that adds to the surface baroclinic wind instead of opposing it, thereby eliminating the damping effect of the barotropic mode on WISHE. The mean meridional circulation will, in a vertical mean, converge zonal momentum into the ascending branch as long as M contours tilt toward the equator with height. Because such a tilt is brought about by advection in a model that conserves M, convergence of zonal momentum into the ascending branch will, in general, be accomplished by any mean meridional flow as long as this flow is directed poleward at low levels. To create barotropic westerlies, this momentum convergence must overcome surface drag and any other horizontal transports:

$$-\left\langle \frac{\partial(vu)}{\partial y} \right\rangle > -\frac{C_D}{H}|\mathbf{V}|u + F \tag{2.33}$$

Here H is the depth of the troposphere and F represents horizontal transports including diffusion and momentum transports by zonally asymmetric eddies (which do not occur in the models examined in this paper).

In the simplified case where F is zero and surface drag is a linear Rayleigh damping, a scale estimate of the terms in (2.33) provides:

$$\frac{V}{\Delta y} > r \tag{2.34}$$

where V is the velocity scale of the meridional wind, r the damping coefficient, and Δy the meridional scale over which the circulation changes. If V responds linearly to the forcing, as in (2.31), then this amounts to a condition on the curvature of the surface entropy flux.

While this scaling is likely too crude to be quantitatively compared with the numerical model results, it does show that there should be a critical surface entropy flux gradient below which no WISHE feedback will occur. We test for the existence of such a threshold by changing the peak amplitude of the SST forcing in the two-mode model (integrated with both WISHE and nonlinear momentum advection). The case examined thus far with $\theta_m =$ 1.0 K seems to nearly coincide with this threshold. A run using $\theta_m = 0.5$ K had no abrupt intensification, and a run using $\theta_m = 1.5$ K had an abrupt intensification reaching a much higher amplitude (Fig. 2-15). Meridional winds in the $\theta_m = 1.5$ K case peaked near 12 m s^{-1}.

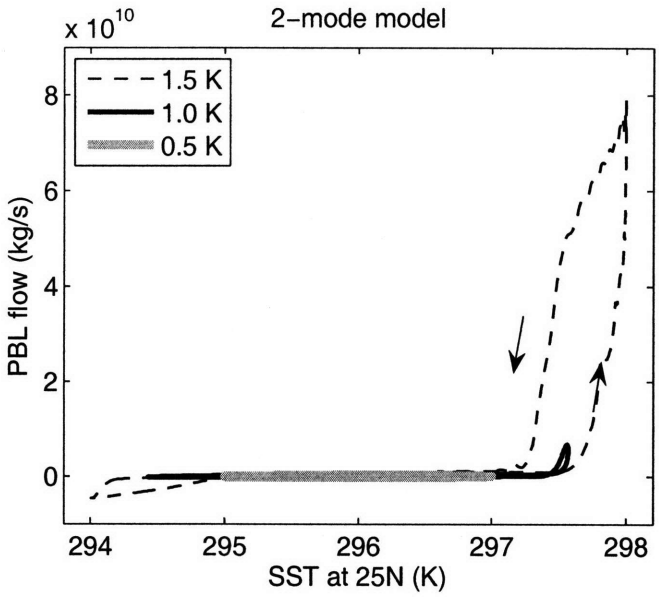

Figure 2-15: As in Fig. 2-8 but for the two-mode model with SST forcings of different strengths. All runs included both WISHE and nonlinear momentum advection. Dashed line is for $\theta_m = 1.5$ K, solid black line for 1.0 K, and solid grey line for 0.5 K. The solid black line is the same trajectory appearing in the left panel of Fig. 2-10.

2.5 Concluding remarks

A seasonal cycle that is long compared to the time scale of meridional M advection should be a necessary, albeit not sufficient, condition for the scalings and thresholds of nonlinear axisymmetric theories (e.g. Held and Hou, 1980; Plumb and Hou, 1992) to apply to an arbitrary planetary atmosphere. We have found that the dry axisymmetric models used by some previous studies (e.g. Fang and Tung, 1999) equilibrate too slowly to be used for study of the time-dependent response to Earth's seasonal insolation forcing, but that moist axisymmetric models equilibrate much faster because of their characteristic stratification and radiative cooling rate. This makes examination of the seasonal cycle in a moist framework, which when properly represented will include effects of WISHE, a logical extension of previous work on nonlinear axisymmetric flow.

This chapter focused on the limiting case of weak SST forcings that do not produce an AMC response. In the axisymmetric models used here, WISHE produced meridional flow that increased nonlinearly as a function of the seasonally-evolving SST gradient, even when the flow was subcritical, in the PH92 sense, to nonlinear intensification by M advection

alone. For Hadley circulations with a strong barotropic component, this WISHE feedback can occur only if the vertically-integrated convergence of zonal momentum into the ascent branch of the circulation is larger than the momentum sink due to surface drag and any other horizontal transports.

Numerous physical processes omitted from the models used here may affect the physics of the WISHE feedback. Using an SST anomaly as a proxy for the thermal forcing of a land surface allows WISHE to operate over the entire domain, whereas the relatively small thermal inertia of a land surface should eliminate WISHE for periods longer than five to ten days. How the WISHE feedback might alter monsoon onset when it operates only over the ocean equatorward of a coast could be easily explored in a variation on the axisymmetric models used here. But the effect of a land surface on WISHE may extend beyond that of its thermal forcing, as topography in the South Asian monsoon is known to strongly organize the flow (e.g. Hoskins and Rodwell, 1995) and increase free tropospheric temperatures (e.g. Molnar and Emanuel, 1999).

The radiative effects of variable clouds and water vapor were also omitted from our models. Ackerman and Cox (1987) estimated horizontal variations in atmospheric radiative flux divergence of about 100 W m^{-2} between clear and cloudy oceanic regions in the 1979 Asian summer monsoon, which is similar to the magnitude of wind-induced surface enthalpy flux variations in our models. Bony and Emanuel (2005) found that moisture-radiation feedbacks can have a scale-selecting effect on WISHE modes and also excite additional small-scale instabilities. Both of these results suggest that the role of moisture-radiation feedbacks in monsoon onset merit further study.

SST in our models was treated as a prescribed forcing, and it is known that surface winds alter SST by driving surface evaporation, horizontal dynamical transports, and the entrainment of thermocline water into the ocean mixed layer. While a common practice in idealized models is to treat the ocean as a dynamically passive bulk mixed layer, it is not obvious that these processes are more important than dynamical ocean transports in monsoon regions. Indeed, Webster and Fasullo (2003) proposed that the seasonally-reversing, cross-equatorial heat flux in the Indian Ocean regulates the strength of the South Asian monsoon. While they focused on interannual variability, dynamical ocean transports might play a role in modulating any abrupt seasonal transitions.

We noted in the introduction that eddy momentum transports may play a role in mon-

soon onset. Eddy transports might even play a direct role in the WISHE feedback because this feedback requires the convergence of zonal momentum to overcome the damping effects of the barotropic wind. However, in the dry model used by Schneider and Bordoni (2007, in press), the ascending branch of the cross-equatorial cell was associated almost entirely with momentum transports by the mean meridional circulation, with eddies extracting zonal momentum primarily from the subsiding branch of the Hadley circulation and depositing it in higher latitudes of the winter hemisphere. There would thus be no *a priori* reason to believe that eddy momentum transports would oppose the momentum convergence required for the WISHE feedback.

Finally, the physics of WISHE may change profoundly with both the structure of the forcing and the breaking of axisymmetry. Prive and Plumb (2007) illustrated the large effect zonal asymmetries in a forcing can have on the dynamical atmospheric response. Yet even with a zonally symmetric forcing, Emanuel (1993) showed that growth rates for WISHE modes peak at a nonzero zonal wavenumber, which suggests that WISHE feedbacks in three dimensions might possess a different sensitivity to SST gradients than in axisymmetric models. Thus, to apply the ideas in this chapter to actual monsoon circulations, it will eventually be necessary to understand the behavior of WISHE modes in a three-dimensional domain with ocean, land and radiative interactions. This issue will be taken up, at least indirectly, in a later chapter by examining the role of WISHE in a three-dimensional GCM with realistic topography and SST.

Chapter 3

Wind-evaporation feedback and the axisymmetric transition to angular momentum conserving flow

Abstract

The effect of wind-induced surface heat exchange (WISHE) on axisymmetric Hadley circulations is examined for forcings strong enough to produce angular momentum conserving meridional flow. Such forcings are known to produce a narrow, off-equatorial ascent zone in the summer hemisphere where the convergence of zonal momentum is balanced by drag on surface westerlies. A quasi-equilibrium model with two vertical modes is used here to show that surface entropy fluxes induced by these surface westerlies can narrow and intensify the ascent zone, and shift both it and the peak subcloud layer entropy toward the equator. This equatorward shift of the entropy peak is associated with a reduction in the forcing amplitude needed to produce angular momentum conserving meridional flow. A previous theory of frontogenesis in tropical cyclones is adapted to axisymmetric Hadley circulations to show that WISHE shifts the peak subcloud layer entropy toward the equator by exerting a frontogenetic tendency on the zonal wind field.

These effects also occur for forcings that vary in a seasonal cycle, with the precise effect of WISHE depending on the peak amplitude of the forcing. For weak seasonally-varying forcings, WISHE can increase the intensity of a local, viscous circulation, while for moderate forcings WISHE produces a transition to angular momentum conserving flow when such a transition would not otherwise occur. For the strongest forcings, WISHE shifts the transition to angular momentum conserving flow to a time earlier in the seasonal cycle. The possible relevance of these results to the seasonal cycle of monsoons is discussed.

3.1 Introduction

The previous chapter showed that a wind-evaporation feedback in axisymmetric models can produce seasonal transitions of the Hadley circulation that are rapid compared to the time evolution of an imposed sea surface temperature (SST) forcing. Study of this feedback was limited to weak SST gradients in order to demonstrate that the abrupt onset due to WISHE can be fundamentally different from an abrupt onset due to the transition to an angular momentum conserving (AMC) circulation. However, thermal forcings on Earth may be stronger than the weak forcings examined in the previous chapter, and it is entirely possible that WISHE may operate together with the transition to an AMC regime in the onset of actual monsoon circulations.

This chapter examines how WISHE alters the dynamics of Hadley circulations driven by forcings sufficiently strong to produce an AMC response. The two-mode model described in the previous chapter is used for this task, both to reduce the computational burden of this exploration of parameter space and to allow for a simpler interpretation of results than would be possible with a primitive equation model. Fortunately, previous authors have already shown that two-mode models faithfully represent important aspects of Hadley circulations dynamics, producing states with weak surface winds, strong upper-level winds, and approximate conservation of absolute angular momentum in the upper troposphere (Burns et al., 2006; Sobel and Neelin, 2006).

The next section briefly reviews the numerical model and discusses some details of momentum conservation in this model. The following section presents the results of a series of integrations using SST forcings of various strengths localized off the equator. One finding from these runs is that WISHE narrows the off-equatorial convergence zone and shifts it toward the equator. The physical mechanism responsible for this effect is discussed. Results for SST forcings with a nonzero cross-equatorial gradient are then presented, to show that these effects of WISHE can operate even when some part of the forcing is always supercritical to AMC flow. The chapter closes with a brief summary and some remarks on the potential relevance of these results to observed monsoons.

3.2 Model details

We employ the same two-mode model used in the previous chapter, but here focus more on the meridional structure of the response and the interaction of WISHE with AMC dynamics. The model is similar to the Quasi-equilibrium Tropical Circulation Model (QTCM) of Neelin and Zeng (2000) in that the momentum equations are projected onto a barotropic and first baroclinic mode. Instead of temperature and humidity, however, the thermodynamics are phrased in terms of the boundary layer moist entropy, s_b, and the saturation moist entropy of the free troposphere, s^*. Convection is assumed to hold changes in s^* constant with height, and convective mass fluxes are obtained by a sub-cloud layer quasi-equilibrium closure (Raymond, 1995). In this framework, we must make some assumption about the entropy just above the subcloud layer, s_m, which we choose to differ from s_b by the constant amount χ. Detailed model equations are contained in the previous chapter.

The lower boundary of the model is entirely oceanic with prescribed SST. To represent, in an idealized manner, the thermal forcing associated with the South Asian land mass, we use the same SST profile employed in the previous chapter, which is similar in meridional structure to the thermal forcing of Plumb and Hou (1992). Between $\phi_0 - \Delta\phi$ and $\phi_0 + \Delta\phi$, the SST is given by:

$$T_{PH} = T_0 + \theta_{PH} \cos^2\left(\frac{\pi}{2}\frac{\phi - \phi_0}{\Delta\phi}\right) \tag{3.1}$$

Outside this range, T_{PH} is set to the constant T_0. This provides a meridionally-confined SST anomaly centered at ϕ_0. To represent SST in the Indian Ocean we use a distribution similar in meridional structure to the thermal forcing of Lindzen and Hou (1988):

$$T_{LH} = T_1 - \theta_{LH}(\sin\phi - \sin\phi_1)^2 \tag{3.2}$$

This provides an SST that peaks at ϕ_1 and has a curvature that is nonzero everywhere except at ϕ_1.

We will first examine the model response to T_{PH}, then to T_{LH}, and finally to a combination of the two obtained by the sum:

$$T_C = T_{PH} + T_{LH} - T_0 \tag{3.3}$$

This combined forcing is meant to represent thermal effects of both the South Asian land

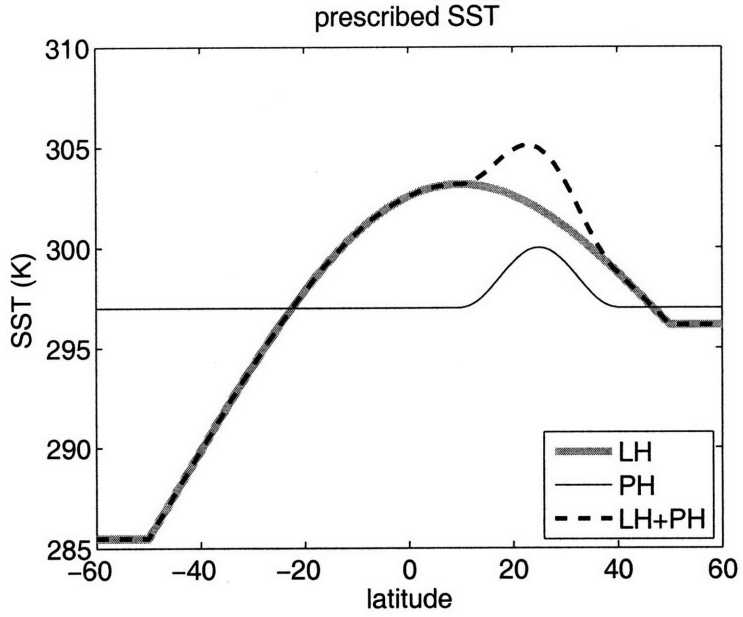

Figure 3-1: Sea surface temperatures used as forcings for the two-mode models. The solid black line shows T_{PH}, a subtropical SST anomaly with a peak amplitude of 3 K, and the grey line shows T_{LH}, an SST distribution peaking at 10°N with nonzero curvature and gradient on the equator. The dashed line shows T_C, a combination of the two aforementioned SST profiles.

mass and Indian Ocean SST. These forcings are illustrated in Fig. 3-1 for $T_0 = 297$ K, $\theta_{PH} = 3$ K, $\phi_0 = 25°$N, $\Delta\phi = 15°$, $T_1 = 303.15$ K, $\theta_{LH} = 20$ K, and $\phi_1 = 10°$N.

For most integrations presented here, a surface gustiness of $v_g = 6$ m s^{-1} is used in the bulk surface flux formula for entropy:

$$\begin{aligned} E &= \rho C_k |\mathbf{V}|(s_o^* - s_b) \\ \mathbf{V} &= \sqrt{u^2 + v^2 + v_g^2} \end{aligned} \tag{3.4}$$

where s_o^* is the saturation entropy corresponding to the prescribed SST. The results are highly sensitive to v_g, as might be expected for solutions in which WISHE plays a major role. The particular value of $v_g = 6$ m s^{-1} was chosen mainly because it is near the smallest value for which solutions without intraseasonal transients were obtained. As discussed in the previous chapter, solutions which contain such transients may be relevant to observed monsoon behavior, but examination of the steady solutions is undertaken as a first step.

Except for the runs with seasonally varying forcings, all model results presented here are

diagnostics taken after the model reached a steady state, which typically happened within 50 days of simulated time.

3.2.1 Angular momentum conservation

A major focus of this chapter is how the dynamics of AMC circulations interact with WISHE. The conserved quantity

$$m \equiv u - \beta y^2/2 \tag{3.5}$$

is the analogue of absolute angular momentum on an axisymmetric β-plane, and hereafter we use absolute angular momentum synonymously with m. Burns et al. (2006) showed that two-mode models approximately conserve m only at one particular level near the tropopause. Following their analysis, an expression for m conservation in two-mode models can be obtained by combining the barotropic and baroclinic zonal momentum equations to eliminate the quantity $u_1 \partial_y v_1$, giving:

$$v_1 \left[\frac{\partial}{\partial y}(u_0 + A u_1) - \beta y \right] = -B \frac{C_D |\mathbf{V}|}{H}(u_0 + u_1) \tag{3.6}$$

where the constants A and B are:

$$A = \frac{\langle T'^3 \rangle}{\langle T'^2 \rangle} + \frac{\langle \Omega T' \partial_p T' \rangle}{\langle T'^2 \rangle} \tag{3.7}$$

$$B = \frac{\langle \Omega T' \partial_p T' \rangle}{\langle T'^2 \rangle^2} + \frac{1}{\langle T'^2 \rangle} \tag{3.8}$$

Burns et al. (2006) derived asymptotic solutions to the two-mode QTCM of Neelin and Zeng (2000) in terms of a small parameter that is the ratio of the meridional advective terms to surface drag terms in the momentum equations. To first order in this parameter, they showed that m conservation holds only at one particular level near the tropopause, and that the surface drag that would violate angular momentum conservation has a magnitude one order smaller. That is, to first order, the right hand side of (3.6) is zero. Then in the presence of nonzero meridional flow, the absolute vorticity will vanish to first order only at the particular level where:

$$\frac{T - \overline{T}}{\Delta T} = A \tag{3.9}$$

This is 263 hPa for the parameters used in our two-mode model, 113 hPa below the specified tropopause. In the diagnostics presented below, the degree of angular momentum conservation is therefore assessed using the absolute vorticity, η, at 263 hPa.

3.3 Results for subtropical forcing

The first two parts of this section present the model response to steady forcings in order to more easily examine the meridional structure of the solutions. Results for forcings of four different magnitudes are presented, with θ_{PH} in (3.1) set to 1 K, 2 K, 3 K, and 7 K. The last part of this section examines the effect of WISHE on the time-dependent response to a seasonally varying version of the forcing with $\theta_{PH} = 7$ K.

3.3.1 Steady forcing without WISHE

The model is first integrated with $|\mathbf{V}|$ in the bulk surface flux formula (3.4) set to a constant value of 10 m s^{-1} everywhere. The value of 10 m s^{-1} for $|\mathbf{V}|$ was chosen, somewhat arbitrarily, to provide a value that exceeded the specified surface gustiness of 6 m s^{-1}. Zheng (1998) used a value of 5 m s^{-1} for $|\mathbf{V}|$; our use of a different value emphasizes that in a quasi-equilibrium framework it is the surface entropy flux, rather than the SST, that determines whether the circulation will achieve an AMC response.

For the three runs with θ_{PH} set to 1 K, 2 K, and 3 K, the meridional circulation is almost entirely confined to the summer hemisphere, and the strength of this circulation increases with the magnitude of the forcing (Fig. 3-2, top three rows). Absolute angular momentum is not homogenized meridionally at upper levels, as indicated by the nonzero values of η. The entire domain is convecting for forcing amplitudes of 1 K and 2 K, while for the 3 K forcing $s^* > s_b$ in much of the subsiding region, indicating that deep convection is suppressed there.

In contrast, for the run with $\theta_{PH} = 7$ K, a strong meridional circulation extends from about 40°S to 25°N, with upper-level m homogenized within 20° of the equator (Fig. 3-2, bottom row). Deep convection is suppressed in the subsiding branch of the circulation. The meridional structure of the circulation is generally consistent with previous theories of solsticial axisymmetric AMC circulations (e.g. Lindzen and Hou, 1988; Plumb and Hou, 1992), and here we discuss a few relevant features. Near the tropopause, the zonal wind

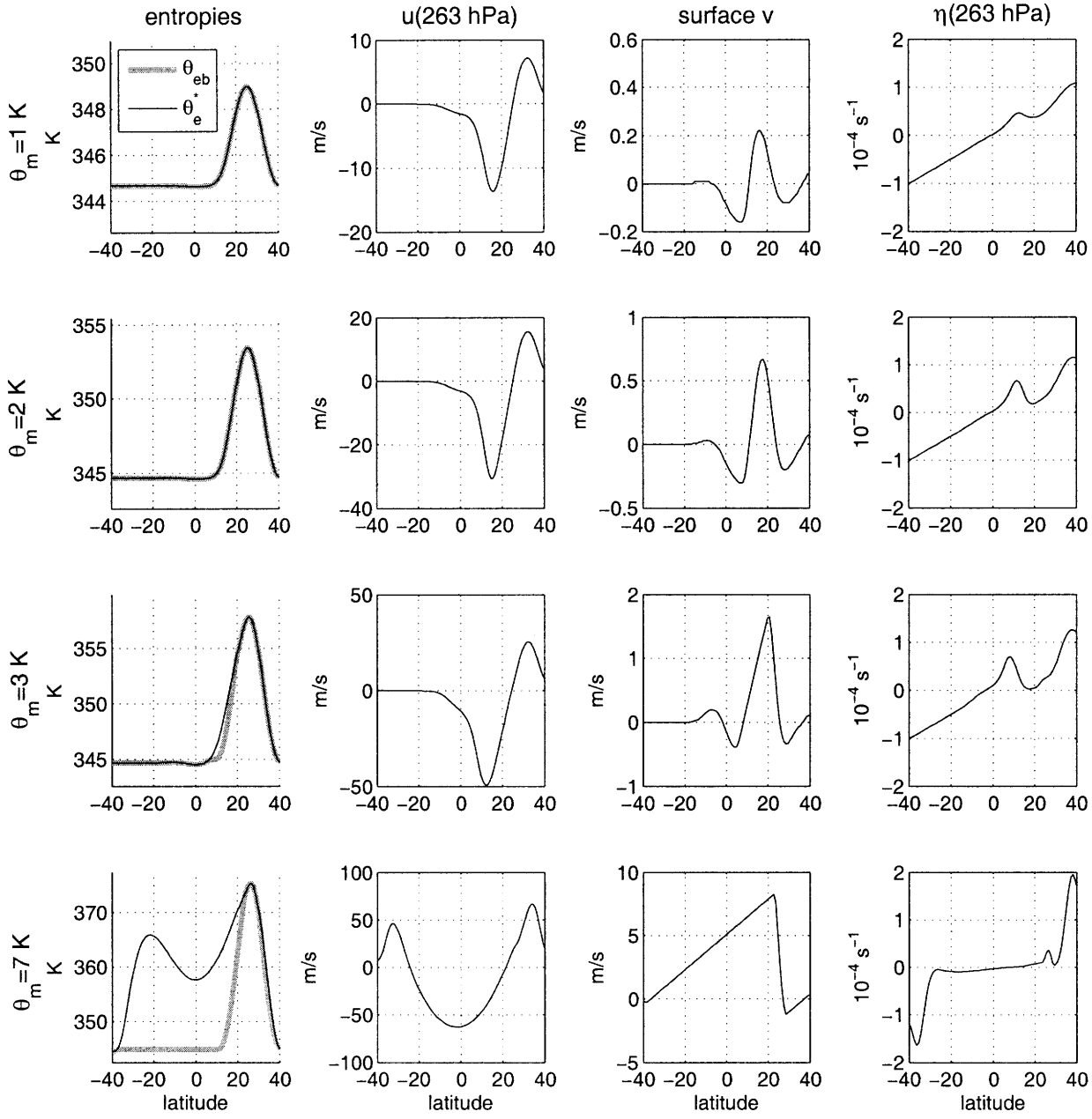

Figure 3-2: State of the equilibrated response of the two-mode model, with wind-independent surface entropy fluxes (no WISHE), to forcings of four different amplitudes. Each row shows the response to a given forcing, with the amplitude of θ_{PH} in (3.1) displayed on the left. The first column shows the subcloud layer equivalent potential temperature (thick grey line) and the saturation equivalent potential temperature of the free troposphere (thin black line). Second column shows the total zonal wind at 263 hPa (the level at which m is approximately conserved), the third shows the surface meridional wind, and the fourth shows the absolute vorticity at 263 hPa.

is constrained by m conservation to vary quadratically with latitude, which is roughly the structure seen in the model results. The s^* distribution has the equatorial minimum and subtropical maxima characteristic of m conservation. Where convection is suppressed, free-tropospheric temperatures are maintained by a balance between subsidence warming and radiative cooling, which when combined with the axisymmetric continuity equation shows that v must increase linearly with latitude:

$$\frac{\partial v}{\partial y} = \frac{R}{N^2 H_b} \tag{3.10}$$

For the parameters of the two-mode model, which include a constant radiative cooling of $R = 1$ K day^{-1}, this produces a surface wind v_1 that increases by about 5 m s^{-1} for every 40 degrees of latitude, consistent with what is seen in the convectively stable region. This results in peak meridional winds several times larger than the observed peak zonal mean meridional wind during boreal summer (e.g. Peixoto and Oort, 1992), but this does not necessarily indicate a deficiency in the numerical model. The wind profile is at least roughly consistent with the axisymmetric GCM used in the previous chapter, in which peak meridional winds of 8 m s^{-1} were obtained for the steady forcing with $\theta_m = 15$ K (not shown). Such SST forcings may simply be considerably stronger than the relevant thermal forcings achieved on Earth. As discussed in the previous chapter, it is difficult to directly compare the SST forcing imposed in an aquaplanet model with the combined ocean and land surface thermal forcing found in observed monsoon circulations.

3.3.2 Steady forcing with WISHE

Now we examine the model response when surface entropy fluxes are allowed to depend on wind speed according to (3.4). A series of integrations is presented with the same forcings used in the runs without WISHE, with θ_{PH} set to 1 K, 2 K, 3 K, and 7 K. The response to the first three of these forcings was examined in a seasonally-varying configuration in the previous chapter. For each of these three forcings, the meridional structure of the peak solsticial response to the seasonally-varying forcing (not shown) is quite similar to that of the equilibrated response to the steady forcing of the same amplitude. The response to the transient forcing did, however, peak at a slightly higher amplitude than the equilibrated response to the corresponding steady forcing. Nevertheless, it seems reasonable to use

the equilibrated response to the steady forcings to characterize the meridional structure of solutions and to determine how WISHE might interact with the constraints of angular momentum conservation.

The response to the weakest two forcings, with amplitudes of 1 K and 2 K, is a viscously-dominated circulation localized in the summer hemisphere with little meridional homogenization of m (Fig. 3-3, top two rows). Comparing the response to that for the runs without WISHE (top two rows of Fig. 3-2) shows that WISHE increases the strength of the circulation for a given value of θ_{PH} for these relatively weak forcings, and that the fractional increase due to WISHE is larger for the 2 K forcing than for the 1 K forcing. That is, WISHE increases the strength of the response to a given forcing, and does so nonlinearly as a function of the forcing. This occurs even though m is not homogenized in the model, for reasons discussed in the previous chapter.

For the slightly stronger forcing of $\theta_{PH} = 3$ K, the circulation enters an AMC regime with the classic structure of a single off-equatorial convergence zone in the summer hemisphere and a broad region of subsidence stretching across the equator well into the winter hemisphere (Fig. 3-3, third row). For the run without WISHE, the 3 K forcing did not produce an AMC circulation. Comparison of the profiles of boundary layer entropy for the two runs with $\theta_{PH} = 3$ K shows that WISHE narrows the s_b peak, increases its amplitude, and shifts it toward the equator (Fig. 3-4). Also plotted in Fig. 3-4 are the corresponding critical distributions of subcloud layer θ_e, calculated using the theory of Emanuel (1995) adapted for the two-mode model (a derivation is given in Appendix C). In the run without WISHE, the subcloud entropy is nowhere supercritical. Subcloud entropy in the run with WISHE is supercritical, with the departure of subcloud layer θ_e from the critical distribution peaking at about 3 K at 13°N. Thus, although the effects of WISHE on the s_b peak may seem small in amplitude, they are sufficient to shift the circulation into an AMC regime.

An AMC circulation is also produced for $\theta_{PH} = 7$ K (Fig. 3-3, bottom row). The main differences with the circulation achieved for the lower forcing of $\theta_{PH} = 3$ K are a meridional expansion of the Hadley circulation to 40°S, a larger s_b peak, and a distribution of free-tropospheric s^* that is shifted nearly uniformly to higher values over the entire Hadley circulation. On first inspection, the zonal and meridional winds seem quite similar to those obtained for the no-WISHE run with the same forcing (bottom row of Fig. 3-2), suggesting that m conservation provides a strong constraint that limits the effect WISHE can have

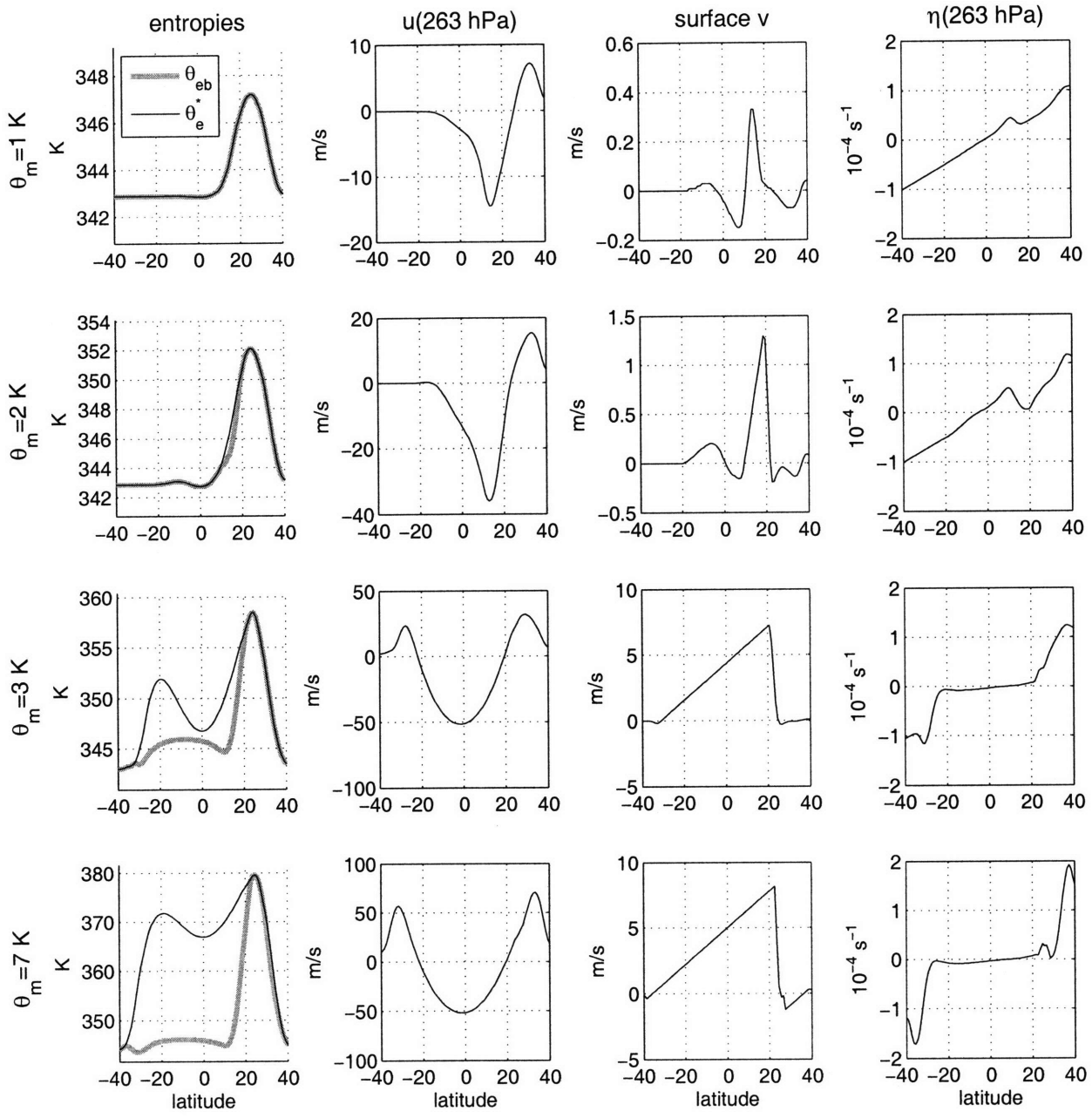

Figure 3-3: As in the previous figure, but for the two-mode model with wind-dependent surface entropy fluxes (with WISHE).

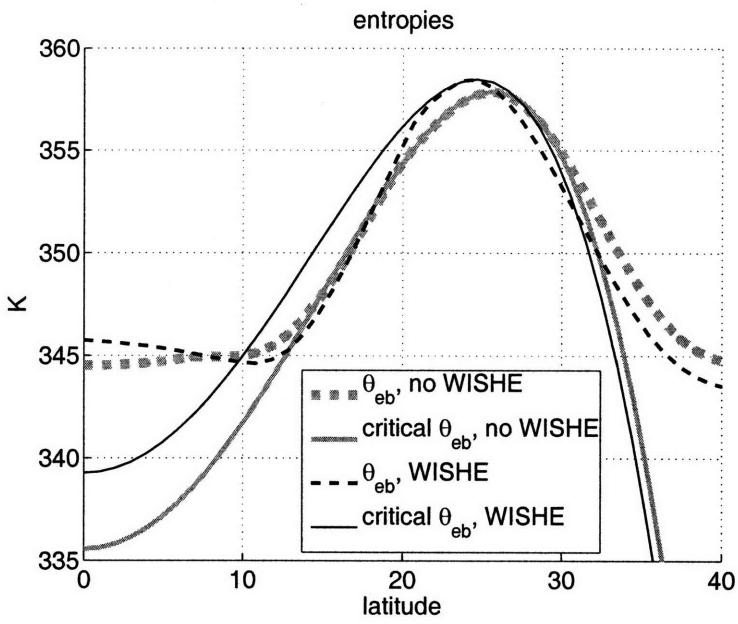

Figure 3-4: Profiles of subcloud layer equivalent potential temperature (solid lines) and the critical distribution of the same quantity (dashed lines). All quantities are for the equilibrated two-mode model with $\theta_{PH} = 3$ K. Grey lines denote results for the integration without WISHE, and black lines for the integration with WISHE.

on the dynamics. However, closer inspection does show some differences. The ascent zone in the run with WISHE is centered about 3° further south, is about half as wide, and has almost twice the peak amplitude when compared to the run without WISHE (Fig. 3-5, top panel). Although this meridional shift of the ascent zone may seem small, zonal winds within the bounds of the AMC circulation are highly sensitive to the latitude of ascent. If, as in previous axisymmetric theory (Held and Hou, 1980; Lindzen and Hou, 1988), ascent is assumed to occur entirely at one latitude ϕ_0 where horizontal winds are zero, and upper-level flow in the cross-equatorial branch of the circulation is assumed to strictly conserve m, then a shift in ϕ_0 from 26° to 23° will make upper-level zonal winds more westerly by about 20 m s^{-1}. Indeed, upper-tropospheric zonal winds within the main Hadley cell are 10 to 15 m s^{-1} more westerly in the run with WISHE than in the run without.

While the mechanism by which WISHE alters the s_b distribution will be discussed in detail in the next section, we make a few comments here. WISHE can be expected to increase vertical velocities in the ascent zone because large surface wind speeds enhance surface enthalpy fluxes there. This relationship between surface enthalpy fluxes and ascent

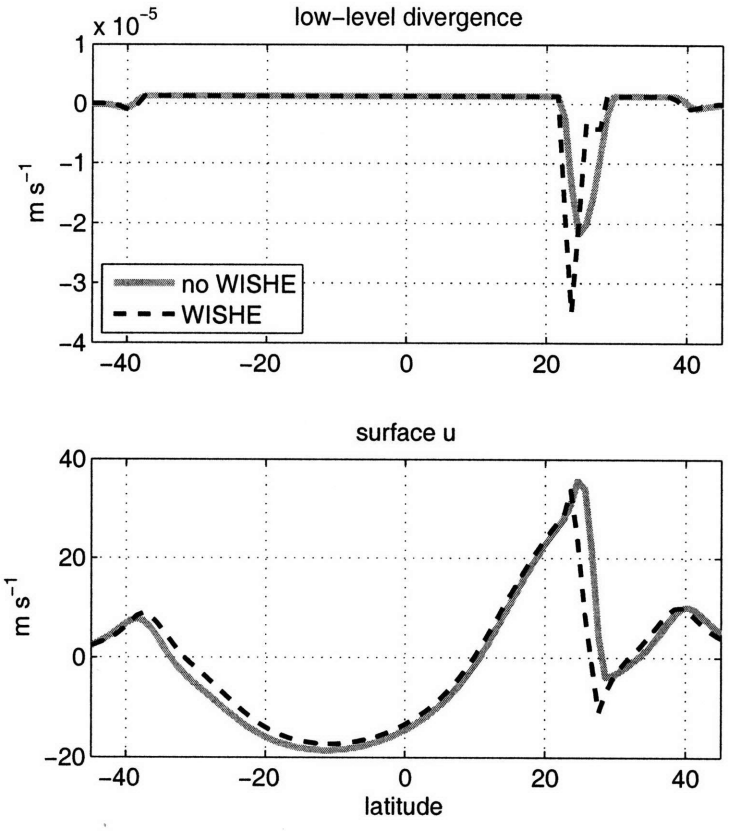

Figure 3-5: Divergence of the surface meridional wind (i.e. $\partial_y v_1$, top panel) and the total surface zonal wind (bottom panel), both for the equilibrated two-mode model with $\theta_{PH} = 7$ K. Solid grey lines denote results for the integration without WISHE, and dashed black lines for the integration with WISHE.

can be seen explicitly by rearranging the steady state budget for s^*, (2.12), under the assumption of strict subcloud layer equilibrium:

$$w = \frac{1}{1-\epsilon}\left(\epsilon C_k |\mathbf{V}| \frac{s_o - s_b}{\chi} - \frac{R}{N^2}\right) \tag{3.11}$$

Since R, N^2, ϵ, and χ are constant in the two-mode model, w can be expected to increase with $|\mathbf{V}|$. For solsticial AMC circulations, surface westerlies must exist in the ascent zone in order for surface drag to balance the convergence of zonal momentum into this region (as discussed by Lindzen and Hou, 1988). In the two-mode model with $\theta_{PH} = 7$ K, these surface westerlies peak near 30 m s^{-1} (Fig. 3-5), which easily produces stronger surface entropy fluxes and ascent than in the model without WISHE, where $|\mathbf{V}|$ was prescribed to be 10 m s^{-1}. These peak surface westerlies are about twice as strong as those observed near the

ascent zone in the South Asian summer monsoon (see next chapter), which could be due to the use of an SST forcing somewhat stronger than that needed to represent typical monsoon forcings on Earth, or some other process not represented in this simple axisymmetric model. Comparison with the GCM results presented in the previous chapter suggest that surface winds in the two-mode model are not unreasonable for axisymmetric solutions despite the lack of a dynamical boundary layer. In particular, for the axisymmetric GCM integrated with $\theta_m = 15$ K, surface westerlies peaked just under 20 m s^{-1}, and westerlies just above that model's boundary layer peaked at 25 m s^{-1} (not shown). In any case, the absolute magnitude of surface zonal winds is somewhat of a side issue, because our main point is that as long as the surface wind speed is larger than the surface gustiness v_g, a condition easily met by typical monsoonal westerlies in observations, WISHE can be expected to enhance vertical velocities in the ascent zone under the assumption of subcloud layer quasi-equilibrium.

The fact that the increase in vertical velocities in the ascent zone is accompanied by a narrowing of that zone is consistent with the conservation of mass. If the magnitude of subsidence is bounded by radiative cooling, and the meridional extent of the subsiding region is not considerably modified by WISHE, as is the case in these integrations, then mass conservation dictates that the ascent zone must narrow as its upward velocities increase.

3.3.3 Seasonally-varying forcing

How does WISHE alter the seasonal cycle of the Hadley circulation when the time-dependent SST forcing reaches sufficient amplitude to produce AMC flow even in the absence of WISHE? To answer this question, we integrated the two-mode model with an SST prescribed to vary in a seasonal cycle:

$$T_{PH} = T_0 + \theta_{PH} cos\left(2\pi \frac{t}{365 \text{ days}}\right) \cos^2\left(\frac{\pi}{2}\frac{\phi - \phi_0}{\Delta\phi}\right) \tag{3.12}$$

This is the same cyclic SST forcing used in the previous chapter, but with the larger peak amplitude of 7 K.

A phase diagram of the meridional mean v_1, plotted against the SST at 25°N, shows that an abrupt increase in meridional flow occurs in runs both with and without WISHE (Fig. 3-6). Here WISHE was turned off by specifying $|\mathbf{V}| = 10$ m s^{-1}, as for the runs with steady forcing. The effect of WISHE is to shift the abrupt onset to a time earlier in the

season and also to increase the peak meridional flow. The fact that the onset occurs earlier in the year is consistent with the finding that, for the runs with steady forcing, WISHE reduced the magnitude of the SST forcing needed to achieve an m-conserving circulation. The larger peak meridional flow achieved in the run with WISHE is actually part of an overshoot behavior where the flow seems to exhibit damped oscillations about some mean value. The period of these oscillations is roughly 15 days (not shown), which is considerably longer than a pendulum day except within a couple degrees of the equator. The reasons for this overshoot behavior are not explored here, although there is some evidence (see next chapter) that meridional flow in the South Asian monsoon does exhibit a transient peak coincident with the onset of the summer circulation.

The phase diagram shown in Fig. 3-6 illustrated the effect of WISHE for a seasonally varying SST forcing sufficiently strong to produce AMC flow even if surface enthalpy fluxes did not depend on wind speed. The previous chapter showed the effect of WISHE for a seasonally varying SST forcing that was sufficiently weak so that an AMC regime was not reached even with WISHE. We do not show the phase diagram for the intermediate case where an AMC circulation would occur only with WISHE, as its individual trajectories resemble those for the other cases: the trajectory for the run with WISHE is similar to that for the strong forcing displayed in Fig. 3-6, while the trajectory for run without WISHE is an approximate ellipse with much weaker peak meridional flow, as seen in the previous chapter. A later part of this chapter examines a seasonally varying version of the combined forcing, (3.3), for which WISHE is needed to produce a transition to AMC flow.

3.4 Moist frontogenesis

The previous section showed that although m conservation constrains the dynamics of the Hadley circulation for sufficiently strong SST forcings, WISHE can alter the response in nontrivial ways. In particular, WISHE reduced the critical forcing amplitude needed to achieve AMC flow by producing a narrowing, intensification, and equatorward shift of both the s_b peak and the ascent zone. This section attempts to explain these effects using an adaptation of a previous theory of eyewall frontogenesis for tropical cyclones (Emanuel, 1997). A heuristic discussion of this theory is presented first, followed by a more detailed analytical treatment.

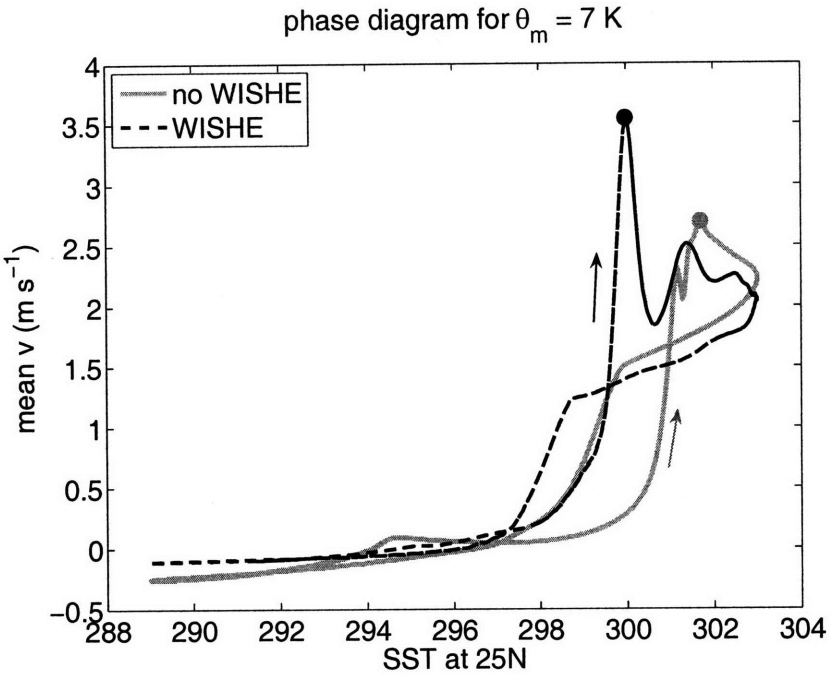

Figure 3-6: The meridional mean surface meridional wind plotted against the SST at 25°N for the two-mode model with the seasonally-varying $\theta_{PH} = 7$ K forcing. Solid grey line denote results for the integration without WISHE, and dashed black line for the integration with WISHE. Time progresses in the direction shown by the arrows.

3.4.1 Heuristic discussion

Emanuel (1997) showed that WISHE and the horizontal advection of subcloud layer entropy can create sharp radial gradients in azimuthal wind in a tropical cyclone and propagate the peak azimuthal wind toward the center of the storm, thereby forming the storm eyewall. It might seem reasonable to expect that a similar frontogenetic mechanism could operate in Hadley flow since idealized Hadley circulations and tropical cyclones are both axisymmetric balanced vortices, albeit with differences in some key parameters (e.g. Wirth and Dunkerton, 2006).

To illustrate the effects of WISHE and s_b advection on the zonal wind field, we begin by examining the idealized case of inviscid thermal wind balance and a convecting domain in strict subcloud layer equilibrium. The linearized meridional momentum and

free-tropospheric temperature equations are then:

$$\beta y u = (T - \overline{T})\frac{\partial s^*}{\partial y} - \frac{\partial \Phi_0}{\partial y} \tag{3.13}$$

$$\frac{\partial s^*}{\partial t} = -N^2(1-\epsilon)w + \epsilon N^2 C_k |\mathbf{V}| \frac{s_o^* - s_b}{\chi} - R \tag{3.14}$$

with the same notation as in the previous chapter. Suppose that a poleward gradient of s^* is imposed, that u maintains thermal wind balance with this distribution of s^*, and that this state is maintained until time t, as shown in Fig. 3-7. Suppose also that after time t, the s^* distribution is allowed to be modified only by the term in (3.14) involving $|\mathbf{V}|$, and that meridional winds and surface gustiness make negligible contributions to $|\mathbf{V}|$. This WISHE tendency will, after the lapse of a short time interval Δt, increase s^* nonuniformly so that both the peak and maximum gradient of s^* are shifted toward the equator (as shown in Fig. 3-7).

If thermally direct meridional flow is assumed to exist in the presence of this s^* distribution, and a quasi-equilibrium state exists with $s_b = s^*$, then a horizontal advective tendency will act on s_b[1]. This advective tendency will be negative within the region of thermally direct flow, and so will shift the maximum gradient of s_b poleward. Although this argument concerns the advection by meridional flow in general, Emanuel (1997) showed that it is the meridional flow induced by surface friction that actually leads to frontogenesis in tropical cyclones.

The s_b distribution is thus altered by both WISHE and s_b advection, with the former shifting the peak toward the equator and the latter shifting it toward the pole. Both processes narrow the peak by enhancing meridional entropy gradients near the peak. These qualitative hypotheses, treated in greater analytic detail below, are confirmed by repeating both the WISHE and no WISHE runs of the two-mode model without horizontal advection of s_b (for the steady forcing $\theta_{PH} = 7$ K). Advection of s_b was turned off simply by omitting the term $v_1 \partial_y s_b$ from the conservation equation for subcloud layer entropy; while this produces a system that does not conserve the relevant analogue of total energy, it proves useful as a process study. Rather than examining the s_b peak directly, we inspect the ascent zone because its width and intensity prove to be more highly sensitive indicators of these

[1]Recall from the previous chapter that s^*, at least in the axisymmetric two-mode model, cannot be directly modified by horizontal advection because it is constant with height. Horizontal advection can alter it only indirectly by acting on s_b.

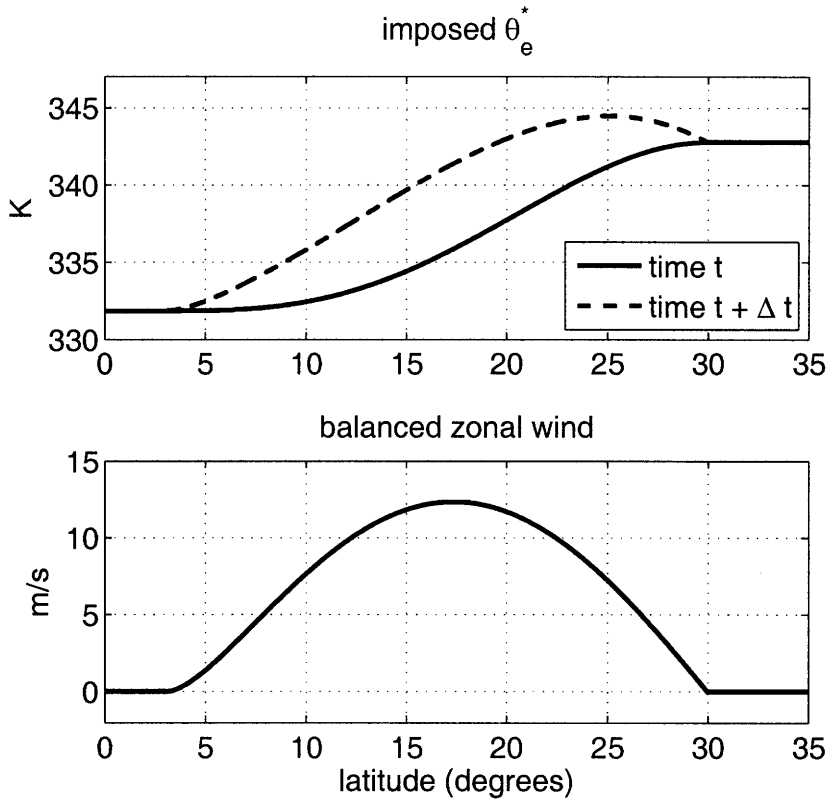

Figure 3-7: Schematic diagram of an imposed distribution of free tropospheric saturation equivalent potential temperature (top, solid line) and the baroclinic zonal wind needed to achieve thermal wind balance on a β-plane (bottom). The dashed line in the top panel shows the change in θ_e^* due only to WISHE after some short time interval Δt. See text for details.

processes. As noted by Emanuel (1995), the ascent zone is expected to be nearly collocated with the s_b peak. Results from these integrations confirm our previous statements: s_b advection generally shifts the ascent peak poleward and WISHE shifts it toward the equator, although more complex interactions between the two processes also seem to occur (Fig. 3-8). Both processes narrow and intensify the ascent zone, though WISHE does so more than s_b advection.

We have thus far implicitly assumed that any frontogenetic tendency in the numerical model will be balanced by horizontal diffusion. This does seem to occur, because the width of the ascent zone was reduced by a factor of two in a version of the model integrated, for $\theta_{PH} = 7$ K, with the horizontal diffusion coefficient κ_H reduced from its default value of 2 $\times$ 10^5 m^2 s^{-1} to 5 $\times$ 10^3 m^2 s^{-1} (not shown). This value of κ_H was near the smallest for which numerically stable solutions could be obtained, and required reducing the model grid

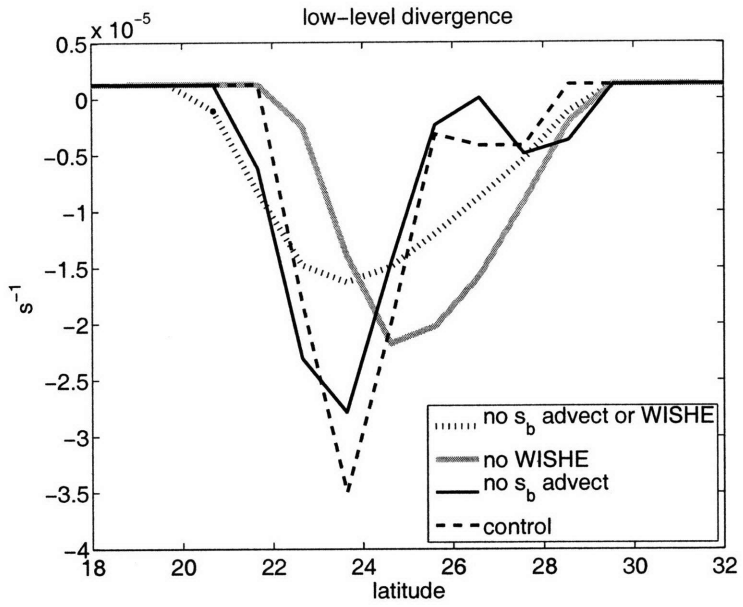

Figure 3-8: Divergence of surface wind (i.e. $\partial_y v_1$) for the equilibrated two-mode model with θ_{PH} = 7 K. Dotted line shows the profile for a run integrated without WISHE or horizontal advection of s_b, solid grey line for a run without WISHE but with s_b advection, solid black line for a run with WISHE but without s_b advection, and dashed line for a run with both WISHE and s_b advection.

spacing to 0.1° of latitude.

The above discussion, as well as the treatment below, assumed a convecting domain, and only a small part of the domain is convecting for strong SST forcings. Nevertheless, it seems that these frontogenetic processes do operate in the relatively narrow region of ascent. Physics arising from the discontinuities between convecting and nonconvecting regions is an active topic of research (e.g. Pauluis et al., 2007) and is not explored further here.

3.4.2 Analytical treatment

Here we show analytically how WISHE can propagate the s_b peak toward the equator, a process made more rapid by nonlinear u advection. We follow a similar treatment to that of hurricane eyewall frontogenesis put forth by Emanuel (1997), though on an axisymmetric β-plane without the centrifugal terms important for tropical cyclones. We make use of the conserved quantity m, defined by (3.5), and note that the absolute vorticity η is equal to

-$\partial_y m$. The zonal momentum equation can be rewritten in terms of m conservation:

$$\frac{Dm}{Dt} = F_u \tag{3.15}$$

where F_u represents dissipation, including surface drag. The following treatment is not specific to the two-mode model in that we do not make any modal decomposition and assume m is conserved everywhere in the absence of dissipation. Following Emanuel (1997), we define a coordinate transformation

$$\frac{\partial}{\partial y} = \frac{dm}{dy}\frac{\partial}{\partial m} = -\eta\frac{\partial}{\partial m} \tag{3.16}$$

The relative vorticity ζ then becomes:

$$\zeta = -\frac{\partial u}{\partial y} = \eta\frac{\partial u}{\partial m} \tag{3.17}$$

and the definition of absolute vorticity allows ζ to be written:

$$\zeta = \frac{\beta y}{1 - \frac{\partial u}{\partial m}} \tag{3.18}$$

Thus ζ becomes singular when $\partial_m u$ increases to unity. Note that for $\partial_m u > 1$, m is no longer monotonic in y and so the use of the definition of m as a coordinate mapping breaks down.

The thermal wind relation can be written in terms of m:

$$\beta y\frac{\partial m}{\partial p} = \frac{\partial s^*}{\partial y}\left(\frac{\partial T}{\partial p}\right)_{s^*} = \frac{ds^*}{dm}\frac{\partial m}{\partial y}\left(\frac{\partial T}{\partial p}\right)_{s^*} \tag{3.19}$$

Dividing through by $\partial_y m$ provides an expression for the slope of an m surface:

$$\beta y\left(\frac{\partial y}{\partial p}\right)_m = -\frac{ds^*}{dm}\left(\frac{\partial T}{\partial p}\right)_{s^*} \tag{3.20}$$

The only assumptions made thus far are those of axisymmetry, m conservation, and thermal wind balance. Now we also assume that the atmosphere is neutral to slantwise convection, so that s^* surfaces are parallel to m surfaces. The previous expression is then

integrated upward along these surfaces:

$$\frac{ds^*}{dm}(T_s - T) = \frac{\beta}{2}y^2\Big|_m = u - u_s \tag{3.21}$$

The last expression on the right was obtained by using the definition of m and represents the vertical shear of zonal wind along an m surface, with u_s the wind at the lower boundary of the atmosphere. For a hurricane, Emanuel (1997) obtained ds^*/dm solely in terms of m and u_s by virtue of the fact that m surfaces flare out to a large radius at the top of the storm and by the assumption that the contribution of u_s to m is much larger than that of the planetary rotation. These extremes do not apply to the monsoonal regime considered here. However, we exploit the baroclinic nature of the circulation by evaluating (3.21) at the level at which the zonal wind vanishes:

$$\Delta T_0 \frac{ds^*}{dm} = -u_s \tag{3.22}$$

where ΔT_0 is defined as the difference between the surface temperature T_s and the temperature at the level of zero zonal wind. If the circulation has a nonzero barotropic component, then $\Delta T_0 \neq T_s - \overline{T}$, with $\overline{T}$ the pressure-weighted mean tropospheric temperature. Indeed, a level of zero zonal wind may not exist given a sufficiently strong barotropic wind. Nevertheless, we proceed with the analysis and simply note that time variations in ΔT_0 (i.e. in the level of zero zonal wind) could alter the behavior.

The time evolution of u in m space can be obtained by differentiating the free-tropospheric temperature balance with respect to m:

$$\frac{\partial^2 s^*}{\partial m \partial t} = \frac{\partial}{\partial m}\left[N^2(\epsilon M - w)\right] \tag{3.23}$$

We assume that convective mass fluxes instantaneously adjust to the value needed to maintain constant subcloud layer entropy:

$$M = M_{eq} \equiv w + \frac{1}{\chi}[C_k|\mathbf{V}|\gamma + H_b \alpha u_s \frac{\partial s_b}{\partial m})] \tag{3.24}$$

where the quantities $\chi \equiv s_b - s_m$ and $\gamma \equiv s_o^* - s_b$ are not necessarily constants. The advective tendency of s_b has been written in m coordinates, using the fact that the only

meridional wind in m space is that induced by surface friction, here assumed to be Rayleigh damping:

$$\frac{Dm}{Dt} = -\alpha u_s \tag{3.25}$$

Using this closure for M together with (3.22) gives:

$$\frac{\partial}{\partial t}\left(\frac{u_s}{\Delta T_0}\right) = N^2\left[-\frac{\epsilon C_k \gamma}{\chi|\mathbf{V}|}\left(\frac{\partial u_s}{\partial m}+\frac{\partial v_s}{\partial m}\right) - \epsilon C_k|\mathbf{V}|\frac{\partial}{\partial m}\left(\frac{\gamma}{\chi}\right) - \epsilon\frac{\partial}{\partial m}\left(\frac{H_b \alpha u_s}{\chi}\frac{\partial s_b}{\partial m}\right) + (1-\epsilon)\frac{\partial w}{\partial m}\right] \tag{3.26}$$

The first and third terms will generally increase u_s by enhancing meridional gradients of s^*. The first term represents the effect of WISHE, and the third term the effect of meridional advection of boundary layer entropy. If we neglect the contribution of the meridional wind to the wind-induced surface entropy flux, and also eliminate $\partial_m s_b$ using (3.22) then, following Emanuel (1997), these two terms can be seen to propagate the u_s distribution meridionally with a phase speed given by

$$c = \frac{\epsilon N^2}{\chi}\left[\frac{\Delta T_0 C_k \gamma}{|\mathbf{V}|} - \frac{2H_b\alpha}{\Delta T_0}u_s\right] \tag{3.27}$$

The first term inside the brackets of this expression is due to WISHE, and serves to propagate the u_s distribution toward higher m (i.e. lower y). Meridional gradients of u_s will be enhanced on the poleward side of the peak surface wind speed and reduced on the equatorward side because the equatorward phase speed varies inversely with $|\mathbf{V}|$. When $\partial_m u_s$ increases to unity, (3.18) shows that a front will exist. The second term inside brackets in (3.27) is due to s_b advection, and propagates the u_s distribution toward lower m, in the opposite direction of the WISHE term. However, this term enhances the frontogenetic effects of WISHE because it also increases $\partial_m u_s$ on the poleward side of the u_s peak, since the poleward phase speed due to s_b advection increases with u_s.

The second and fourth terms on the right hand side of (3.26) damp frontogenesis by reducing meridional gradients of s^*. The second term represents the effect of surface entropy fluxes increasing with the difference between subcloud layer and ocean surface entropies. The fourth term represents the tendency of vertical velocities in a thermally direct circulation to adiabatically reduce the horizontal temperature gradients that drive the circulation. While the above development does not address the nature of the equilibrium achieved be-

tween the four terms on the right hand side of (3.26), the two-mode model runs in which WISHE and s_b advection were selectively omitted confirm that these processes do shift the u_s maximum toward the equator and the pole, respectively (as in Fig. 3-8, discussed above). It is difficult to discern any considerable increase in $\partial_y u_s$ on the poleward side of the u_s peak in the two-mode model due to either WISHE or s_b advection because this gradient is already large simply due to the sharp northern boundary of the Hadley circulation. Thus, our focus is on the meridional propagation of the s_b maximum rather than the associated frontogenesis, although we henceforth refer to the physics responsible for this propagation as the frontogenetic mechanism.

The two-mode model used in this paper has a vertical structure simplified by the assumption that variations in s^* are constant with height. This simplification involved taking the thermal wind relation:

$$\beta y \frac{\partial u}{\partial p} = \frac{\partial s^*}{\partial y}\left(\frac{\partial T}{\partial p}\right)_{s^*} \tag{3.28}$$

and integrating it along an s^* surface to obtain:

$$\beta y(u - u_s) = (T - T_s)\frac{\partial s^*}{\partial y} \tag{3.29}$$

This last step assumes that $\partial_y s^*$ is constant along s^* surfaces, which is true only if s^* surfaces are vertical (i.e. parallel to y surfaces). Thus, the two-mode model assumes that s^* and m surfaces are not parallel; the former are vertical while the latter are tilted in this model.

The expression (3.26) derived for a slantwise neutral fluid would thus seem to be inapplicable to the two-mode model. However, a similar procedure can be followed in physical space, rather than m space, to obtain:

$$\frac{\partial^2 s^*}{\partial t \partial y} = \frac{1}{\beta y \Delta T}\frac{\partial u_s}{\partial t} = N^2\left[\epsilon C_k \frac{\gamma}{\chi|\mathbf{V}|}\left(\frac{\partial u}{\partial y} + \frac{\partial v}{\partial y}\right) + \epsilon C_k |\mathbf{V}| \frac{\partial}{\partial y}\left(\frac{\gamma}{\chi}\right) - \epsilon \frac{\partial}{\partial y}\left(\frac{Hv}{\chi}\frac{\partial s_b}{\partial y}\right) - (1-\epsilon)\frac{\partial w}{\partial y}\right] \tag{3.30}$$

While the WISHE and advective terms here also increase gradients of u_s on the poleward side of the surface wind maximum, $\partial_y u$ must become singular in order for the relative vorticity to become singular. This means that it takes infinite time to form a discontinuity in u by (3.30), consistent with the fact that nonlinear u advection was not used to derive

(3.30). Thus, while the slantwise neutral solution (3.26) is not directly applicable to the two-mode model, the mechanisms that produce velocity fronts in this model seem similar even though they may operate on longer time scales.

3.5 Results for equatorial forcings

3.5.1 Steady forcings

Thermal forcings with a first or second meridional derivative that is nonzero on the equator are expected to produce an AMC circulation regardless of the magnitude of the forcing, as discussed by Plumb and Hou (1992). For such forcings, m conservation is expected to constrain the dynamics as it did for the subtropical forcings, although we find that there are a few features worth noting. For this purpose, the two-mode model is integrated with the T_{LH} forcing given in (3.2), with $T_1 = 303.15$ K and $\theta_{LH} = 20$ K. Several values of ϕ_1 are examined.

For an SST maximum at $\phi_1 = 10°$N, a cross-equatorial AMC circulation is produced that extends to nearly 40°S, regardless of whether WISHE is included in the model (Fig. 3-9). Convection is suppressed in the winter hemisphere branch of the circulation. Consistent with the results for subtropical forcings, the ascent zone is narrower for the run with WISHE, and although the peak ascent is actually shifted slightly poleward by WISHE, the bounds of the ascent region are shifted toward the equator (Fig. 3-10). The fact that zonal winds near the equatorial tropopause are slightly more westerly in the run with WISHE is consistent with the equatorward shift in mean ascent.

The equatorially symmetric forcing, with $\phi_1 = 0$ in (3.2), is a special case in that ascent peaks on the equator only when WISHE is not included (Fig. 3-10). The use of WISHE produces two ascent zones symmetric about the equator, with a local minimum in ascent on the equator. This same effect of wind-dependent ocean evaporation was obtained by Numaguti (1993) in a three-dimensional aquaplanet GCM with a zonally symmetric SST forcing peaking on the equator, and we present a brief discussion consistent with his explanation of the underlying physics. As shown by Held and Hou (1980), to balance the convergence of zonal momentum produced by an AMC response with ascent peaking on the equator, surface winds must consist of easterlies between the equator and some intermediate latitude, westerlies poleward of this latitude, and zero wind on the equator in

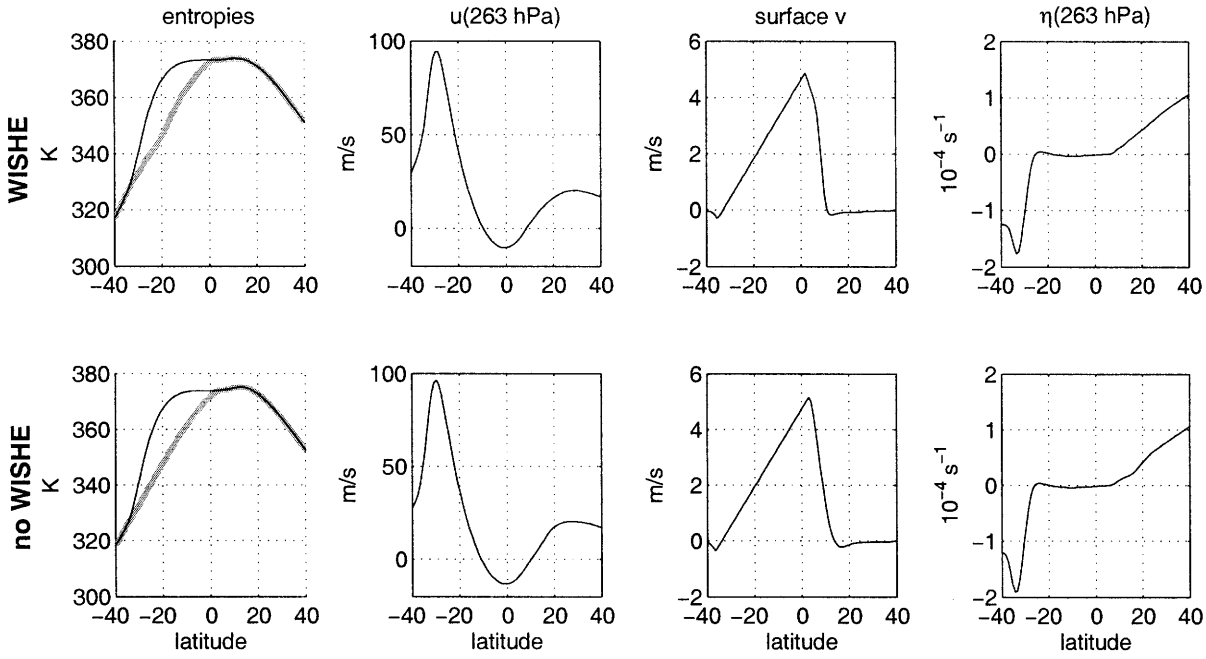

Figure 3-9: As in Fig. 3-2 but for the equilibrated response to the steady T_{LH} forcing centered at $\phi_1 = 10°$N, with WISHE (top row) and without WISHE (bottom row).

the inviscid limit. With WISHE, however, this surface wind distribution is incompatible with an equatorial peak of free-tropospheric temperatures, as can be seen by combining the steady state version of the budget for s^*, (3.23), under the assumption of strict boundary layer quasi-equilibrium, (3.24):

$$0 = -\epsilon \frac{\partial}{\partial m}\left(\frac{E}{\chi}\right) - \epsilon \frac{\partial}{\partial m}\left(\frac{H_b \alpha u_s}{\chi}\frac{\partial s_b}{\partial m}\right) + (1-\epsilon)\frac{\partial w}{\partial m} \tag{3.31}$$

For an equatorial SST peak without WISHE, peak ascent is maintained on the equator because surface entropy fluxes peak there, and the negative first term and positive third term in the above expression roughly balance. For an equatorial SST peak with WISHE, the fact that m conservation requires a local minimum in $|\mathbf{V}|$ on the equator means that the first term in (3.31) will become positive, unless gradients in χ or $(s_o^* - s_b)$ are sufficiently large to compensate for the poleward gradient in $|\mathbf{V}|$. Observational estimates of E presented in the next chapter show that a local minimum does generally exist on the equator even when SST peaks there, so an equatorward gradient in χ would seem to be the only candidate for keeping the first term negative. While χ is fixed in the two-mode model, its variations could

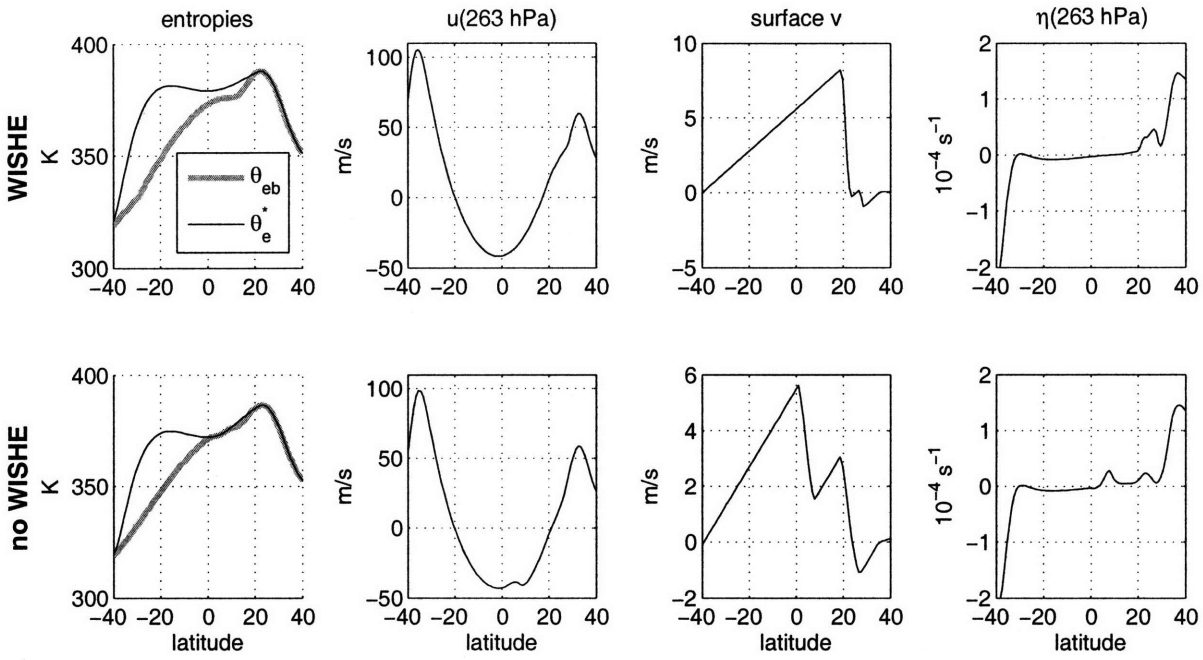

Figure 3-11: As in Fig. 3-9 but for the equilibrated response to the steady T_C forcing (the combination of the equatorial and subtropical SST distributions).

only when WISHE was included in the model. The response to T_C largely seems to be a superposition of the responses to the individual components of the forcing (T_{LH} and T_{PH}) with the AMC circulation dominating wherever it exists. That is, for the run with WISHE, ascent occurs only in a narrow zone just south of the subtropical SST maximum, and no ascent occurs just north of the equator despite the cross-equatorial gradient of SST and s_b (Fig. 3-11, top row). The main effect of the T_{LH} component of the forcing is to extend the poleward boundary of the AMC circulation to higher latitudes in the winter hemisphere (compare top row of Fig. 3-11 with third row of Fig. 3-3). In the run without WISHE, the subtropical component of the forcing does not generate a cross-equatorial AMC response, so ascent occurs both near 20°N and just north of the equator due to the equatorial component of the forcing (Fig. 3-11, bottom row).

3.5.2 Seasonally-varying forcings

Finally, the combined forcing is varied in a seasonal cycle, which can be thought of as an idealization of seasonal variations in the thermal forcing associated with both the South

produce a moisture-convection feedback (e.g. Grabowski and Moncrieff, 2004) in which the convective mass flux increases as the lower free-troposphere moistens. We do not explore this further here, but simply note that this is one candidate mechanism for maintaining equatorial maxima in convection and ascent when E has a local minimum on the equator. Advection of s_b, represented by the second term in (3.31), is another such candidate, but this advective tendency should be quite weak near the equator because of the flatness of the m-conserving distribution of s_b there. Thus, if variations in χ or advection of s_b do not compensate, the poleward gradient in E near the equator that is produced by WISHE must be balanced by a poleward gradient in w.

By a similar argument, a bimodal profile of w with a near-equatorial local minimum is expected to exist for SST distributions that peak very near the equator. This is seen in the two-mode model, where a northward shift of ϕ_1 from the equator to 5°N produces a similar northward shift in the two ascent zones (Fig. 3-10). This is consistent with the results of Lindzen and Hou (1988), in that the peak surface easterlies in the winter hemisphere tropics of their steady, dry model moved toward the equator as the forcing maximum was shifted off the equator into the summer hemisphere. The surface easterly peak in the winter hemisphere is expected to be associated with a local maximum of ascent until the thermally direct circulation is strong enough to suppress convection in the winter trade wind region.

Although this shift in the ascent zone off the equator for near-equatorial forcings may seem to contradict the previous statement that WISHE shifts ascent zones toward the equator, it is not at odds with the frontogenetic mechanism. That mechanism can be viewed as simply providing a lower bound for the latitude of the s^* peak. That is, if the SST peak were moved quasi-statically from the subtropics to the equator, the equatorially symmetric peaks of the m-conserving s^* distribution would move toward the equator to a limiting latitude some distance from the equator. These s^* peaks would only move onto the equator if the meridional gradient of the surface entropy flux between the peaks became zero, a process that WISHE prevents from occurring. Furthermore, for SST peaking on or very near the equator, the frontogenetic mechanism must take into account that easterlies may exist at all heights near the ascent zone so that no level of zero zonal wind exists.

We also examine the response to a forcing that contains both cross-equatorial and subtropical components, represented by T_C in (3.3). The subtropical SST anomaly is given an amplitude of $\theta_{PH} = 3$ K, which for the isolated subtropical forcing of T_{PH} was supercritical

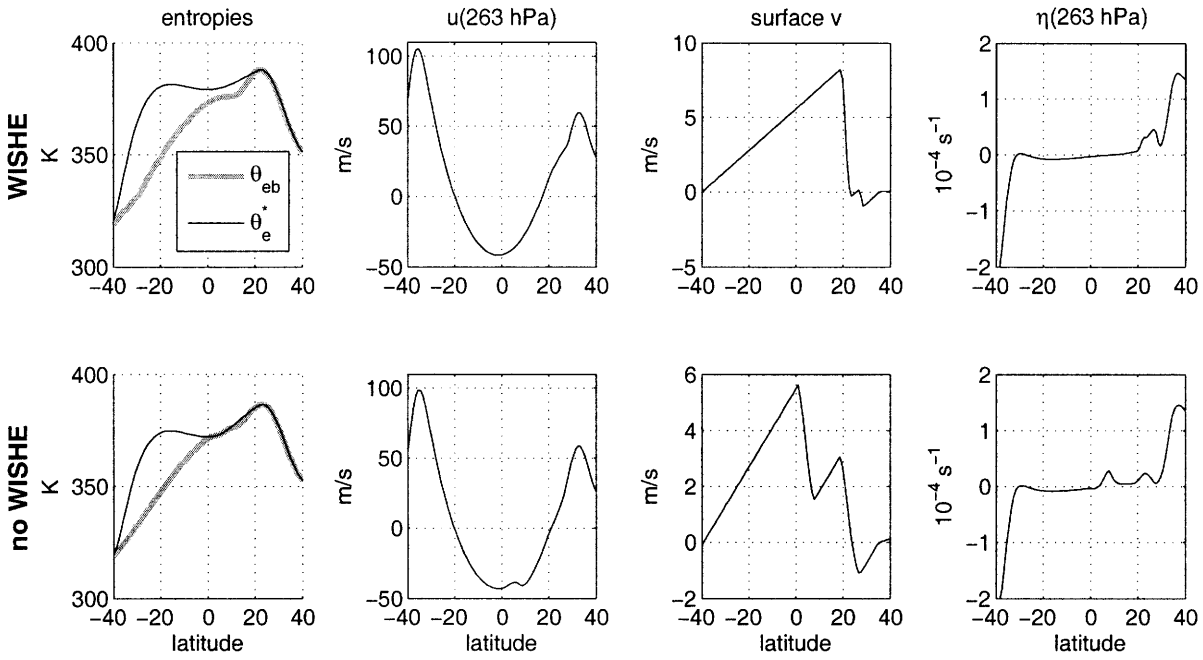

Figure 3-11: As in Fig. 3-9 but for the equilibrated response to the steady T_C forcing (the combination of the equatorial and subtropical SST distributions).

only when WISHE was included in the model. The response to T_C largely seems to be a superposition of the responses to the individual components of the forcing (T_{LH} and T_{PH}) with the AMC circulation dominating wherever it exists. That is, for the run with WISHE, ascent occurs only in a narrow zone just south of the subtropical SST maximum, and no ascent occurs just north of the equator despite the cross-equatorial gradient of SST and s_b (Fig. 3-11, top row). The main effect of the T_{LH} component of the forcing is to extend the poleward boundary of the AMC circulation to higher latitudes in the winter hemisphere (compare top row of Fig. 3-11 with third row of Fig. 3-3). In the run without WISHE, the subtropical component of the forcing does not generate a cross-equatorial AMC response, so ascent occurs both near 20°N and just north of the equator due to the equatorial component of the forcing (Fig. 3-11, bottom row).

3.5.2 Seasonally-varying forcings

Finally, the combined forcing is varied in a seasonal cycle, which can be thought of as an idealization of seasonal variations in the thermal forcing associated with both the South

Asian land mass and SST in the Indian Ocean. This is accomplished by prescribing ϕ_1 in (3.2) and θ_{PH} in (3.1) to vary in phase with the same annual frequency:

$$\phi_1 = 10^\circ \cos\left(2\pi \frac{t}{365 \text{ days}}\right) \tag{3.32}$$

$$\theta_{PH} = 3 \text{ K} \cos\left(2\pi \frac{t}{365 \text{ days}}\right) \tag{3.33}$$

At any point in the resulting seasonal cycle, the response is generally consistent with the steady results discussed above. In the run without WISHE, ascent occurs both near the equator and near the subtropical SST peak at the boreal summer solstice (Fig. 3-12, top panel). The near-equatorial ascent zone has a single peak that migrates back and forth across the equator in a continuous annual cycle, and is confined closer to the equator in boreal summer than in boreal winter because of subsidence forced by the subtropical SST peak. In the run with WISHE, ascent occurs only near 20°N at the boreal summer solstice, as it did in the equilibrated response to the steady combined forcing. During spring and fall in the run with WISHE, a region of ascent migrates across the equator, but within this region a local minimum of ascent exists between two maxima positioned on opposite sides of the equator. During the transition from spring to summer, the ascent zone jumps discontinuously from its near equatorial position to the location just south of the subtropical SST peak. This jump is a signature of the transition to an AMC circulation forced by the subtropical SST peak, and WISHE simply causes this transition to occur for the intermediate value of 3 K used here for the subtropical forcing. A similar jump of the surface convergence zone from the equator to 20°N occurs if the subtropical SST anomaly is increased to 7 K in the run without WISHE (not shown).

The run with the seasonally-varying combined forcing is repeated with the gustiness parameter v_g in the surface bulk flux formula for latent and sensible heat reduced from its default value of 6 m s^{-1} to 2 m s^{-1}. The gross meridional structure of the solution resembles that for the default value of v_g, with an abrupt transition to an AMC circulation in early summer and two ascent zones on opposite sides of the equator during spring and fall. However, during boreal winter an ascent zone persists just north of the equator and the southern hemisphere ascent zone undergoes several poleward migrations. This is of interest because observations show the convective maximum undergoing poleward migrations in the northern hemisphere during the South Asian summer monsoon, with a secondary time-mean

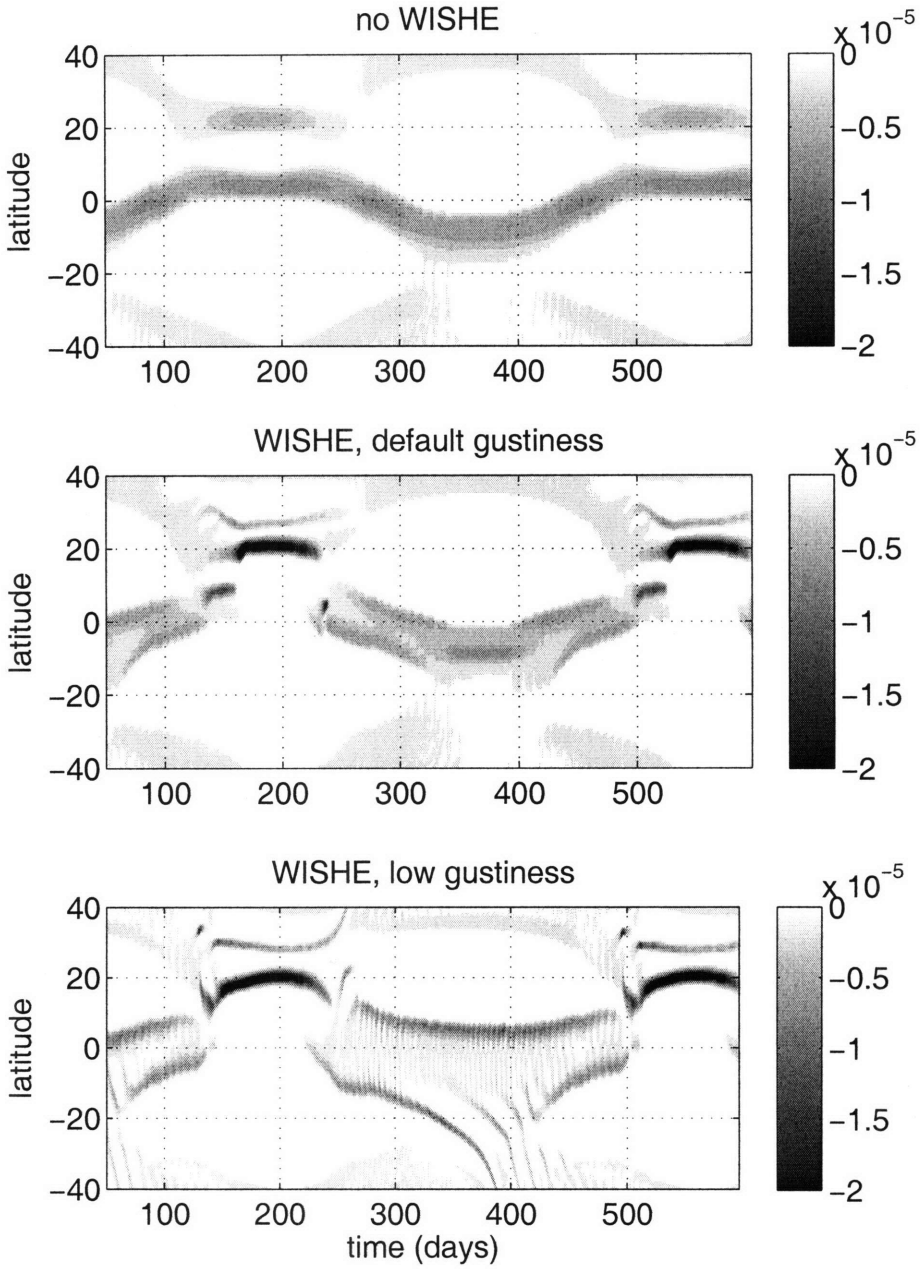

Figure 3-12: Hovmuller diagrams of surface divergence for the response to the seasonally varying T_C forcing. Top panel shows the run without WISHE, middle panel the run with WISHE, and bottom panel the run with WISHE and the surface gustiness parameter decreased to a value of v_g = 2 m s^{-1}. Time is the number of days after the winter solstice.

maximum of convection existing just south of the equator (Sikka and Gadgil, 1980). Thus, the southern hemisphere austral summer regime of the two-mode model with $v_g = 2$ m s^{-1} exhibits some of the observed features of the boreal summer South Asian monsoon. A number of factors could be responsible for the fact that such propagating anomalies do not occur during boreal summer in the two-mode model while they do occur in observations: the subtropical forcing used in this run could be too strong, the small thermal inertia of a land surface poleward of the equator could be important, or zonally asymmetric disturbances could be needed to excite the propagating anomalies in regions where convection would otherwise be continually suppressed in the axisymmetric model.

These poleward propagating anomalies resemble axisymmetric WISHE modes, as discussed by Emanuel (1993). Bellon and Sobel (2008, in press) also obtained northward migrations of an ascent zone starting from about 5°S in a version of the QTCM with a dynamical boundary layer. Their model was forced with a prescribed SST field that resembled the T_{LH} distribution, except that the peak was flattened to provide uniform SST between the equator and 18°N. They found that both WISHE and a dynamical boundary layer were needed to obtain the poleward propagating modes in their model, although here we obtain the modes without a dynamical boundary layer.

3.6 Concluding remarks

The effect of WISHE on axisymmetric Hadley circulations can be summarized by considering four different regimes. For the weakest SST forcings localized off the equator, WISHE only mildly enhances the strength of the circulation because surface drag suppresses the positive feedback on the baroclinic component of the circulation. For slightly stronger SST forcings, the convergence of zonal momentum into the off-equatorial ascent zone can overcome the effects of surface drag, allowing WISHE to more strongly enhance the sensitivity of the circulation strength to the forcing. These are the two cases discussed in the previous chapter, and upper tropospheric meridional flow does not homogenize absolute angular momentum in either of these regimes. For still stronger SST forcings, WISHE can cause the circulation to enter an AMC regime when, in the absence of WISHE, only a local, near-linear response would be produced.

Finally, for the strongest SST forcings, an AMC circulation is achieved regardless of

whether WISHE has any effect. Angular momentum conservation provides a strong constraint on the dynamics; together with the upper bound on the magnitude of subsidence provided by the conservation of potential temperature in nonconvecting regions, it imposes a meridional structure on both winds and free-tropospheric temperatures within the cross-equatorial Hadley cell. Within these constraints, WISHE exerts a frontogenetic tendency in the off-equatorial ascent zone, narrowing and intensifying this zone and shifting it toward the equator. These effects of WISHE reduce the forcing amplitude needed to achieve an AMC response and, for forcings that are supercritical even without WISHE, slightly increase the mean absolute angular momentum of upper-tropospheric winds in the Hadley cell.

These results hold even when the SST has a nonzero gradient on equator, which results in a boundary layer entropy distribution that is always supercritical to m-conserving flow. When a subtropical SST anomaly is superimposed on an SST distribution with a cross-equatorial gradient, the origin of the m-conserving flow can be shifted from the equator nearly into the subtropics, thereby suppressing any near-equatorial convection. This shift in the origin of the m-conserving flow occurs once the subtropical SST anomaly exceeds the critical threshold discussed by Plumb and Hou (1992), and WISHE can reduce the magnitude of this threshold.

It is not obvious where either the Earth's zonal mean Hadley circulation or actual monsoon circulations fall in this series of regimes. That is, are the thermal forcings associated with the off-equatorial land masses in monsoon climates sufficiently strong to produce AMC flow in the absence of WISHE? This question will be addressed, albeit somewhat indirectly, in Chapter 5 by use of a three-dimensional GCM. Without answering this question, however, it may be possible to assess the consistency of observations with some features of the axisymmetric models used here, thereby providing evidence for or against the role of WISHE in the onset of monsoons. This is the task taken up in the next chapter.

THIS PAGE INTENTIONALLY LEFT BLANK

Chapter 4

Annual intensification of the Somali jet in a quasi-equilibrium framework: Observational composites

Abstract

The annual intensification of the southwesterly Somali jet, which accompanies the onset of the Indian monsoon, is rapid compared to the evolution of the seasonal insolation forcing. This chapter presents a 27-year composite of the onset of this jet, based on reanalyzed winds. The abrupt component of jet onset occurs over the Arabian Sea at least 1000 km east of the East African highlands, and is accompanied by large increases in both deep convection and baroclinic circulation. The core of the cross-equatorial jet, located over land adjacent to the East African highlands, evolves more slowly than the winds over the Arabian Sea. This topographically-bound flow accounts for about one quarter of the global cross-equatorial mass flux in the solsticial Hadley cell, while the flow that intensifies abruptly over the Arabian Sea accounts for another quarter.

The onset of the southwesterly jet is examined in a convective quasi-equilibrium framework. Changes in low-level geopotential accompanying jet onset are estimated to be consistent with an increase in subcloud entropy over the Arabian Sea, which is in turn roughly collocated with increases in both ocean evaporation and deep-tropospheric ascent. These results suggest that a wind-evaporation feedback may be responsible for the abrupt nature of jet onset. In contrast, the peak increase in free-tropospheric temperature accompanying jet onset occurs about 15° north of the peak increase in subcloud entropy, mostly in a region of subsidence estimated to be strong enough to thermodynamically decouple the free troposphere and the subcloud layer. Possible mechanisms for this temperature increase are suggested, but a detailed investigation is left for future work.

4.1 Introduction

The two previous chapters showed that wind-evaporation feedback in axisymmetric models can play an important role in producing seasonal transitions of the Hadley circulation that are rapid compared to the evolution of an imposed thermal forcing. Although that work was motivated by a desire to explain the abrupt onset of monsoon circulations, the connection between idealized, axisymmetric Hadley circulations and the highly three-dimensional flow in monsoons is far from obvious. Here we suggest that, for the South Asian monsoon, such a connection can be found in the Somali jet, and we present evidence that this jet is a convectively coupled phenomenon with a characteristic seasonal evolution set in large part by a wind-evaporation feedback.

The Somali jet is an important component of the South Asian monsoon, with most low-level cross-equatorial monsoon flow concentrated in a narrow band of longitudes near the East African highlands (Findlater, 1969; Krishnamurti and Bhalme, 1976). The jet turns anticyclonically in the northern hemisphere to become the westerlies that sweep over India during the summer monsoon, with peak low-level wind speeds typically observed near 10°N off the east coast of Somalia. Here we distinguish between the peak southerly winds that flow across the equator, which we call the cross-equatorial jet, and the intense southwesterlies over the off-equatorial Arabian Sea, which we call the southwesterly jet.

Like the monsoon, the jet undergoes a seasonal cycle, with northward cross-equatorial flow typically starting in April over the ocean east of Africa, then shifting westward in May to become zonally focused near the East African highlands (Krishnamurti and Bhalme, 1976). In June the northern branch of zonal flow associated with the jet shifts poleward and abruptly increases in speed to become the low-level monsoon westerlies. The rapid increase in wind speed of this southwesterly jet is one of the most dramatic pieces of evidence for the abrupt onset of the South Asian monsoon circulation. As in Chapter 1, we define "abrupt" or "rapid" relative to the seasonal cycle of insolation: an abrupt event has a time series that projects onto frequencies higher than those of the first three Fourier harmonics of Earth's annual cycle. Using data from a field campaign in 1979, Krishnamurti et al. (1981) found that the kinetic energy of the 850 hPa horizontal wind over the Arabian Sea increased from its mean winter to its mean summer value over a single week prior to the start of monsoon rains over central India, which easily qualifies as abrupt by the above definition.

The abrupt nature of the onset of the southwesterly jet has also been documented more recently in scatterometer data: Halpern and Woiceshyn (1999) showed that surface wind speeds in this jet increased to their summer mean over a two-week interval in 1997, with peak surface winds exceeding 16 m s^{-1}.

The start of summer monsoon rains over India is closely associated with the onset of the jet, but no comprehensive multi-year study of jet onset has been published. Halpern and Woiceshyn (2001) verified the close association between jet intensification and Indian monsoon onset, but they focused on interannual variations in the date of onset and did not present any sort of composite time series for the seasonal intensification itself. Krishnamurti et al. (1981) and Halpern and Woiceshyn (1999) examined only single years of jet onset. Compiling a composite picture of how winds and other variables evolve with the onset of the jet is one of the main tasks of this paper.

The other main task is to examine these composites in a convective quasi-equilibrium framework that takes the distributions of pressure and cumulus heating as part of the solution, rather than as the forcing. Previous studies of the structure of the Somali jet have employed numerical models in which the distributions of either pressure (Krishnamurti and Wong, 1979) or convective heating (e.g. Rodwell and Hoskins, 1995) were prescribed as the forcing. While such studies have provided valuable insight on certain aspects of the dynamics, they presuppose a forcing which cannot truly be seen as external. Ideally, the structure and evolution of the jet would be determined, and dynamically understood, given only the distributions of insolation and topography, and perhaps of SST if two-way ocean coupling is not considered. This chapter serves as a first step toward this task, as we limit our focus to observations and do not attempt to obtain the jet as a solution of a model system.

Studies concerned with the seasonal evolution of the Somali jet are typically framed in terms of the onset of the South Asian summer monsoon and consider the evolution of the jet as part of a broader-scale circulation. It is possible that the low-level zonal monsoon flow would exhibit an abrupt seasonal onset even if Africa and the East African highlands did not serve to zonally focus the flow. Indeed, an off-equatorial surface westerly jet is a characteristic feature of axisymmetric models forced by an off-equatorial thermal maximum (e.g. Krishnamurti et al., 1976; Lindzen and Hou, 1988). So any theory that successfully explains the abrupt onset of a zonally symmetric monsoon might also explain the abrupt

onset of the southwesterly jet. This chapter does not present a comprehensive assessment of previous theories for monsoon onset in the context of observations, but instead examines the concurrent evolution of winds and thermodynamic variables in a quasi-equilibrium framework where convection is seen as part of the response, rather than as the external forcing. We do briefly discuss, however, theories invoking inertial or symmetric instability as a mechanism for abrupt onset (e.g. Krishnakumar and Lau, 1997).

The next section of this chapter outlines the data used in this study, and is followed by the definition of a dynamical index of Somali jet activity. This index is then used to make composites of the onset of the southwesterly jet. Composites of both winds and thermodynamic variables are assessed in a quasi-equilibrium framework, with particular attention given to the effect of wind-driven surface entropy fluxes on boundary layer entropy. Changes in some terms of the moist static energy budget are also briefly examined. We conclude with a short summary and some remarks on the consistency of the observationally-based composites with the results of the previous two chapters.

4.2 Data

Daily-mean data from the NCEP/NCAR Reanalysis (Kalnay et al., 1996) is used for estimates of winds for the years 1979-2005. While some details of the spatial and temporal variance of the Somali jet may be poorly represented in the low resolutions used in reanalysis data sets, no relevant *in situ* measurements of full-tropospheric behavior seem to exist for periods of multiple years (though it should be noted that the NCEP Reanalysis does assimilate satellite derived winds). Using scatterometer-derived surface wind speeds, Halpern et al. (1999) estimated the horizontal e-folding scale of the jet to be 200 km near the equator, and found that operational ECMWF analyses contained errors in the position and variance of surface winds associated with the southwesterly jet. However, Goswami and Sengupta (2003) examined the surface southwesterly jet in two years of the NCEP Reanalysis and found that although the reanalyzed winds contained errors in the seasonal mean intensity and intraseasonal variance of the jet, the timing and general character of its seasonal intensification were nearly identical with that seen in scatterometer data. For this reason, it seems reasonable to use reanalyzed winds in this first attempt at creating a composite of jet intensification. There is no obvious better alternative, because the use of

scatterometer data would limit our results to surface winds over ocean, and the core of the cross-equatorial jet is estimated to be positioned over the East African land surface (e.g. Findlater, 1971; Krishnamurti et al., 1983).

The only radiosonde stations that exist in the Arabian Sea are located on several islands about 500 km west of southern India, well east of the peak southwesterly jet but within the low-level westerlies that stretch across India to the Bay of Bengal during boreal summer (Durre et al., 2006). No radiosonde stations exist over the central or western Arabian Sea, or over the country of Somalia. Of the three stations off the southwest coast of India, only Minicoy at 8.3°N and 73°E has more than a few years of data, so we use 850 hPa wind speeds from this station to provide some evaluation of the reanalyzed winds. While this is not independent data because radiosonde winds are assimilated by the NCEP model, it provides some reassurance that the results are not model artifacts. The Minicoy wind speeds are linearly interpolated in pressure to 25 hPa resolution, and then averaged in time to daily resolution. No time interpolation was performed, so that days on which wind speeds were not collected were omitted from the composite averaging described in the next section.

We also examine how several other variables evolve in concert with the jet. As a proxy for deep moist convection, we use daily satellite-estimated outgoing longwave radiation (OLR) from NOAA, interpolated in both space and time, for the same period as the reanalyzed winds (1979-2005). For surface fluxes of latent and sensible heat we employ daily data from the Objectively Analyzed Air-Sea Fluxes project (OAFlux) at the Woods Hole Oceanographic Institute (Yu and Weller, 2007; Yu et al., 2004). The time range of this dataset is limited to 1981-2002, which is what we use here. Yu et al. (2007) examined the statistics of this OAFlux dataset in the Indian Ocean and found that, although the time mean was biased compared to in situ data from the Arabian Sea and Bay of Bengal, there was no major bias in the seasonal cycle of surface heat fluxes. They stated that ocean surface heat fluxes from the NCEP Reanalysis and the ERA40 products also had little bias in their seasonal cycle over the Indian Ocean, even though they exhibited a large bias in the time mean. Finally, we estimate the net source of atmospheric moist static energy, vertically integrated from the surface to the top of the atmosphere (TOA), using energy fluxes from the NCEP Reanalysis. In particular, we use the net surface fluxes of latent heat, sensible heat, and radiation, together with the net radiative flux at the top of the atmosphere (TOA). These are employed only in one diagnostic discussed in section 4.5.

4.3 Jet index definition

We create a scalar index of jet intensity by computing the square root of twice the spatial mean kinetic energy of 850 hPa horizontal wind over the Arabian Sea, in the same spatial domain examined by Krishnamurti et al. (1981): 5S - 20N, 50E - 70E. We use the square root of the kinetic energy, rather than the kinetic energy itself, to avoid the possibility that jet intensification may appear rapid only because of the use of a quadratic metric. Our choice of metric can also be viewed as a weighted average intended to emphasize the highest wind speeds occurring near the core of the jet, which is why the square root of twice the domain mean kinetic energy will henceforth be called the "jet speed".

The onset of the Somali jet was defined to occur at the start of the first three-day period, within each calendar year, during which the jet speed maintained a value more than one standard deviation above its 27-year mean. All statistics were computed with daily-mean data. A composite of the seasonal intensification was formed by averaging the jet speed over all 27 years of data relative to the onset date within each year. The mean onset date is June 5, with a standard deviation of 9 days. In the composite, the jet speed takes less than two weeks to completely transition from a mean winter to a mean summer value, while a best fit of the first three seasonal harmonics takes about seven weeks to undergo the same change (Fig. 4-1). Even a calendar-based climatological mean of the jet speed intensifies faster than the first three seasonal harmonics, although it evolves more slowly than the composite. Similar results were obtained when this analysis was repeated using the domain maximum wind speed as the index instead of the square root of twice the domain mean kinetic energy.

Radiosonde data at Minicoy confirm that wind speeds at 850 hPa downstream of the peak southwesterly jet increase abruptly during the week prior to jet onset (Fig. 4-2). The composite wind speed at 850 hPa for the 2.5 $\times$ 2.5° grid box in the NCEP data containing the Minicoy location exhibits a similar increase, though the NCEP composite time series is less noisy than the radiosonde composite. The large peak about 20 days after jet onset in the composite radiosonde time series seems to be the result of several tropical cyclones occurring near this time in some years of the dataset, and this peak disappears when wind speeds over 80 m s^{-1} are excluded from the composite averaging.

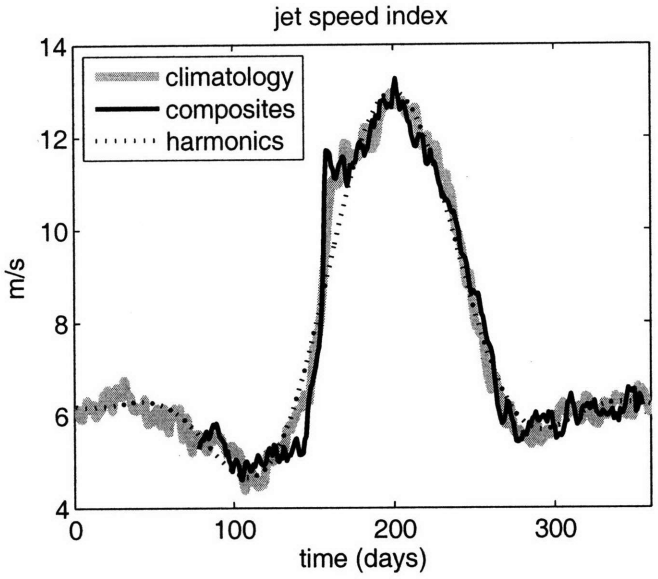

Figure 4-1: Annual cycle of the jet speed index in 27 years of NCEP Reanalysis data. The black line represents the composite evolution relative to the date of jet onset, the grey line is a calendar-based climatology, and the dotted line is the best fit of the first three Fourier harmonics of Earth's annual cycle to the composite evolution. Time is the number of days since January 1, with the composite time series shifted so that jet onset occurs at day 156, the mean onset date.

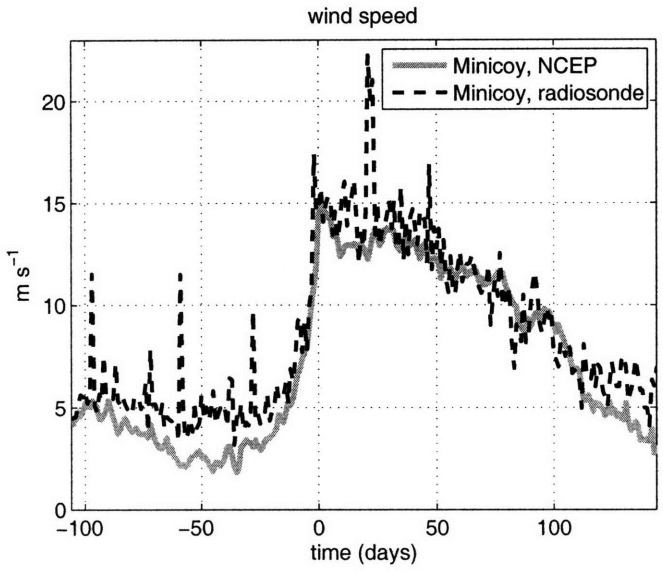

Figure 4-2: Composite evolution of the 850 hPa wind speed in the Minicoy radiosonde archive for 1979-2005 (black dashed line), and in the single grid point of the NCEP Reanalysis containing the Minicoy site for the same years (grey line). Time is the number of days after jet onset, as defined in the text.

4.4 Wind composites

This same compositing procedure is now used to examine how the dynamics over South Asia evolve with the onset of the jet (i.e. composites are formed by averaging wind fields relative to the date of jet onset). A composite of 850 hPa wind shows that before the onset of the jet, northern hemisphere westerlies peak south of India and have a magnitude around 5 m s^{-1} over the Arabian Sea (Fig. 4-3, top panel). Easterly trades persist in the southern hemisphere tropics, and low-level cross-equatorial flow occurs primarily over the east coast of Africa. Over the ten days preceding jet onset, the maximum wind speed increases by over 12 m s^{-1} near 10°N over the Arabian Sea, so that the jet speed index is most directly a measure of off-equatorial oceanic behavior (Fig. 4-3, bottom panel). Over the same ten day period, zonal winds also increase over southern India and the Bay of Bengal, cross-equatorial southerlies expand eastward from the coast of Africa, and flow becomes more northerly over the Arabian Peninsula.

The changes in wind accompanying jet onset extend through the full depth of the troposphere. At 60°E and 10°N, where the 850 hPa wind speed peaks, winds become more westerly from the surface up to 300 hPa over the ten days preceding jet onset (Fig. 4-4). An easterly tendency centered at 150 hPa has a similar magnitude over this ten day period, though at 60°E it is much less meridionally confined than the low-level westerly tendency.

Examination of the meridional wind averaged between 5°N and 5°S shows peak cross-equatorial southerlies of 10 m s^{-1} ten days before jet onset at 42°E and 925 hPa, adjacent to the East African highlands (Fig. 4-5, top panel). This is consistent with the location and intensity of cross-equatorial winds obtained by flight surveys (Findlater, 1972; Hart et al., 1978), bearing in mind that the winds and surface pressure obtained from the NCEP data represent averages over horizontal grid boxes several hundred kilometers in size. Cross-equatorial flow is also organized around the topography of the maritime continent, with local maxima of southerly flow occurring near the mountains of Sumatra, Borneo, and New Guinea, consistent with the analysis of scatterometer-derived surface winds by Chang et al. (2005). The increase in southerly flow over the ten days before jet onset is centered near 55°E, well separated from the East African highlands (Fig. 4-5, bottom panel). This increase in southerlies is also centered at a slightly higher altitude and extends deeper into the free troposphere than the peak topographically-bound flow. Upper-tropospheric northerlies

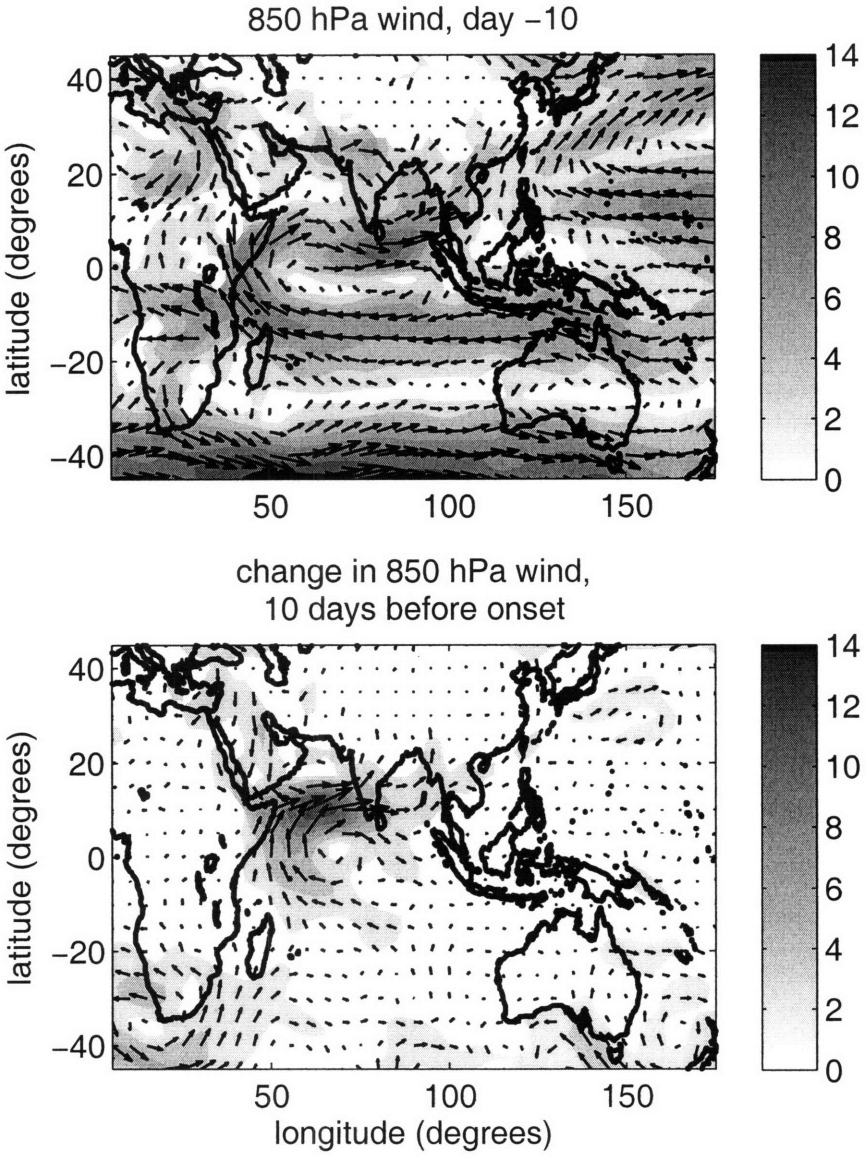

Figure 4-3: Vector wind at 850 hPa (arrows) and the magnitude of the vector wind (shading, in m s^{-1}). Top panel is a composite ten days before jet onset, and bottom panel is the composite change in vector wind over the ten day period preceding jet onset (shading in the bottom panel denotes the magnitude of the vectors, not the change in wind speed). Coastlines are shown by the thick black line.

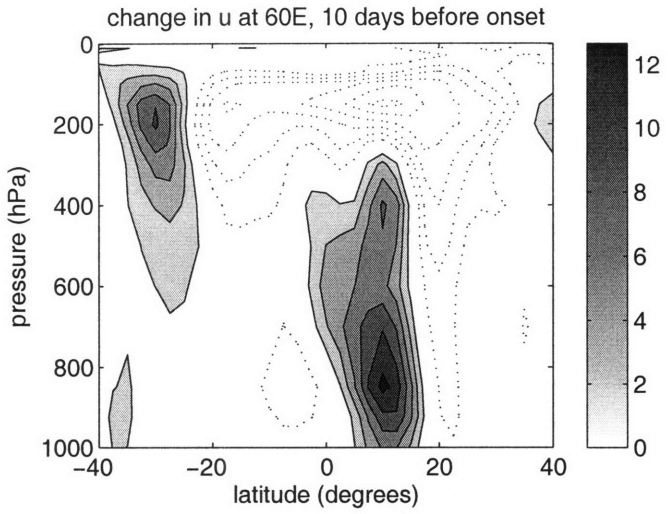

Figure 4-4: Vertical section of the composite change in zonal wind at 60°E over the ten day period preceding jet onset. Solid contours with shading denote winds becoming more westerly and dotted contours winds becoming more easterly. Contour interval is 2 m s^{-1} with the zero contour omitted.

intensify over a zonally broader band extending from East Africa to the Bay of Bengal. The rapid onset of the Somali jet should thus be thought of as an increase in off-equatorial southwesterlies over the Arabian Sea and an eastward expansion of cross-equatorial flow over the western Indian Ocean. It is not a rapid increase in the flow immediately adjacent to the East African topography, at least in reanalyzed winds.

The slower evolution of the core of the cross-equatorial jet can be seen in a composite time series of the southerly cross-equatorial mass flux integrated vertically through the troposphere and between 38.75°E and 48.75°E, which encompasses the peak flow immediately adjacent to the topography of the East African highlands (Fig. 4-6). Rapid intensification synchronous with jet onset is instead seen in the eastern periphery of the cross-equatorial jet, between 48.75°E and 71.25°E. These two regions, the core and eastern periphery of the cross-equatorial jet, each account for about one-quarter of the mass flux in the zonal mean cross-equatorial Hadley cell during boreal summer, consistent with the estimate by Findlater (1969) that flow between 35°E and 75°E makes up about half the global low-level mass flux. The fraction of zonal mean cross-equatorial flow associated with the abrupt onset of the southwesterly jet is thus at most 25 percent. The impact of this abrupt intensification on the zonal mean may be reduced by the fact that some low-level northerly

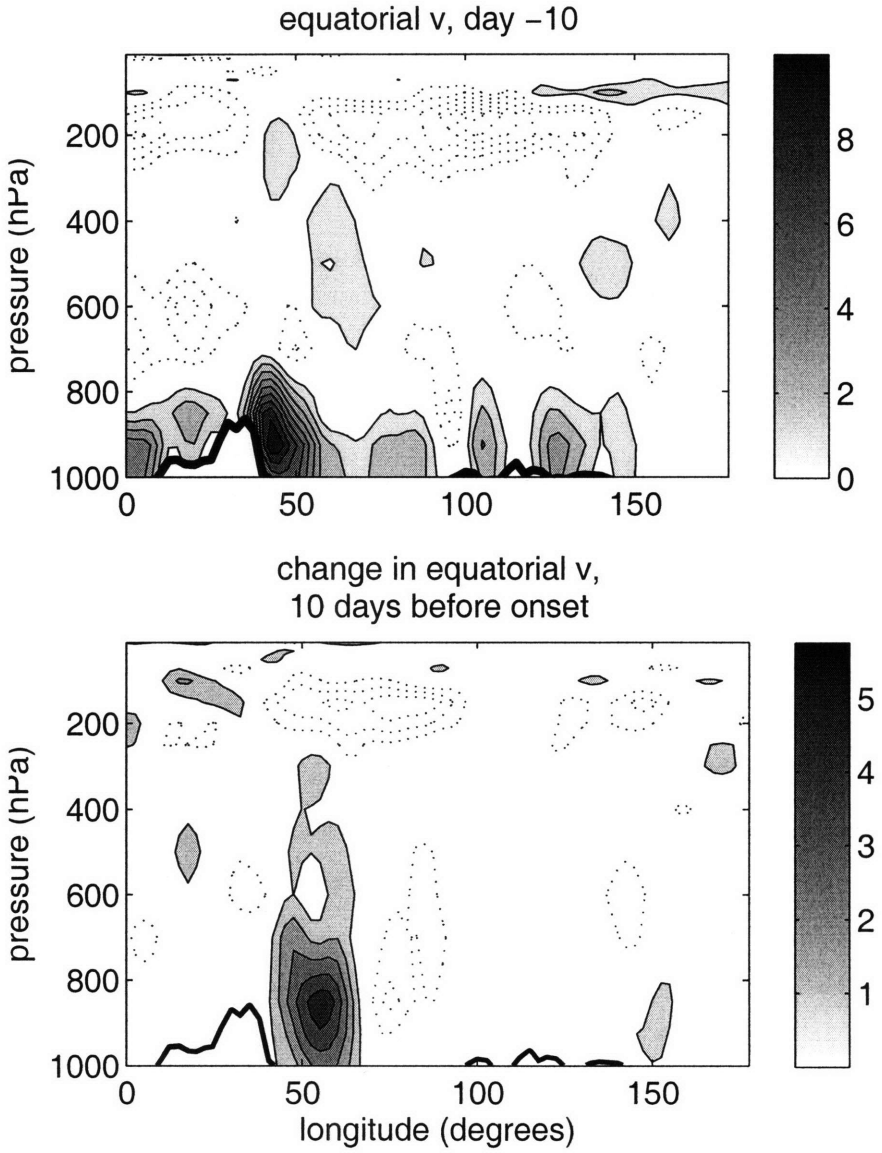

Figure 4-5: As in Fig. 4-3, but for a vertical section of the cross-equatorial meridional wind (mean between 5°S and 5°N, in m s^{-1}). Solid contours with shading denote northward flow and dotted contours southward flow. The contour interval is 1 m s^{-1} with the zero contour omitted.

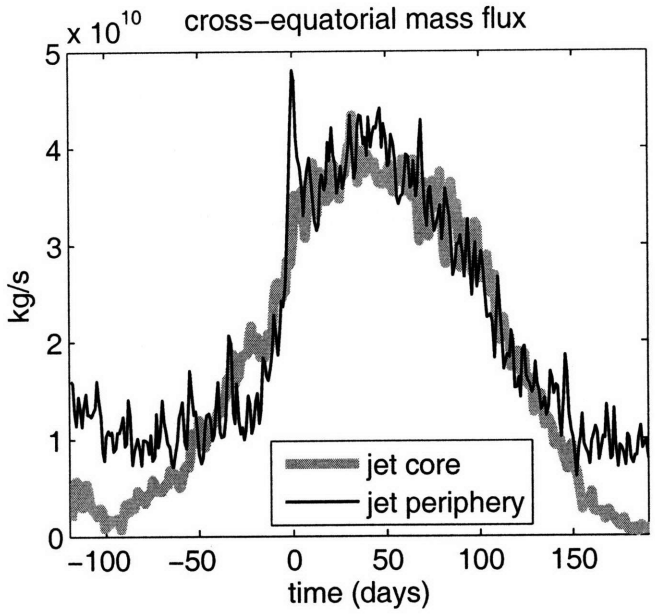

Figure 4-6: Composite evolution of the northward cross-equatorial mass flux in the NCEP Reanalysis for the core of the cross-equatorial jet (38.75°E - 48.75°E, grey line), and the eastern periphery of this jet (48.75°E - 71.25°E, black line). Time is the number of days after jet onset.

return flow seems to occur east of the jet periphery (around 75°E, see bottom panel of Fig. 4-5), consistent with the southward turning of the jet discussed by previous authors (e.g. Rodwell and Hoskins, 1995). Together, these findings may explain why Dima and Wallace (2003) did not find any abrupt signal of monsoon onset in a scalar index of the zonal mean Hadley circulation, despite the strong projection of South Asian summer monsoon flow on the boreal summer Hadley circulation.

Composites of the absolute vorticity, η, of the 850 hPa horizontal wind show that the $\eta = 0$ contour shifts from about 3°N to 8°N over the central Arabian Sea during the ten days before jet onset (Fig. 4-7). Directly over the east coast of Africa, the vorticity distribution changes little over these ten days, consistent with the slower evolution of winds in this region. Over the Arabian Sea, the meridional gradient of η increases and a local maximum of η forms just south of the Arabian Peninsula during the ten days before jet onset. The poleward shift of the $\eta = 0$ contour is accompanied by the formation of a low-level vertical velocity dipole over the Arabian Sea that is nearly bisected by this contour, with ascent north of the contour and weaker subsidence on and to the south of the contour (Fig. 4-8).

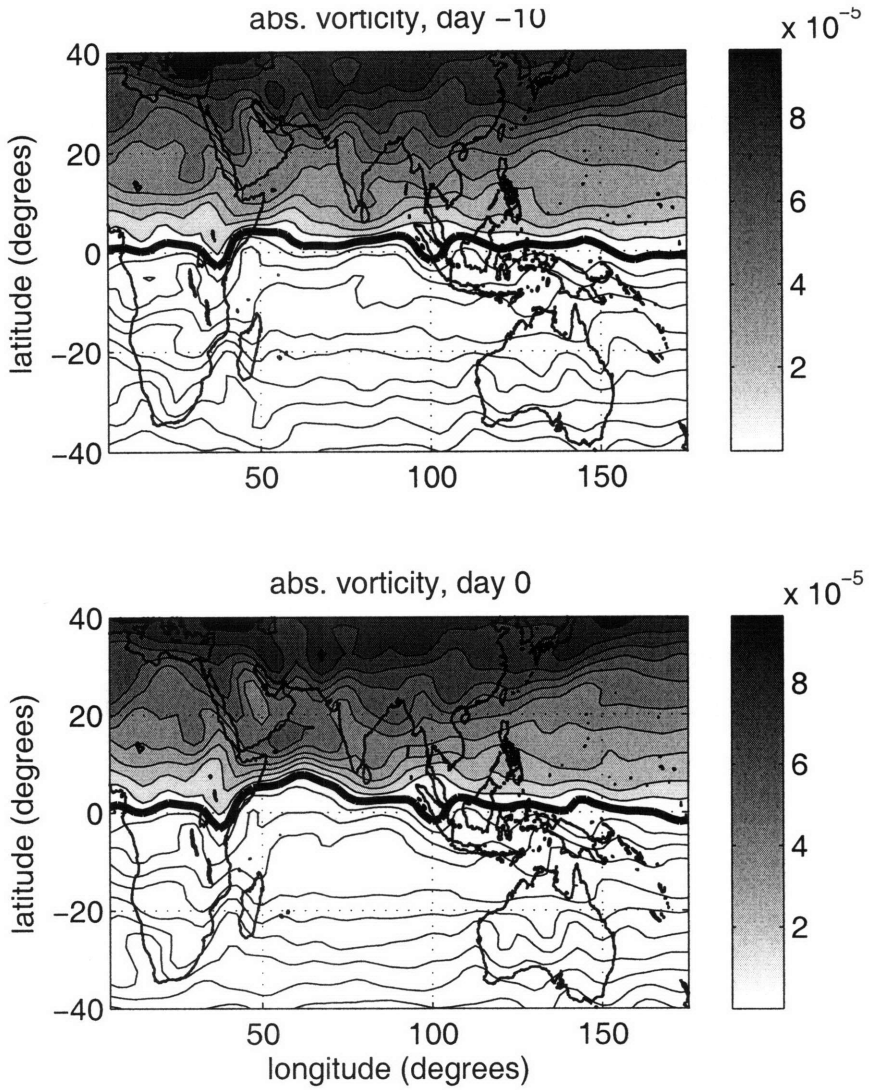

Figure 4-7: The composite absolute vorticity of the 850 hPa horizontal wind ten days before jet onset (top) and on the day of jet onset (bottom). Note that, unlike previous figures, the bottom panel shows the total quantity on the day of onset. Positive values are shaded with a contour interval of 1×10^{-5} s^{-1}, and the thick solid line is the zero contour.

Low-level ascent also increases just south of the Arabian Peninsula even though the $\eta = 0$ contour does not undergo a large poleward shift at these longitudes. The zonally elongated band of ascent that stretches across northern Africa and the ascent maximum just south of the Tibetan plateau exhibit little coherent change over the ten days before jet onset. The significance of the poleward shift of the $\eta = 0$ contour is discussed in a later section of this chapter.

The composite potential vorticity (PV) exhibits some fairly rapid changes at upper levels. For a limited zonal mean encompassing the western half of South Asia (50-110°E), the zero contour of Ertel's PV at 350 K shifts from the equator to about 8°S over the 20 days *after* the onset of the Somali jet (Fig. 4-9). While the 350 K isentrope may be as much as 100 hPa below the tropopause over South Asia during boreal summer, it is used here because it is the closest isentropic surface to the tropopause for which PV is provided directly in the NCEP Reanalysis; calculation of PV on a slightly higher isentrope could be performed in future work. The location of the zero PV contour may not be the most dynamically relevant quantity, as the transition to a thermally direct flow regime is theoretically associated with upper-level PV that approaches zero in the region of upper-level divergence (Plumb, 2007). PV is considerably reduced over South Asia during boreal summer, with the onset of the jet occurring during a poleward shift of the 0.5 PVU contour from 20 to 30°N. This poleward shift is actually due to a large reduction in the PV at 350 K centered over the southwest edge of the Tibetan Plateau, with strong reductions also seen near Japan and northeastern Africa (Fig. 4-10).

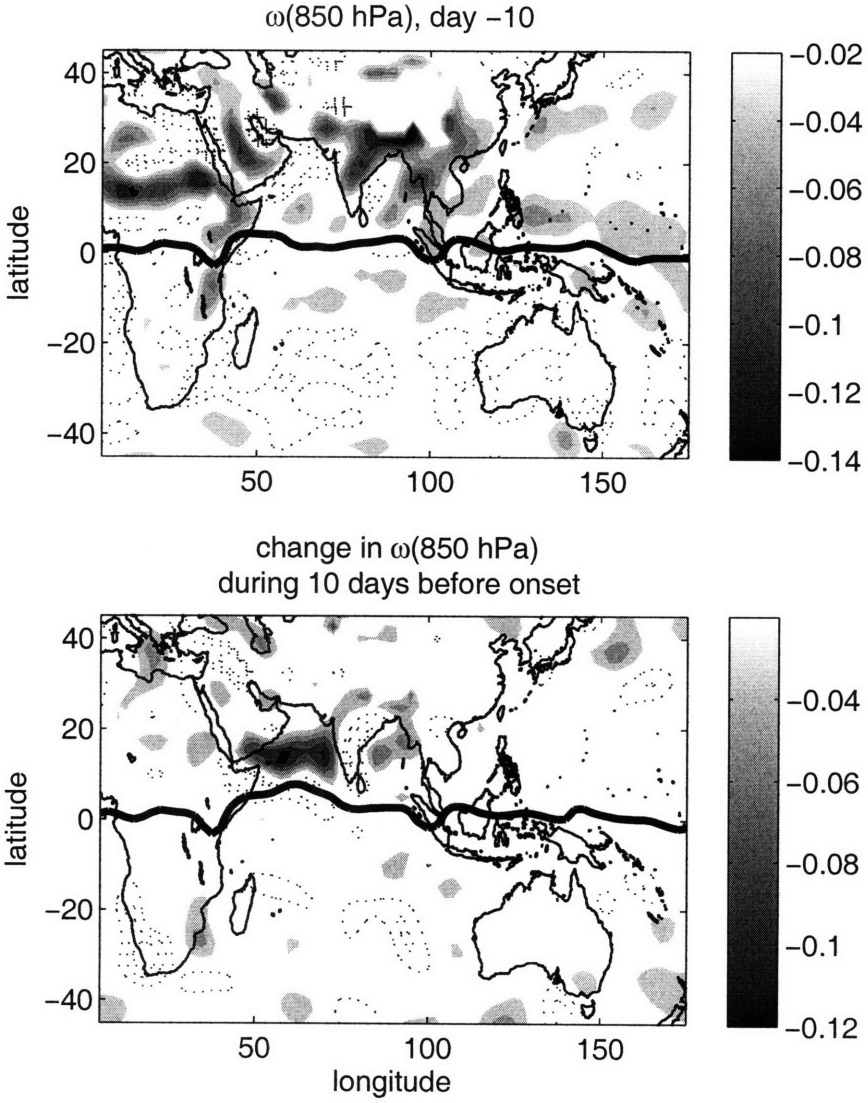

Figure 4-8: As in Fig. 4-3, but for the vertical velocity at 850 hPa. Shading denotes ascent and dotted contours subsidence. Contour interval is 0.02 Pa s^{-1} with the zero contour omitted. Thick solid line is the zero contour of 850 hPa absolute vorticity; note that this contour in the bottom panel is the total absolute vorticity (not the change) on the day of jet onset.

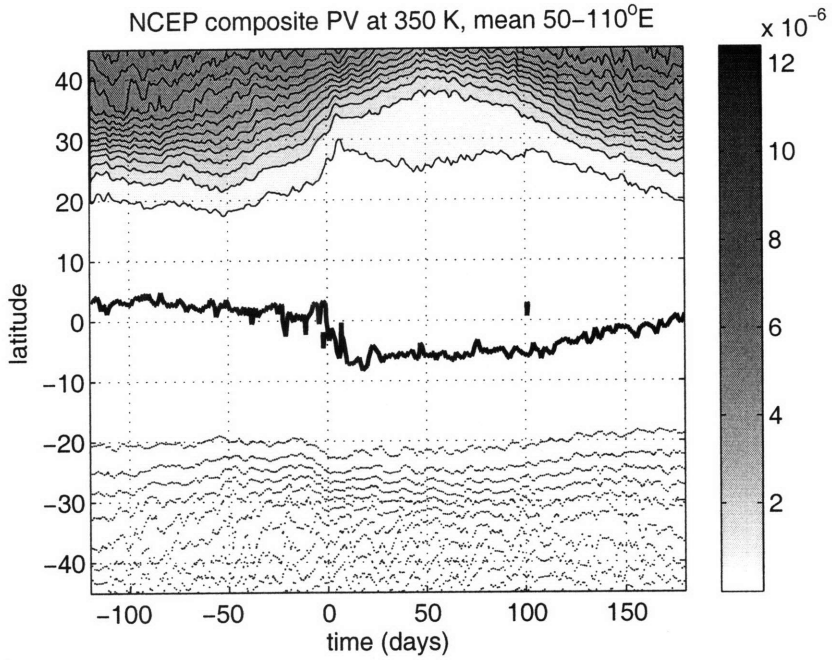

Figure 4-9: Composite evolution of potential vorticity at 350 K, from the NCEP Reanalysis, averaged 50-100°E. Time is number of days before jet onset. Contour interval is 0.5 PVU, with negative contours dotted, positive contours solid, and the zero contour denoted by a thick black line.

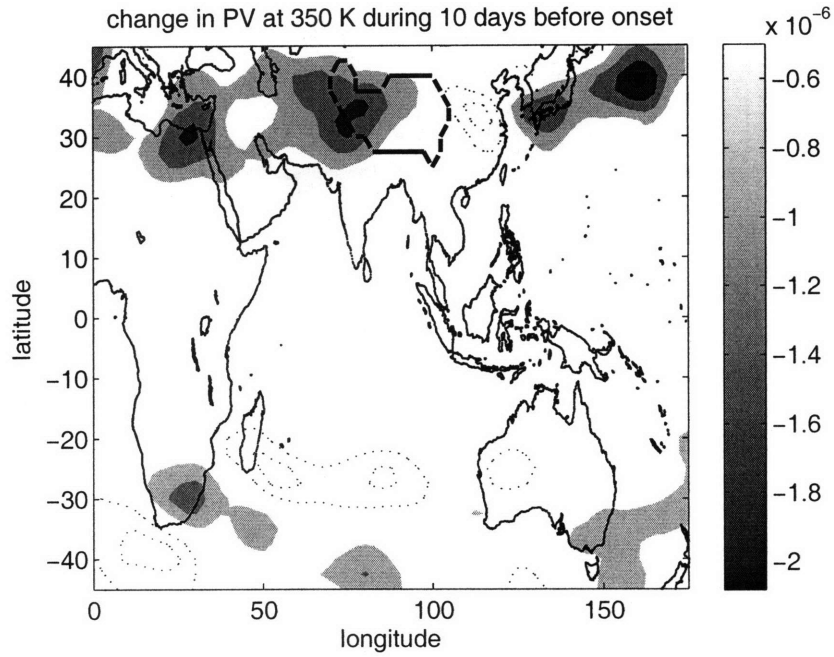

Figure 4-10: Composite change in potential vorticity at 350 K, from the NCEP Reanalysis, over the 10 days before jet onset. Shading denotes a decrease and dotted contours an increase, with a contour interval of 0.5 PVU and the zero contour not shown. Thick dashed line surrounds regions with surface pressures lower than 700 hPa.

4.5 Thermodynamic composites

The composites just discussed show that changes associated with the onset of the southwesterly jet have a strong baroclinic component, with an increase in low-level convergence occurring concurrently with an increase in the vertical shear of both zonal and meridional winds. These baroclinic changes are accompanied by an increase in deep convective activity, as evidenced by a reduction in OLR peaking at more than 70 W m^{-2} over the Arabian Sea and stretching across India into the northern Bay of Bengal (Fig. 4-11). This change in OLR is similar to behavior described by previous authors for the onset of the Indian monsoon (e.g. Webster et al., 1998; Li and Yanai, 1996), and supports the association of the start of Indian monsoon rains with the onset of the Somali jet.

As noted in the introduction, a number of previous studies of the structure of the Somali jet have specified either a cumulus heating or a pressure gradient as an external forcing (e.g. Krishnamurti and Wong, 1979; Rodwell and Hoskins, 1995). The composite of OLR just discussed shows that the convective forcing evolves in concert with the southwesterly jet. Geopotential over the Arabian Sea also changes abruptly with the onset of the jet (Fig. 4-12, top panel), which is expected to the degree that the jet is in balance with the height field. Indeed, the 35 m depression of geopotential height over the Arabian Sea has a meridional scale of about 10° of latitude and would thus balance a geostrophic wind of 12 m s^{-1}, which is almost exactly equal to the change in wind speed in this region (compare with bottom panel of Fig. 4-3). The fact that increased deep convection and geopotential gradient occur synchronously with jet onset makes it difficult, at best, to treat either of these as an external forcing for the jet.

In the remainder of this section we examine the onset of the Somali jet in a convective quasi-equilibrium framework, following many of the ideas set forth by Emanuel et al. (1994). In such a framework, latent heating is assumed to simply maintain the temperature structure of the free troposphere near that of a moist adiabat, thereby tying free tropospheric geopotential to the entropy of the subcloud layer. The changes in convection and low-level geopotential accompanying jet onset can then be seen as part of a convectively-coupled response, rather than as an external forcing for the dynamics.

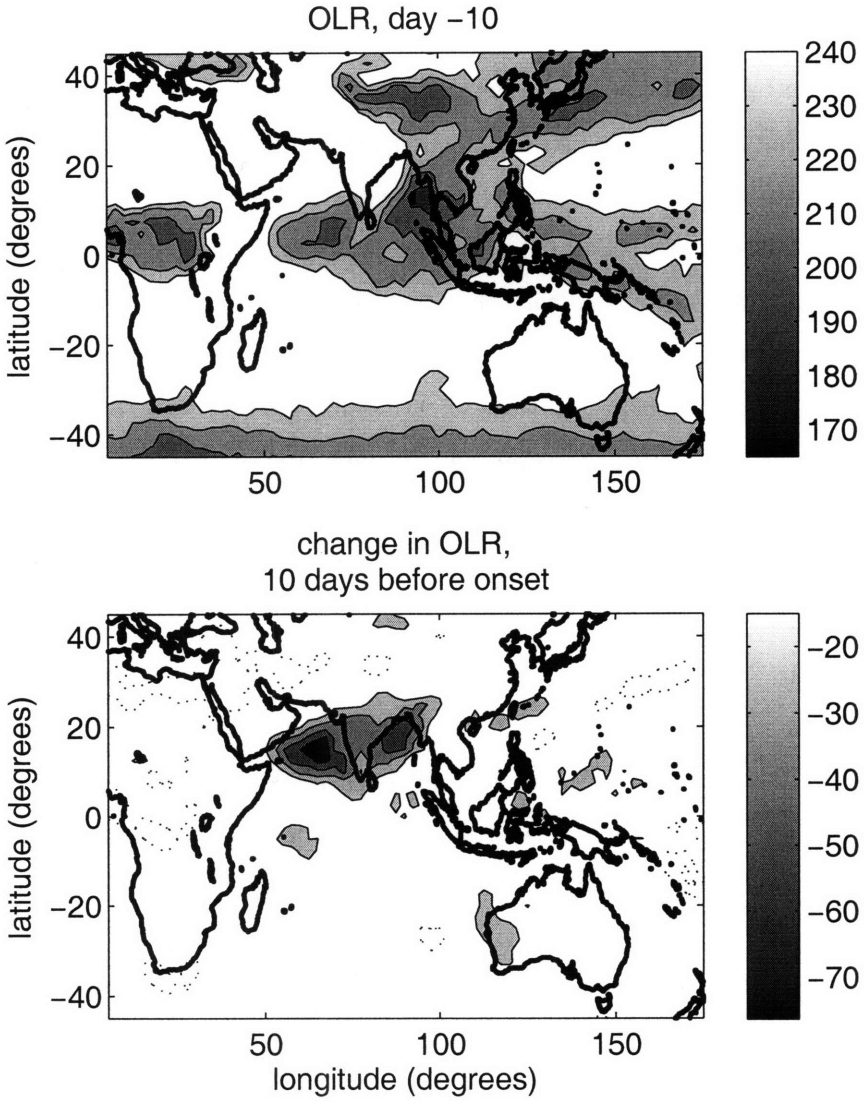

Figure 4-11: As in Fig. 4-3, but for NOAA OLR. In the top panel, only values below 240 W m^{-2} are contoured. In the bottom panel, solid contours with shading denote a reduction in OLR, while dotted contours denote an increase. The contour interval in both panels is 15 W m^{-2}, with the zero contour omitted in the bottom panel.

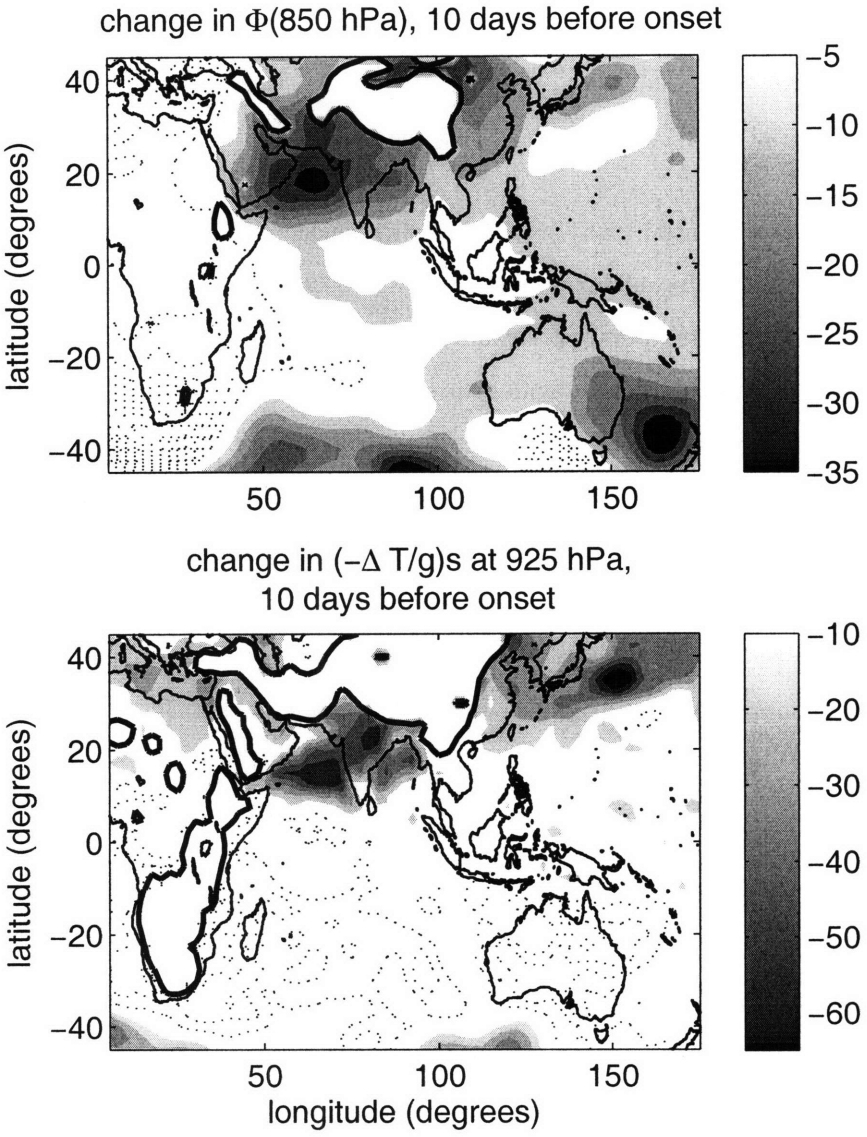

Figure 4-12: Top panel shows the composite change in the NCEP Reanalysis geopotential height at 850 hPa over the ten day period preceding jet onset. Contour interval is 5 m. Bottom panel shows the change in geopotential height at the top of the subcloud layer expected in the quasi-equilibrium framework if the 925 hPa entropy from the NCEP Reanalysis is used for the subcloud entropy. Contour interval is 10 m. In both panels, shading denotes a decrease, dotted contours an increase, and the zero contour is omitted. Regions with surface pressure less than 850 hPa and 925 hPa are masked out of the top and bottom panels, respectively.

4.5.1 Assessment in a quasi-equilibrium framework

In the quasi-equilibrium framework discussed by Emanuel et al. (1994), changes in free tropospheric temperature, or equivalently in the thickness of the convecting layer, are directly related to changes in the subcloud layer entropy, s_b:

$$\delta\Phi(p) - \delta\Phi_b = \delta s_b(T_b - T(p)) \tag{4.1}$$

Here Φ is the geopotential of a certain pressure surface, and the subscript b denotes a property at the top of the subcloud layer. The temperature T acts as a vertical coordinate, and its horizontal and temporal variations are henceforth presumed to be small compared to its vertical variations. This provides an expression for changes in the thickness of the convecting layer if $\delta\Phi$ and T are evaluated at the top of that layer. As shown by Emanuel (1987), if we are concerned only with the baroclinic aspects of the system and assume $\omega = 0$ at the top of the convecting layer and at the bottom of the subcloud layer, then changes in the thickness of the convecting layer must be accompanied by equal and opposite changes in the thickness of the subcloud layer. That is, vertical integration of (4.1) gives an expression for changes in subcloud layer height for purely baroclinic anomalies:

$$\delta\Phi_b = -\delta s_b(T_b - \overline{T}) \tag{4.2}$$

Here the overbar denotes a vertical, mass-weighted integral from the surface to the top of the convecting layer.

It may be possible to view the abrupt changes in wind over the Arabian Sea as a baroclinic anomaly because, as noted in the previous section, upper-tropospheric easterlies increase concurrently with lower-tropospheric westerlies during the ten days before jet onset (Fig. 4-4). If these changes in wind can be well-represented by a baroclinic anomaly in the quasi-equilibrium framework, then (4.2) should describe the accompanying changes in boundary layer geopotential and entropy. To test this, we compare the change in Φ at 850 hPa with the change in s at 925 hPa over the ten days preceding jet onset. While a more theoretically correct procedure would involve using the geopotential of the lifted condensation level for Φ_b and the mean, mass-weighted entropy below this level for s_b, this is computationally more difficult and of questionable accuracy when using soundings from

reanalyzed data. Given the absence of radiosonde stations in the Arabian Sea, a dataset may not exist, outside of isolated field campaigns, with which this more detailed procedure could be performed for the peak southwesterly jet. So here we use Φ(850 hPa) and s(925 hPa) to represent Φ_b and s_b, respectively, with s_b scaled by the factor $[\overline{T} - T(850\text{ hPa})]/g$ for direct comparison with the geopotential height. The temperatures $\overline{T}$ and T(850 hPa) are assumed to be spatially and temporally invariant, and are computed assuming a surface temperature of 30°C, a dry adiabat up to 900 hPa, and a moist pseudoadiabat between 900 hPa and 150 hPa.

The resulting plots of $\delta\Phi_b$ and the scaled δs_b for the ten days preceding jet onset both show minima over the Arabian Sea, with strong meridional gradients nearly coincident with the zonal jet (Fig. 4-12; note that the entropy has increased where the scaled δs_b is negative). The scaled δs_b minimum is centered slightly south of the $\delta\Phi_b$ minimum, and has almost twice the peak amplitude and a narrower distribution. The scaled entropy also has a secondary minimum over India which is not clearly evident in the $\delta\Phi_b$ distribution. Some of these differences might be accounted for by horizontal homogenization of free-tropospheric temperatures by gravity waves, which would be consistent with $\delta\Phi_b$ appearing as a smoothed version of δs_b. Overall, the two distributions are sufficiently similar that it seems reasonable to describe the onset of the southwesterly jet as being roughly in balance with subcloud layer entropy under the assumption of convective quasi-equilibrium. Note that the distributions of $\delta\Phi_b$ and δs_b are not expected to be similar where deep convection is suppressed (e.g. in much of the Southern Hemisphere).

The Tibetan Plateau has long been thought to play an important role in the dynamics of the South Asian monsoon (e.g. Flohn, 1974; Hahn and Manabe, 1975), so it may seem inappropriate to exclude elevated terrain by using entropy at 925 hPa as a proxy for s_b. Computation of the change in subcloud layer entropy over the highly variable topography of South Asia, however, would best be accomplished in a terrain-following σ coordinate system. We intend to perform this task in future work, but emphasize here that the Tibetan Plateau should not be thought of as a region of peak subcloud entropy at any point in the seasonal cycle. A climatological summer mean of θ_e on the near-surface 0.995σ layer in the NCEP Reanalysis shows oceanic maxima over the northernmost parts of the Arabian Sea, Bay of Bengal, and South China Sea (Fig. 4-13). Values of θ_e over the southern Tibetan Plateau are similar to those over non-elevated regions of China at the same latitude, and θ_e decreases

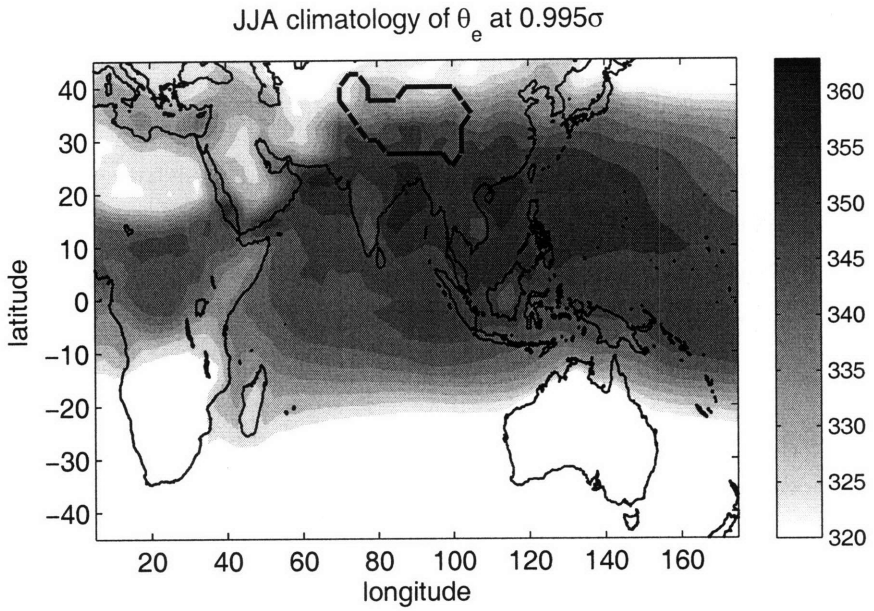

Figure 4-13: The climatological mean equivalent potential temperature on the 0.995σ surface of the NCEP Reanalysis for June-August. Contour interval is 4 K, with shading starting at 320 K. The dashed line surrounds regions with surface pressure 700 hPa or lower (i.e. the Tibetan Plateau).

poleward over the plateau at a faster rate than over the nonelevated terrain to the east. While it is the location of maximum change in subcloud entropy that is relevant to the phenomenon of monsoon onset, it is nevertheless interesting to see the absence of a large signal of the Tibetan plateau in the time mean quantity. In the next section, assessment of some terms in the moist static energy budget will shed some additional light on behavior on or near the Tibetan Plateau.

A fairly obvious candidate for the cause of the change in s_b over the Arabian Sea is a wind-driven increase in surface entropy flux, which would be consistent with the abrupt onset of the jet being caused by wind-evaporation feedback. A composite from the OAFlux dataset shows an increase in surface enthalpy fluxes of over 80 W m^{-2} over the Arabian Sea during the ten days before jet onset (Fig. 4-14). Surface enthalpy fluxes also increase by about 50 W m^{-2} over the southern Indian Ocean. Over ocean, the total enthalpy flux as well as the increase are made up almost entirely of the latent heat flux (not shown). This increase in ocean evaporation is consistent with measurements collected over the course of one year from a surface mooring deployed in the Arabian Sea along the climatological axis of the southwesterly Somali jet (Weller et al., 1998). In that study, ocean evaporation peaked

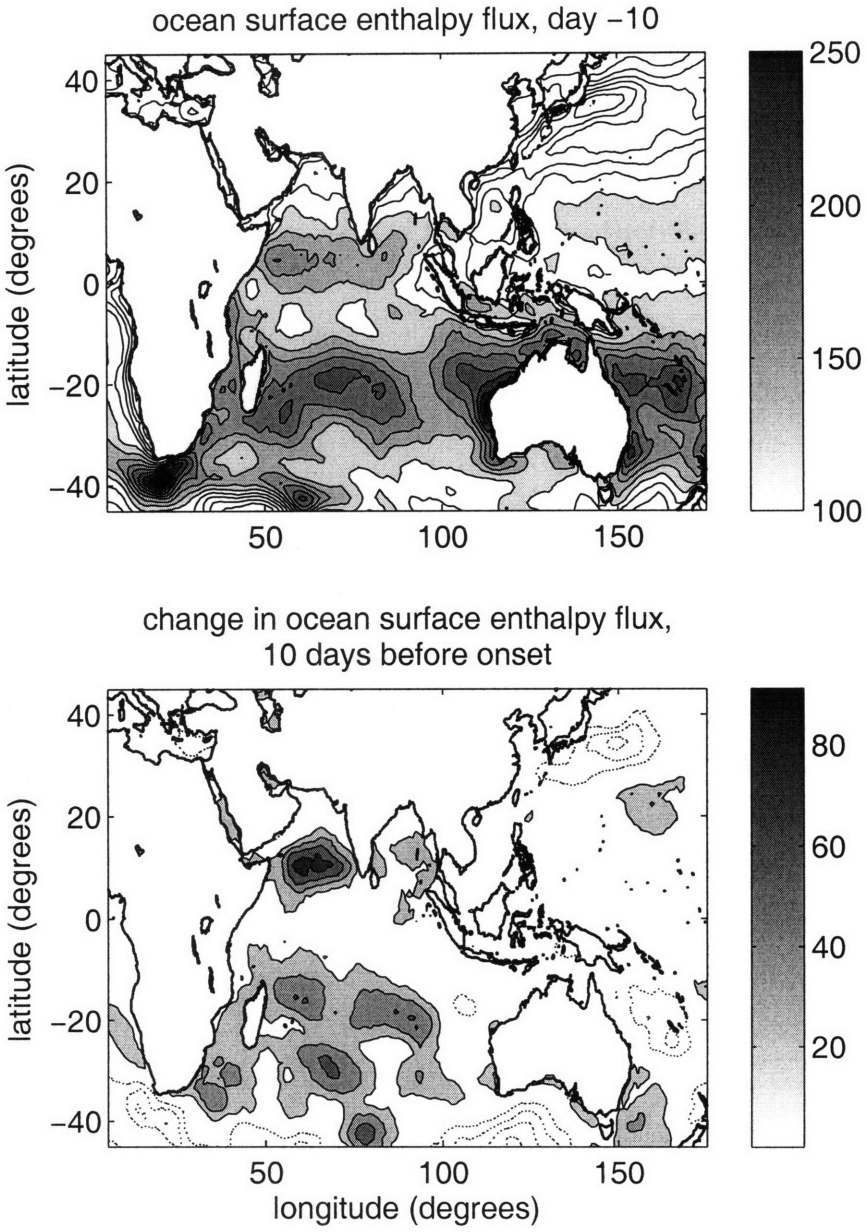

Figure 4-14: As in Fig. 4-3, but for the ocean surface enthalpy flux from the OAFlux project. Contour interval is 20 W m^{-2} in both panels. Shading in the top panel starts at 100 W m^{-2}. In the bottom panel, solid contours with shading denote an increase and dotted contours a decrease, with the zero contour omitted.

shortly after the onset of the southwesterly jet, then decreased as the summer monsoon season progressed due to both a reduction in SST and an increase in the relative humidity of surface air over the Arabian Sea. Our composites should thus be taken as representative of conditions only at the time of jet onset and not during the mean summer monsoon.

The increase in surface enthalpy fluxes over the ten days before jet onset is about ten times larger than that needed to produce the composite increase in s_b, assuming that the entropy is mixed over a boundary layer depth of 100 hPa and that there is no change in processes that reduce subcloud entropy. This suggests that a large part of the increase in surface entropy fluxes is balanced by changes in convective downdrafts, horizontal advection, or subsidence between cumulus clouds. In fact, it would be surprising if all of these processes did not play a role in setting s_b, given the concurrent increases in deep convection and horizontal flow. The fact that the increase in surface enthalpy fluxes seems to be collocated with the increase in s_b and is not completely compensated for by some other negative tendency suggests that the system is gaining energy. Indeed, a positive correlation between surface enthalpy fluxes and s_b (which are the analogues of heating and temperature in quasi-equilibrium) is responsible for the linear instability of WISHE (wind-induced surface heat exchange) modes in analytical theories (Yano and Emanuel, 1991; Emanuel, 1993). An increase in the potential energy of the system and the conversion of potential to kinetic energy would be expected to accompany the intensification of the baroclinic circulation associated with the Somali jet. Closer inspection shows that the increase in surface enthalpy fluxes is centered about 5° south of the increase in s_b over the Arabian Sea, with the reduction in OLR more closely collocated with the s_b change. This slight offset is not inconsistent with a wind-evaporation feedback, as disturbance growth does not require that anomalies of evaporation and s_b be precisely in phase, but only that they have a positive correlation over the whole domain. We have not computed this correlation because it is unclear whether the data are sufficiently reliable for such a detailed assessment of the energetics of jet intensification.

The relation (4.2) was derived by assuming Φ_b is altered only by purely baroclinic dynamics, an assumption that can be quantitatively tested by comparing changes in free-tropospheric wind to those expected from the simple theory outlined above. For a strictly baroclinic anomaly in the quasi-equilibrium framework, the moist adiabatic temperature structure can also be used to define the vertical structure of a first baroclinic mode in

horizontal wind:

$$u(p) = u_0 + u_1 \left(\frac{T(p) - \overline{T}}{\Delta T} \right) \tag{4.3}$$

where $\Delta T \equiv T_b - \overline{T}$ and u_1 is then the wind speed at the top of the subcloud layer. A vertically uniform barotropic wind speed is represented by u_0. This is the same definition of the first baroclinic mode used in the two-mode model of the previous two chapters, and is similar to that used in the Quasi-Equilibrium Tropical Circulation Model (QTCM) of Neelin and Zeng (2000). We compare this vertical structure with that of the composite change in zonal wind over the ten days before jet onset at the location of peak low-level southwesterlies, 60°E and 10°N. Employing the same moist adiabat used previously to scale s_b, a decent fit is obtained using $u_0 = 7.3$ m s^{-1} and $u_1 = 8.1$ m s^{-1} (Fig. 4-15). While the composite vertical structure shows a secondary maximum at 400 hPa and a secondary minimum at 600 hPa that may project onto higher baroclinic modes, the fit seems a good approximation to the gross vertical structure in the free-troposphere. We have not attempted to fit the wind below 850 hPa because the idealized quasi-equilibrium theory discussed here does not account for boundary layer dynamics. While the presence of a strong barotropic component in the abrupt changes in wind over the Arabian Sea introduces additional complexity, it is consistent with the WISHE feedback discussed in the previous two chapters.

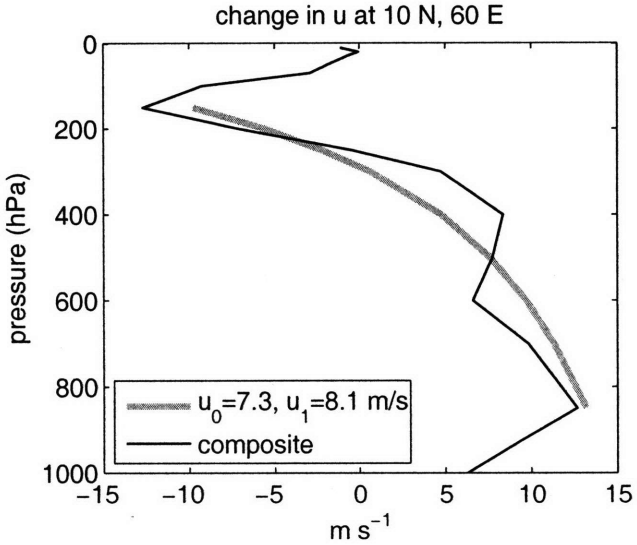

Figure 4-15: Vertical profile of the composite change in zonal wind at 60°E and 10°N from the NCEP Reanalysis over the ten days preceding jet onset (solid line), and the best fit to this profile of two modes (one barotropic and one baroclinic) from the quasi-equilibrium framework (dashed line).

The relation (4.1) was derived by assuming convection constrains free tropospheric temperatures to be moist adiabatic, so that any change in subcloud layer entropy results in the same change in the saturation entropy of the free troposphere:

$$\delta s^* = \delta s_b \tag{4.4}$$

Examination of changes in free-tropospheric s^* can thus provide an additional check on the idealized quasi-equilibrium framework used here. We compute the mass-weighted vertical mean s^* between 450 hPa and 175 hPa, take the composite relative to the date of jet onset, then convert this composite s^* to θ_e^* using the definition of saturation equivalent potential temperature. The lower bound of 450 hPa was used to minimize any contribution of boundary layer air over the Tibetan Plateau to the vertical mean. Ten days before jet onset, the composite θ_e^* peaked over coastal regions of the northeast Bay of Bengal, near the latitude of the s_b peak but with a clear bias toward the eastern part of South Asia (Fig. 4-16). Over the ten days preceding jet onset, the increase in θ_e^* is centered over the western edge of the Tibetan Plateau, about 15° poleward of the peak δs_b. A large part of the increase in θ_e^* occurs in a region of subsidence, and in quasi-equilibrium subcloud entropy is expected to be decoupled from free-tropospheric temperature where the adiabatic warming due to subsidence is large enough to balance radiative cooling. That is, (4.4) is not expected to hold where convection is suppressed by strong subsidence. The thick dashed line in the bottom panel of Fig. 4-16 surrounds regions where subsidence at 300 hPa is larger than that needed to balance a 1 K day^{-1} radiative cooling, assuming a stratification equal to the spatial mean stratification found in the NCEP data within 40° of the equator at 60°E on the day of jet onset. This region of strong subsidence encompasses a large part of the region in which δs^* peaks, suggesting that the offset between the peaks of δs_b and δs^* is not inconsistent with the quasi-equilibrium hypothesis.

Nevertheless, this leaves open the question of what mechanism is responsible for the peak increase in s^* over the western edge of the Tibetan Plateau. Here we note several potentially relevant processes, but leave a detailed exploration of this issue for future work. The fact that the peak increase in s^* occurs immediately west of the Tibetan Plateau suggests that topography may play an important role in setting δs^*, through either thermal or mechanical effects. Another possibile mechanism might involve the transient dynamics

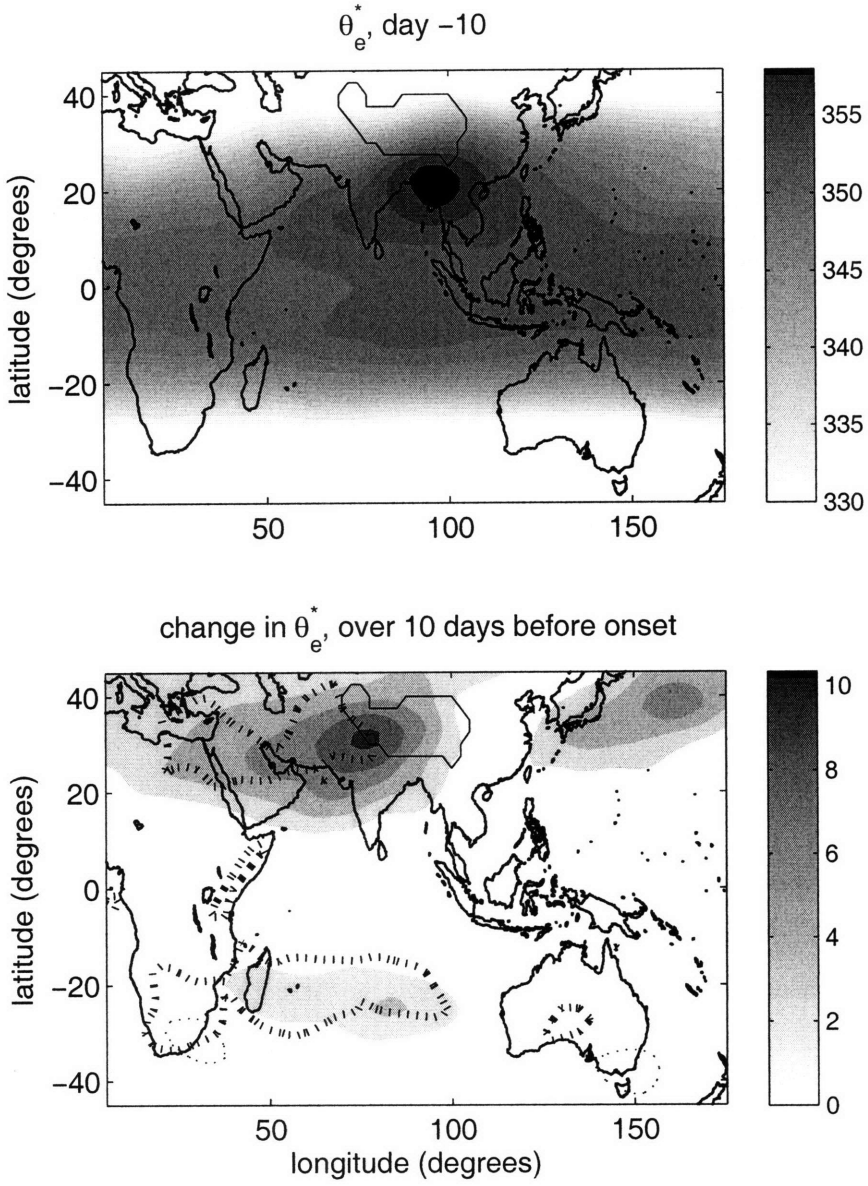

Figure 4-16: As in Fig. 4-3, but for the vertical mean from 450 hPa to 175 hPa of the saturation entropy, displayed as the saturation equivalent potential temperature. In both panels, the contour interval is 2 K and the thin line surrounds regions with surface pressure 700 hPa or lower. Shading starts at 320 K in the top panel. In the bottom panel, shading denotes an increase and thin dotted contours a decrease, with the zero contour omitted. The thick dashed line in the bottom panel surrounds regions where subsidence at 300 hPa is stronger than that needed to balance a 1 K day^{-1} radiative cooling (see text for details).

of a transition to angular momentum conserving (AMC) flow. We make this suggestion because the distribution of δs^* is zonally elongated with an equatorial minimum suggestive of a temperature distribution needed to balance AMC flow, and the peak increase in s^* is nearly collocated with the peak reduction in PV seen at 350 K (compare the bottom panel of Fig. 4-16 with Fig. 4-10). Also, the free-tropospheric stratification (i.e. $-\partial_p\theta$) in the NCEP Reanalysis increased by about 30 percent over the ten days before jet onset in the regions of peak δs^*, both near the δs^* peak at 25°N and near the peak at 25°S (not shown). Some part of the increase in s^* might thus be due to subsidence warming, perhaps even as part of a transient wave response to the deep ascent occurring over the Arabian Sea and Bay of Bengal.

4.5.2 Assessment of the moist static energy budget

Rather than viewing the evolution of the southwesterly jet as being controlled by boundary layer entropy, changes in the circulation can be related directly to changes in the source of moist static energy, an approach used by Neelin and Held (1987). The vertically integrated, steady state budget for moist static energy, h, is:

$$\langle \mathbf{v_h} \cdot \nabla h \rangle + \left\langle \omega \frac{\partial h}{\partial p} \right\rangle = Q \tag{4.5}$$

where triangle brackets denote mass-weighted vertical integrals from the surface to the top of the atmosphere, and $\mathbf{v_h}$ is the horizontal wind. Here Q is the net source of moist static energy in an atmospheric column, which is equal to the net surface enthalpy flux plus the net atmospheric radiative flux convergence. We consider the idealized case where horizontal advection is negligible and the vertical velocity has a constant vertical structure given by the function $\Omega(p)$:

$$\omega(p) \equiv \overline{\omega}\Omega(p) \tag{4.6}$$

where $\overline{\omega}$ is a scalar. The vertical velocity then increases with the net column source of moist static energy:

$$\overline{\omega} = \frac{Q}{\left\langle \Omega(p)\frac{\partial h}{\partial p} \right\rangle} \tag{4.7}$$

It is entirely possible that the gross moist stability $\left\langle \Omega(p)\frac{\partial h}{\partial p} \right\rangle$ will vary in both space and time. Elevated terrain, in particular, might be expected to alter $\partial h/\partial p$ to the degree

that surface temperatures and humidities are invariant with surface height [see Molnar and Emanuel (1999) for details on this invariance in radiative-convective equilibrium]. Here we limit our scope to the idealized case where the gross moist stability is constant in space and time, leaving an examination of the seasonal cycle of gross moist stability for future work.

The moist static energy source Q is computed by summing the surface enthalpy flux and the net atmospheric radiative flux divergence, both obtained from the NCEP Reanalysis. Although the NCEP estimates of surface enthalpy fluxes are presumably less accurate than the OAFlux estimates used in the composites, they are used here because they contain data over both land and ocean and provide a dataset expected to be at least roughly internally consistent in its energetics. Ten days before jet onset, this Q field has maxima roughly collocated with the peak low-level zonal winds. Then over the ten days before jet onset, Q increases by 200 W m^{-2} at the location of the peak southwesterly jet (Fig. 4-17). Weaker increases also occur in the Bay of Bengal and the southwest Indian Ocean. A reduction in the atmospheric radiative flux divergence accounts for about one-quarter of the increase in Q over the Arabian Sea in the NCEP data (Fig. 4-18). The composite increase in the NCEP net surface enthalpy flux over the Arabian Sea (not shown) is almost twice as large as that found in the OAFlux data, although the two do have a similar spatial pattern.

The change in Q over nearly all land surfaces during the ten days before onset is less than 20 W m^{-2}, which is likely due to the constraint that the land surface heat capacity places on the energy budget. The energy budget for a near-surface soil layer is:

$$C_s \frac{\partial T_s}{\partial t} = -E - R_s + G \tag{4.8}$$

where C_s is the heat capacity of this soil layer, E is now the surface enthalpy flux into the atmosphere, R_s the net upward surface flux of radiative energy, and G the upward flux of heat from lower soil layers. This budget can alternatively be written:

$$Q = R_{TOA} + G - C_s \frac{\partial T_s}{\partial t} \tag{4.9}$$

where R_{TOA} is the net radiative energy flux at TOA. If we consider only a thin near-surface soil layer and average over a sufficiently long time period for the last term to be negligible (i.e. several days), then a change in Q that is rapid compared to the insolation forcing must be due to either a rapid change in the ground heat flux or a change in the radiative balance

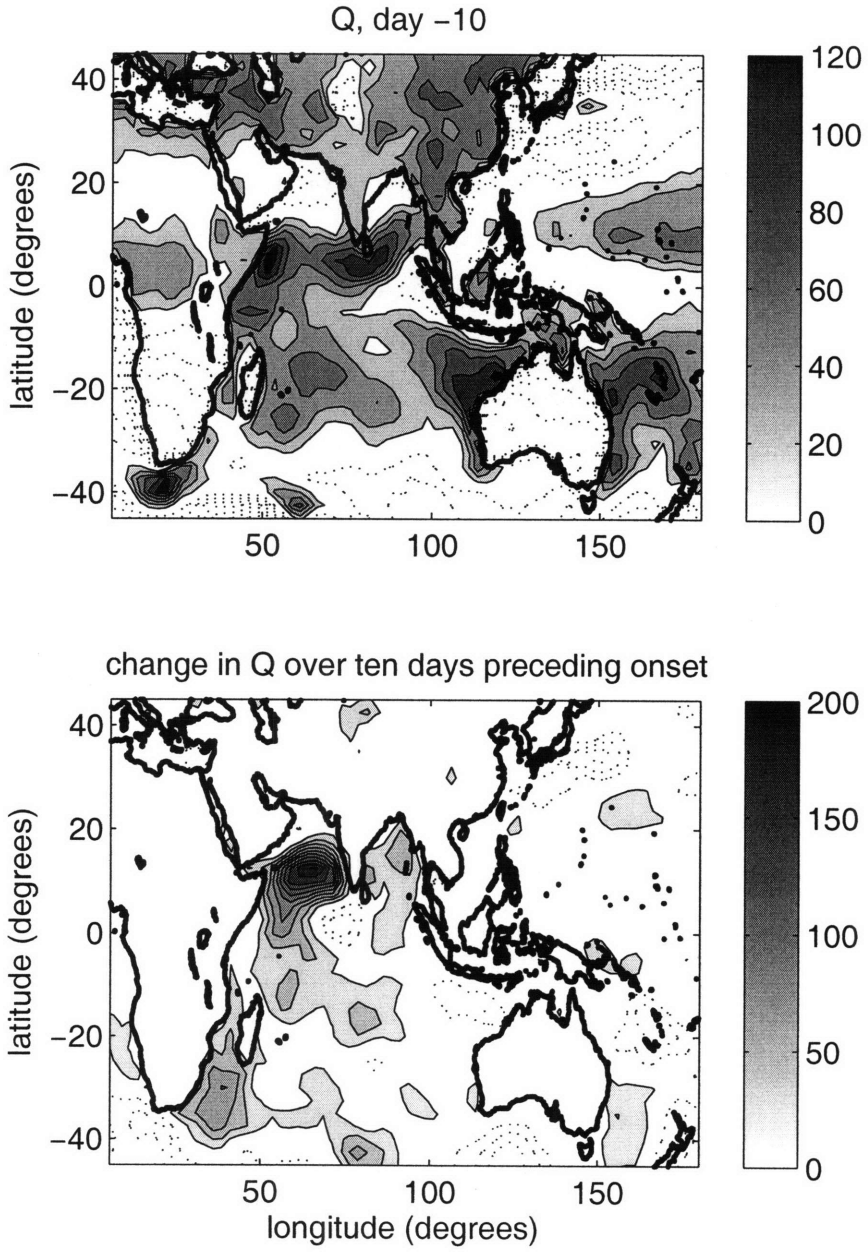

Figure 4-17: As in Fig. 4-3, but for the vertically-integrated source of moist static energy in each atmospheric column in the NCEP Reanalysis. In both panels, solid contours with shading denote positive values, dotted contours negative values, and the contour interval is 20 W m^{-2} with the zero contour omitted.

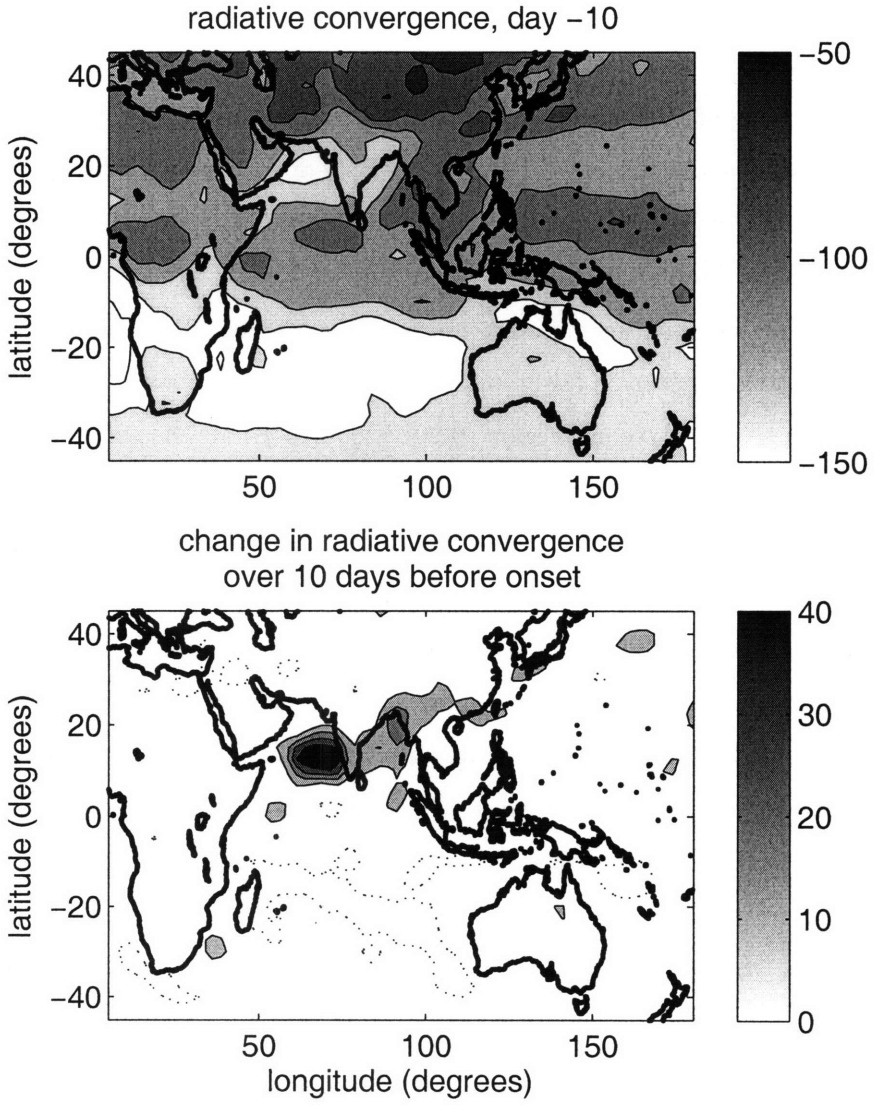

Figure 4-18: As in Fig. 4-3, but for the vertically-integrated convergence of radiative energy in each atmospheric column in the NCEP Reanalysis. Contour interval is 20 W m^{-2} in the top panel. In the bottom panel, solid contours with shading denote positive values, dotted contours negative values, and the contour interval is 10 W m^{-2} with the zero contour omitted.

at TOA. While neither of these processes should be ruled out during the process of monsoon onset, none of the terms in (4.9), as calculated from NCEP data, exhibit abrupt changes over land concurrent with jet onset. Averaged over the South Asian longitudes of 60-110°E, Q goes through a fairly smooth seasonal cycle over the predominantly terrestrial region of 20-40°N, which includes the Tibetan plateau (Fig. 4-19). In this region, Q is about 20 W m^{-2} less than the TOA flux during boreal summer, presumably due in large part to the warming and melting of fairly deep layers of frozen soil on the Tibetan plateau. Over the predominantly oceanic domain of 0-20°N, 60-110°E, Q does increase abruptly by about 30 W m^{-2} over the ten days before jet onset, mostly because of the wind-driven increase in evaporation over the Arabian Sea.

When the same regional averages are applied to ω at 300 hPa (the level at which ω typically peaks in this region), a fairly linear relationship is seen between ω and the moist static energy source in the oceanic region (0-20°N, 60-110°E) for the 100 days surrounding jet onset (Fig. 4-20). An abrupt increase in ascent is also seen in the land region (20-40°N, 60-110°E). The fact that no similar abrupt change occurs in the moist static energy source for this land region implies that abrupt changes must occur in the gross moist stability or in the horizontal advection of moist static energy over land. The spatial patterns of δQ and $\delta\omega$ over the ten days before jet onset are quite similar over ocean, with both peaking over the eastern Arabian Sea (Fig. 4-21, compare with Fig. 4-17). The abrupt change in ω over the predominantly land region of 20-40°N, 60-110°E appears as the periphery of a signal centered in the northern Bay of Bengal.

4.6 On the shift of the $\eta = 0$ contour

The fact that the $\eta = 0$ contour at 850 hPa is displaced to nearly 10°N at jet onset, at which time it is roughly bisected by a low-level divergence dipole (see bottom panel of Fig. 4-8), has been used to suggest that symmetric or inertial instability may be responsible for the abrupt onset of the South Asian monsoon (Krishnakumar and Lau, 1997). Rodwell and Hoskins (1995) showed that fluid parcels did accelerate, in a Lagrangian sense, along the trajectory of a simulated Somali jet in regions where the potential vorticity (PV) was locally anticyclonic and thus satisfied a necessary condition for symmetric instability. However, any circulation resulting from an instability is generally expected to relax the fluid toward a neutrally stable

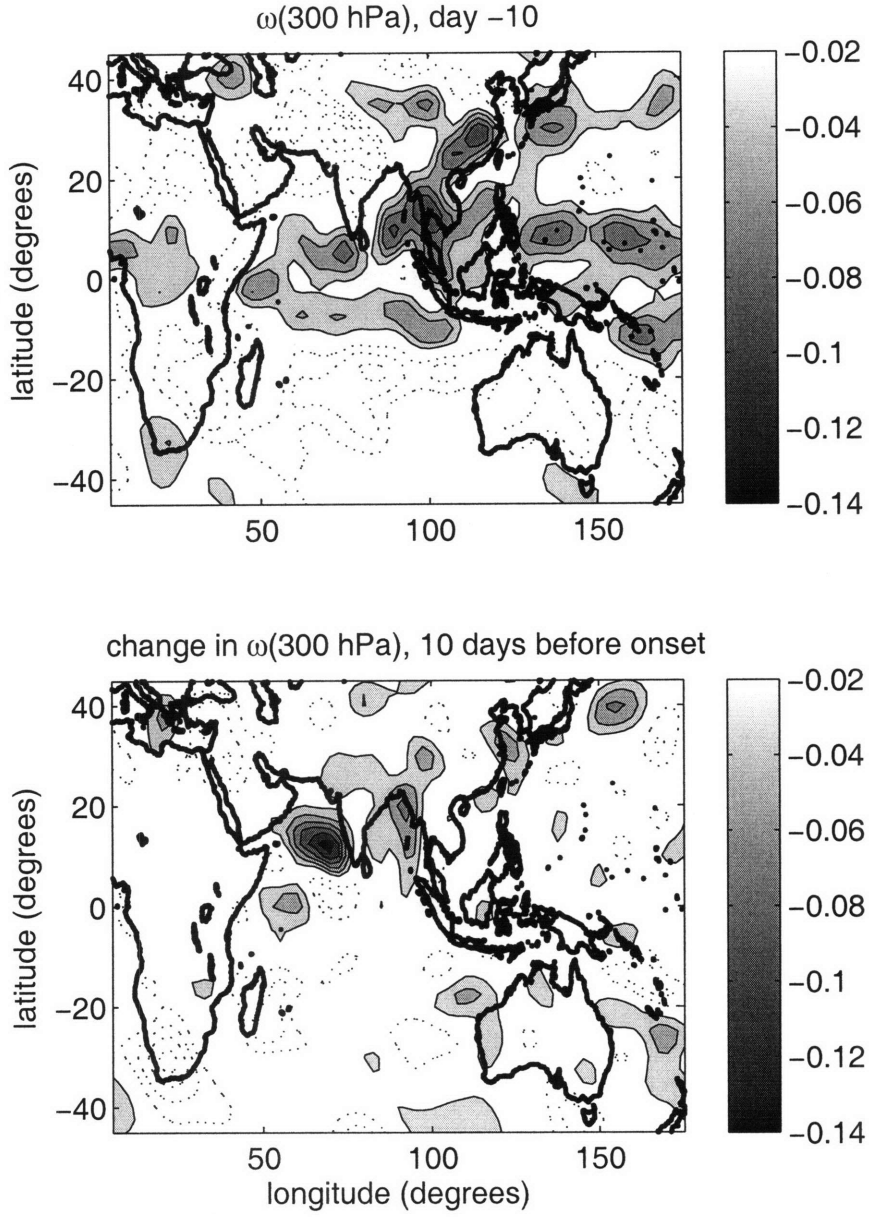

Figure 4-21: As in Fig. 4-3, but for the vertical velocity at 300 hPa from the NCEP Reanalysis. In both panels, solid contours with shading denote negative values (ascent), dotted contours positive values (subsidence), and the contour interval is 0.02 Pa s^{-1} with the zero contour omitted.

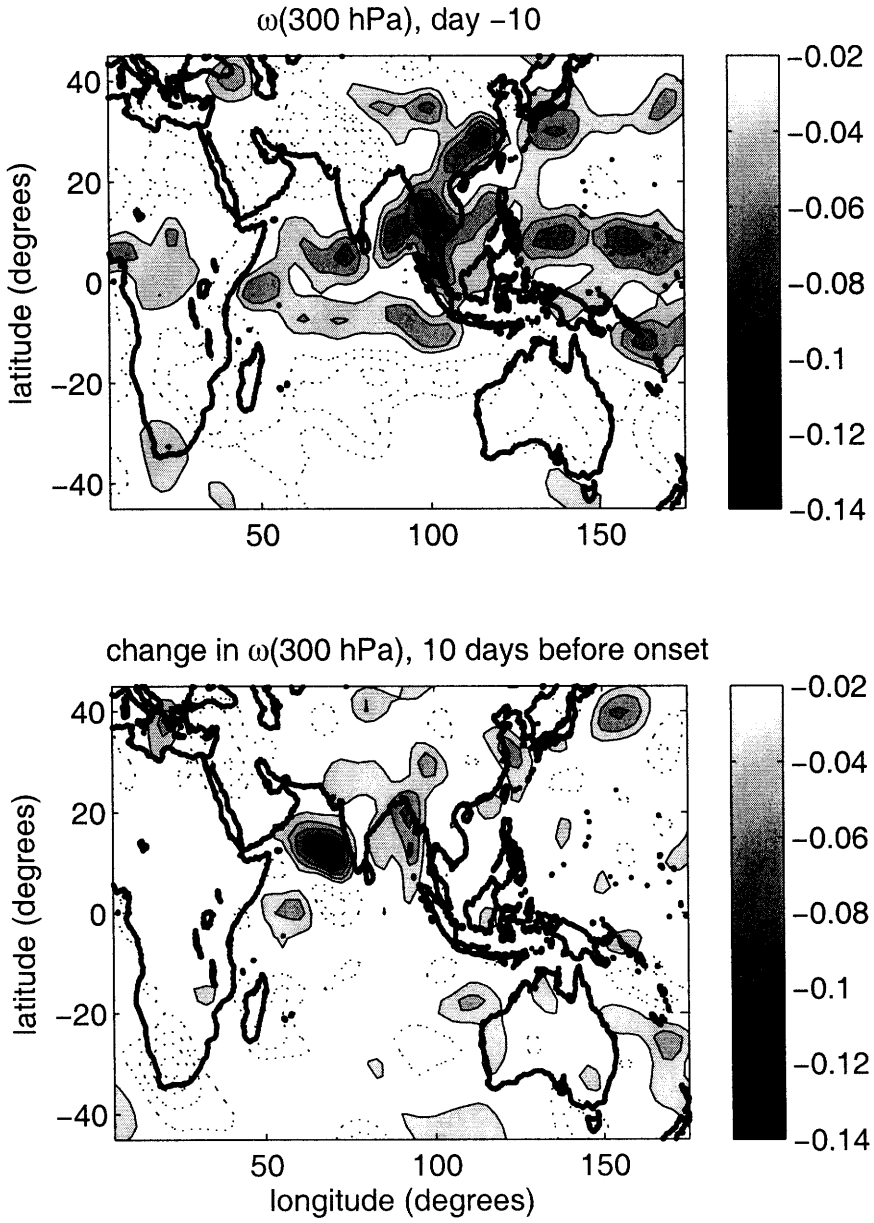

Figure 4-21: As in Fig. 4-3, but for the vertical velocity at 300 hPa from the NCEP Reanalysis. In both panels, solid contours with shading denote negative values (ascent), dotted contours positive values (subsidence), and the contour interval is 0.02 Pa s^{-1} with the zero contour omitted.

state. That is, the circulation induced by a symmetric instability is expected to relax the PV toward a distribution where it is nowhere locally anticyclonic. During the course of jet onset, however, the latitude of the $\eta = 0$ contour actually increases. A similar increase in the latitude of the zero PV contour over the course of monsoon onset occurred in the GCM used by Krishnakumar and Lau (1998). They found that this change in the PV distribution resulted primarily from an increase in cumulus heating, which they in turn attributed to the release of convective available potential energy (CAPE) in a conditionally unstable atmosphere. They posited that the trigger for this release of CAPE was the low-level moisture convergence resulting from the release of symmetric instability associated with an initial, small shift of the zero PV contour off the equator by meridional flow. This hypothesis involves the same physics as conditional instability of the second kind (CISK), in which a positive feedback between low-level moisture convergence and latent heating produces a transfer of energy from a reservoir of available potential energy (APE) to the motion of the circulation. Explaining abrupt onset by symmetric instability thus requires a reduction in a reservoir of APE to continually destabilize the PV distribution, otherwise any increase in meridional flow caused by the symmetric instability would be expected to relax the zero PV contour back toward the equator.

The hypothesis that changes in the circulation are caused by the release of a large amount of potential energy is at odds with the concept of convective quasi-equilibrium, in which convection quickly eliminates anomalies of CAPE that are created by the destabilizing effects of surface entropy fluxes and radiation (e.g. Arakawa and Schubert, 1974). While results from the previous section show that further work is needed to determine whether or not some form of convective quasi-equilibrium holds during the onset of the South Asian monsoon, there are some theoretical problems with using moisture convergence as a closure for convective heating. In particular, Emanuel et al. (1994) discussed how the moisture convergence closures on which CISK theories rely largely ignore the fact that moist convection is a response to a local convective instability. These closures allow APE to accumulate when the precipitation is not strongly positive, then cause this APE to be released when low-level moisture convergence is strong, instead of when the atmosphere is convectively unstable. If WISHE, rather than CISK, is responsible for the abrupt intensification of the southwesterly jet, a positive feedback will exist between the circulation and the rate at which energy is supplied to the system via surface sensible and latent heat fluxes. There is then no need to

postulate a reduction in a reservoir of APE to further destabilize the PV distribution over the course of jet onset, because any increase in the energy of the atmosphere is obtained from the heat content of the ocean. That is, in a wind-evaporation feedback the shift of the $\eta = 0$ contour away from the equator is a result of the intensification of the baroclinic circulation, rather than a cause of that intensification.

This is not to say that the existence of locally anticyclonic PV has no effect on the speed or structure of the Somali jet. Rodwell and Hoskins (1995) showed that larger southwesterlies over the Arabian Sea were achieved in a model state having a larger region of negative PV in the Northern Hemisphere. However, they obtained this larger region of locally anticyclonic PV by reducing the frictional and diabatic modification of PV in the cross-equatorial jet. It is thus possible that the poleward shift of the $\eta = 0$ contour over the ten days before jet onset is accompanied by an intensification of Arabian Sea southwesterlies due to symmetric instability, but as discussed above, this instability should not necessarily be seen as a cause of the poleward shift of the $\eta = 0$ contour. The time-dependent effect of symmetric instability during the course of jet onset, and its interaction with convection, thus seems to merit further investigation. Tomas et al. (1999) examined time-dependent effects of the poleward shift of the $\eta = 0$ contour on meridional flow in an axisymmetric boundary layer model, but this model employed a basic state with prescribed geopotential and so could not represent the intensification of zonal flow.

4.7 Concluding remarks

Composites of the seasonal intensification of the Somali jet were compiled with the intent of understanding the mechanism responsible for the abrupt onset of this component of the South Asian summer monsoon. A jet index was defined and used to show that the speed of low-level southwesterlies over the Arabian Sea increases faster than the insolation forcing. Cross-equatorial flow associated with the Somali jet was found to consist of a zonally focused core of southerlies near the East African highlands that increases in speed nearly linearly over about two months, and a broader region of southerly flow to the east of this core that evolves more rapidly, in concert with the off-equatorial southwesterlies.

Accompanying the increase in off-equatorial southwesterlies is an increase over the Arabian Sea in low-level convergence, deep convection, surface entropy fluxes, and boundary

layer entropy. The change in boundary layer entropy was estimated to be consistent with the change in low-level geopotential expected in a quasi-equilibrium framework. The corresponding increase in free-tropospheric temperature peaks in a region of subsidence located poleward of the increase in subcloud entropy.

We also examined some components of the vertically integrated budget of moist static energy, h. The increase in wind-driven ocean evaporation was estimated to be consistent with an abrupt increase in ascent over ocean. Differences in the time evolution of ascent and the vertically integrated source of h over land suggest that horizontal advection or changes in the gross moist stability may be important there, although the coherent increase in ascent occurring over land is weak compared to that occurring over ocean.

In the composites of jet onset, the vertical profile of changes in zonal wind near the Arabian Sea convergence zone were decently described by the superposition of barotropic westerlies and a baroclinic mode of roughly equal magnitude. This is consistent with the WISHE feedback seen in Chapter 2, in which the creation of barotropic westerlies by the convergence of zonal momentum was needed for the feedback to occur. Composites of upper-level PV indicate that the onset of the jet may be accompanied by a transition to a circulation that conserves absolute angular momentum in its free-tropospheric branch. The next chapter presents some evidence that WISHE may be required for such a transition to occur in the South Asian monsoon.

THIS PAGE INTENTIONALLY LEFT BLANK

Chapter 5

Wind-evaporation feedback and the South Asian summer monsoon in a three-dimensional model

Abstract

A three-dimensional atmospheric primitive equation model was integrated with realistic topography and a prescribed climatology of sea surface temperature to examine the role played by wind-induced surface heat exchange (WISHE) in the seasonal cycle of the South Asian summer monsoon. Two multi-year integrations of the model were performed, one with and one without wind-dependent surface fluxes of latent and sensible heat. In the integration with WISHE, zonal winds and precipitation in the mean summer monsoon were stronger than observations, and the southwesterly Somali jet did not intensify abruptly as it does in observations. Despite these deficiencies, the spatial structure of the seasonal monsoon transition was well simulated by the model. In particular, the onset of the southwesterly Somali jet projected strongly onto a first baroclinic mode structure, and the precipitation maximum migrated from the equator to about 20°N with a secondary maximum persisting near 5°S over the Indian Ocean. The summer monsoon was much weaker in the integration performed without WISHE, with the bulk of the precipitation centered just north of the equator and a factor of two reduction in the strength of both the monsoon westerlies and the precipitation near 20°N. In the absence of WISHE and some associated radiative effects, the thermal forcing of the South Asian land mass seems to be too weak to produce a meridional circulation that conserves absolute angular momentum at upper levels. Thus, although it was not possible to use this model to test the hypothesis that WISHE produces an abrupt monsoon onset, these results do support the idea that WISHE plays an important role in setting both the amplitude and the spatial structure of the mean summer monsoon.

5.1 Introduction

The previous chapter showed that the South Asian summer monsoon circulation begins more rapidly than can be explained by a linear response to the insolation forcing, and that this abrupt onset is accompanied by a large increase in wind-driven surface enthalpy fluxes over the Arabian Sea. In this chapter we examine how eliminating the wind-dependence of surface enthalpy fluxes in a simulation of the South Asian monsoon alters the evolution of that circulation.

The model we use, a three-dimensional version of the atmospheric MIT general circulation model (MITgcm), is far more complex than the idealized models used in Chapters 2 and 3 of this thesis, and contains an interactive land surface, realistic topography, and prescribed, realistic sea surface temperature (SST). This model should thus include at least some processes proposed by previous authors to be involved in monsoon onset that were not represented in the axisymmetric aquaplanet models used in previous chapters. For example, the three-dimensional MITgcm can be expected to represent with at least some fidelity the effects of eddy transports of momentum, the thermal and orographic effects of land surfaces, and the radiative effects of clouds and water vapor. We will not diagnose the effects of all these processes in the model, but will instead focus on the role played by wind-induced surface heat exchange (WISHE) in the seasonal cycle of the South Asian summer monsoon by conducting one integration with and another without wind-dependent surface enthalpy fluxes. If WISHE is of little import in the onset of the South Asian monsoon, then the changes in winds and convection that accompany this onset should proceed largely the same in both integrations.

This model is used instead of one of more intermediate complexity (e.g. Xie and Saiki, 1999; Prive and Plumb, 2007) partly because a model with realistic topography and SST can be directly compared to observations, and partly for expediency: model development was completed and a seasonal climatology assessed by Molod et al. (2007). We will show in this chapter that the South Asian summer monsoon in the model possesses several important deficiencies when compared to observations. In particular, low-level westerlies are too strong and the monsoon onset is not abrupt. However, these deficiencies may not be particularly worse than those found in other GCMs. For example, Martin (1999) found that low-level westerlies in the Asian summer monsoon were too strong and began about a month

too early in the UK Meteorological Office's Unified Model, which was forced by observed SSTs. Kang et al. (2002) examined climatologies of the Asian summer monsoon in ten atmospheric GCMs, and noted that models with Arakawa-Schubert convection schemes typically obtained low-level monsoon winds stronger than observed, while models with other types of convection schemes generally obtained winds weaker than observed (the model used in this chapter employs an Arakawa-Schubert scheme). Two different GCMs using cloud-resolving models to predict convective tendencies within each GCM grid cell [i.e. the superparameterization approach of Grabowski (2001)] obtained Asian summer monsoons with precipitation significantly larger than in observations (Khairoutdinov et al., 2005; Luo and Stephens, 2006). Luo and Stephens (2006) proposed that this is due to an enhanced wind-evaporation feedback in these models. Although they did not determine why such an enhanced feedback occurs, they suggested that it might be related to the duration of convective events being artificially prolonged by the use of cyclic boundary conditions in the cloud-resolving models; an alternative mechanism for an artificially strong wind-evaporation feedback is suggested in this chapter.

It is difficult to know how well existing GCMs simulate the abrupt onset of monsoon winds because studies have typically focused on how well models represent the meridional migrations of precipitation maxima on seasonal time scales. For example, Gadgil and Sajani (1998) examined precipitation in 30 models participating in the Atmospheric Model Intercomparison Project, and found that although almost all models simulated the seasonal cycle of precipitation over Africa well, model skill in representing precipitation in the Asia-West Pacific region was much more diverse. They found that in some models the precipitation peak even remained over the equatorial ocean and did not migrate poleward over South Asia during boreal summer. When models cannot reliably simulate the summer mean state, it does seem sensible to postpone examination of the abrupt character of monsoon onset. However, even in models that better simulate the mean summer monsoon, diagnostics of monsoon onset are often limited to a climatology of the meridional position of precipitation. Meehl et al. (2006) examined monsoon regimes in version 3 of the Community Climate System Model (CCSM3). South Asian monsoon precipitation in an atmosphere-only version of this model, forced by observed SST, began about one month too early each year and was at least 20 percent stronger than observations. Meehl et al. (2006) found that this bias was reduced when the same model was coupled to an interactive ocean, but

the coupled model exhibited systematic SST errors that may have artificially compensated for the precipitation bias. Our main point is that modern GCMs exhibit considerable bias in both the summer mean monsoon state and in the timing of monsoon onset, and that diagnostics of the dynamical changes accompanying monsoon onset are rarely presented. The MITgcm thus seems as good a model as any to use for assessing the role WISHE might play in monsoon onset.

The next section of this chapter gives a brief overview of the version of the MITgcm used here, with particular attention paid to representations of moist convection and surface fluxes of latent and sensible heat. Then we present diagnostics of the mean South Asian summer monsoon and its onset. We frequently refer to results from previous chapters to tie these model results to both the observations presented in Chapter 4 and to the idealized model results of Chapters 2 and 3.

5.2 Model details

The MIT general circulation model (MITgcm) can simulate either atmospheric or oceanic flow using the same dynamical core (Marshall et al., 2004; Adcroft et al., 2004). Several atmospheric versions of the MITgcm exist, and we use the one with the most detailed treatment of subgrid scale physics (the Fizhi package). This version was part of the Aqua-Planet Experiment (Neale and Hoskins, 2000), and the seasonal climatology of an integration forced by a prescribed sea surface temperature (SST) was described by Molod et al. (2007, hereafter M07). This model is discussed briefly here, and more detailed documentation can be found in M07.

The horizontal grid of this version of the MITgcm is a cubed sphere with six faces of 32×32 grid points each, resulting in a maximum grid spacing of 2.8×2.8 degrees at the center of each face. An eta coordinate is used in the vertical with a resolution of 25 hPa. An additional five vertical levels are included near the surface in the calculation of subgrid scale physics. Surface topography and coastlines were specified by the Navy dataset supplied by the National Center for Atmospheric Research (NCAR).

The model uses parameterizations adapted from the Goddard Earth Observing System 3 (GEOS-3). Turbulence in the MITgcm is parameterized by the 2.5 level, Mellor-Yamada type scheme of Helfand and Labraga (1988), and the top of the atmospheric boundary

layer is diagnosed as the level at which the turbulent kinetic energy falls to one tenth of its near-surface maximum. A land surface model contains several soil layers, a snow pack, and a canopy reservoir. Additional parameterizations, though not discussed here, predict radiation, large scale precipitation, gravity wave drag, and cloud cover.

Moist convection is represented by a relaxed Arakawa-Schubert (RAS) scheme (Moorthi and Suarez, 1992), with a Kessler-type scheme for the re-evaporation of precipitation (Sud and Molod, 1988). The RAS scheme uses a closure for the cloud-base mass flux based on the assumption that a quasi-equilibrium is maintained between the generation of convective instability by large scale forcings and the dissipation of that instability by moist convection. This differs from the closure used in the idealized models of preceding chapters, that was based on the assumption of quasi-equilibrium of subcloud layer entropy. Another difference is that those idealized models incorporated a time lag for the effect of convection on the large scale environment by relaxing the convective mass flux toward its equilibrium value over a specified time scale. In contrast, the RAS scheme relaxes the large scale environment itself toward the quasi-equilibrium state by applying a specified fraction of the adjustment needed to instantaneously achieve that state. RAS convection thus responds instantaneously to perturbations in the large scale forcing, and does not explicitly include the phase lags that are theoretically important for WISHE modes (e.g. Emanuel, 1993).

Fluxes of sensible heat, momentum, and moisture from ocean and land surfaces are treated using stability-dependent bulk formulae in a Monin-Obukhov scheme (Helfand and Schubert, 1995). For surface fluxes of sensible heat, the transfer formula can be put in the familiar form:

$$\overline{w'\theta'} = C_H|\mathbf{V}|\Delta\theta \tag{5.1}$$

where $\Delta\theta$ is the difference in potential temperature between the surface and the lowest atmospheric layer, and the left hand side uses the usual notation for a Reynolds decomposition. The dimensionless transfer coefficient in this bulk formula, however, varies with the atmospheric stability:

$$C_H = \frac{k^2}{\psi_m(\psi_h + \psi_g)} \tag{5.2}$$

where k is the Von Karman constant. Nondimensional vertical gradients of momentum and temperature in the surface layer are given by ψ_m and ψ_h, respectively, which have values predicted by similarity theory with different functional forms for stable and unstable surface

layers. The nondimensional temperature gradient in the viscous sublayer (the layer immediately adjacent to the surface in which gradients are controlled by molecular processes), is represented by ψ_g, which depends on both surface roughness and wind speed. Details on how the ψ terms are calculated can be found in M07. The same transfer formula is used to obtain $\overline{w'q'}$ (the surface evaporation), but with ψ_g representing the moisture gradient in the viscous sublayer, and $\Delta\theta$ replaced by Δq, the difference between the specific humidity of the lowest atmospheric layer and the saturation specific humidity of the surface.

The dependence of surface enthalpy fluxes on wind speed enters into (5.1) through both C_H and $|\mathbf{V}|$. To examine the role that WISHE plays in the onset of the South Asian monsoon, we integrate both a control run where these coefficients vary prognostically, and another run where their product, defined as

$$K_H \equiv C_H|\mathbf{V}| \tag{5.3}$$

is fixed at a constant, spatially uniform value. This prescribed value was obtained by diagnosing K_H from the control run, then taking a time mean over one year and a spatial mean within 30° of the equator. This approach renders surface enthalpy fluxes independent of both wind speed and stability. The coefficient K_H was fixed over both land and ocean, with the expectation that changes in wind speed cannot directly enhance the net surface enthalpy flux from a land surface over time scales longer than a few days, due to the small heat capacity of land surfaces. This is verified in the model, with the monthly mean difference between the net downward surface radiation and the net upward surface enthalpy flux peaking at about 10 W m^{-2} over the South Asian land mass.

Two three-year integrations of the MITgcm were performed, one with fully prognostic values of K_H (henceforth called the control, or WISHE run) and the other with the prescribed uniform distribution of K_H (the no-WISHE run). In both integrations, the model was forced by seasonally- and diurnally-varying insolation and prescribed, time-varying SST. The SST forcing was obtained by linearly interpolating in time to the weekly analyzed data of Reynolds and Smith (1994), which had been spatially smoothed with a binomial filter of $(\frac{1}{4}, \frac{1}{2}, \frac{1}{4})$. The model state was initialized to conditions on January 10, 1993 from the GEOS-3 reanalysis (Schubert et al., 1993), and SSTs through the end of 1995 were used to force the model. This is exactly the same configuration examined by M07, except that

M07 used a 30-year climatology of weekly SSTs (with no interannual variability), while here we use weekly SSTs from 1993-1995.

5.3 Model results

5.3.1 Control run mean monsoon

The seasonal climatology of the model was compared to observations by M07, and here we discuss some details relevant to the South Asian summer monsoon. M07 concluded that the global seasonal mean climate of the MITgcm was generally realistic. Inspection of the summer (June-August) mean wind at 850 hPa shows strong low-level monsoon westerlies over South Asia, as well as an organized southwesterly jet over the Arabian Sea (Fig. 5-1, top right). These low-level westerlies are over 5 m s^{-1} stronger in the model than in the NCEP Reanalysis, with the enhanced westerlies extending from the African monsoon domain all the way to the West Pacific (Fig. 5-1, bottom left). The enhanced monsoon westerlies are actually accompanied by a summer Hadley circulation that is weaker in the model than in the NCEP Reanalysis (M07), with the peak zonal mean ascent located further from the equator in the model. Although northward flow at 850 hPa over the western Indian Ocean is stronger in the model than in observations, this flow is shallower and thus produces a smaller total meridional mass flux in the model. Reanalyzed meridional winds are not as well constrained by observations as zonal winds, so this may partly be a comparison of cross-equatorial flow in two different models.

Many of the theoretical ideas discussed in the previous chapters frame the monsoon circulation as being closely tied to horizontal gradients in the vertically-integrated source of atmospheric moist static energy, so it seems natural to ask whether the bias in model winds is accompanied by a bias in these energy sources. Components of the seasonal mean energy budget were examined by M07, and we note a few relevant points here. Evaporation from the Indian Ocean was about 50 percent larger in the model than in the observational estimate of the Comprehensive Ocean-Atmosphere Data Set (da Silva et al., 1994). This larger evaporation rate is consistent with the stronger surface westerlies found in the model. The model also showed considerable bias in the radiative energy budget, with tropical clouds that were generally too low, yielding overly large values of outgoing longwave radiation (OLR). In the zonal mean, the model also underpredicted the amount of incident shortwave

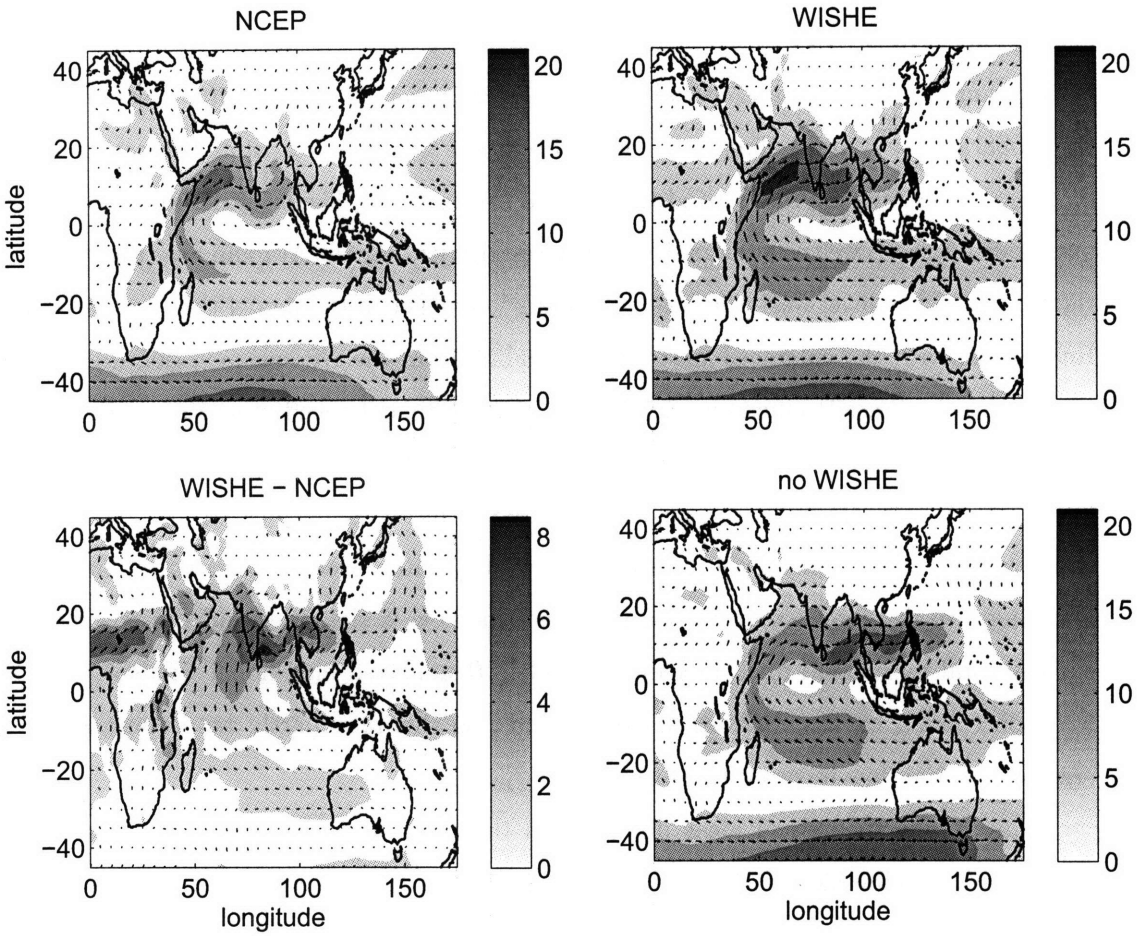

Figure 5-1: Summer mean (June-August) horizontal wind at 850 hPa (arrows) and isotachs (shading). Isotach contour interval is 5 m s^{-1} in all panels except for the bottom left, where it is 3 m s^{-1}. Top left panel is for the NCEP/NCAR Reanalysis, top right for the MITgcm control run, bottom left the difference between the MITgcm control run and the NCEP Reanalysis, and bottom right for the MITgcm run without WISHE.

reflected by clouds. This underestimate of the shortwave cloud forcing occurred primarily off the west coast of continents, in typical stratocumulus regions, suggesting that the model underpredicts the radiative forcing of shallow clouds. The bias in net downward radiation at the top of the atmosphere (TOA) was not of a uniform sign over South Asia: it was about 30 W m^{-2} smaller than satellite observations over India and the Indochina Peninsula, and about 15 W m^{-2} larger over the Tibetan Plateau.

Some of these errors in energy sources may arise directly from deficiencies in a parameterization scheme, and that particular scheme can then be seen as causing the energy imbalance. Other errors, such as the overestimate of both ocean evaporation and low-level westerlies, may result from an interaction between parameterized and resolved physics that has some other cause. The assertion by Luo and Stephens (2006), that the South Asian monsoon in one GCM is too strong because of an overactive wind-evaporation feedback, is intriguing because the MITgcm exhibits winds and ocean evaporation that are both too strong, and we shall show that reducing horizontal gradients of surface evaporation does weaken the circulation. Although the cause of such an overactive wind-evaporation feedback is unclear, it is worth noting that the strength of an overactive monsoon was reduced in another GCM by use of interactive SST, even though the prescribed SST in the atmosphere-only model was taken from observations (Meehl et al., 2006). One hypothesis consistent with these results is that small, precisely phased changes in SST have a large effect on the growth rates of WISHE modes, similar to the way in which a small but nonzero phase lag in deep convection alters the growth rates of such modes (Emanuel, 1993). This is not explored further here, but simply mentioned as one possible explanation for the bias of the MITgcm.

5.3.2 WISHE and monsoon onset

Consistent with overly strong low-level westerlies in the model's mean summer monsoon, southwesterlies associated with the Somali jet are stronger and begin earlier in the year than in the NCEP Reanalysis. This is shown by calculating the jet speed index defined in the previous chapter, then constructing composites relative to the date this index exceeds a defined threshold, as in the previous chapter. The NCEP composite jet speed index was recalculated for the years 1993-1995, to match the years for which SST was used to force the MITgcm. The onset of the jet index is considerably less abrupt in the model than in

the NCEP data and, outside of "noise" in the signal that seems nearly constant throughout the year, the model's index does not project strongly onto frequencies higher than the first three seasonal harmonics (Fig. 5-2, top two panels). There may be a very low-amplitude signal of an abrupt onset, as well as a slightly higher amplitude abrupt reduction in jet speed about 130 days after the date of onset, but these are both weak compared to the rapid intensification seen in the NCEP jet speed. The best fit of the harmonics to the control run index is not visibly changed even if only the first two seasonal harmonics are used.

In the no-WISHE run, the jet speed index exhibits a seasonal cycle with only about one-third the amplitude of that in the control run and about half that of observations (Fig. 5-2, bottom). The transition from winter to summer does occur more abruptly than the first three seasonal harmonics, but this signal of abrupt onset has a similar amplitude to the increase in jet speed seen in the control run within a few days of the onset date, and in the control run this signal is indistinguishable, at least by eye, from noise. In the no-WISHE run, the largest 850 hPa wind speeds in the tropics actually occur over the southern Bay of Bengal and just west of the Indochina Peninsula rather than over the Arabian Sea (Fig. 5-1, bottom right).

Although the onset of the Somali jet in the control run occurs over a longer time scale than in the NCEP data, the changes in horizontal wind that occur during this onset process are largely consistent with those seen in the NCEP data. To show this, we construct composites similar to those detailed in the previous chapter, but because of the longer time scale of onset in the model, we show the composite change over a 20 day period centered on the date of onset (rather than the 10 day period preceding onset used in the previous chapter). The cross-equatorial jet is focused near the East African highlands in both model runs. Ten days before onset, the cross-equatorial jet in the control run is several m s^{-1} stronger than both the NCEP jet and the jet in the no-WISHE run. Southerly winds in the control run's cross-equatorial jet do not extend as high or as far east as in the NCEP data (Fig. 5-3, top left, compare with Fig. 4-5 of previous chapter). In both runs, the increase in cross-equatorial flow during the 20 days surrounding jet onset is separated from the topography, although in the control run the increase in equatorial southerlies exhibits a westward tilt with height not seen in the NCEP Reanalysis and actually peaks near 700 hPa ((Fig. 5-3, bottom panels). The model's composite cross-equatorial flow has more spatial

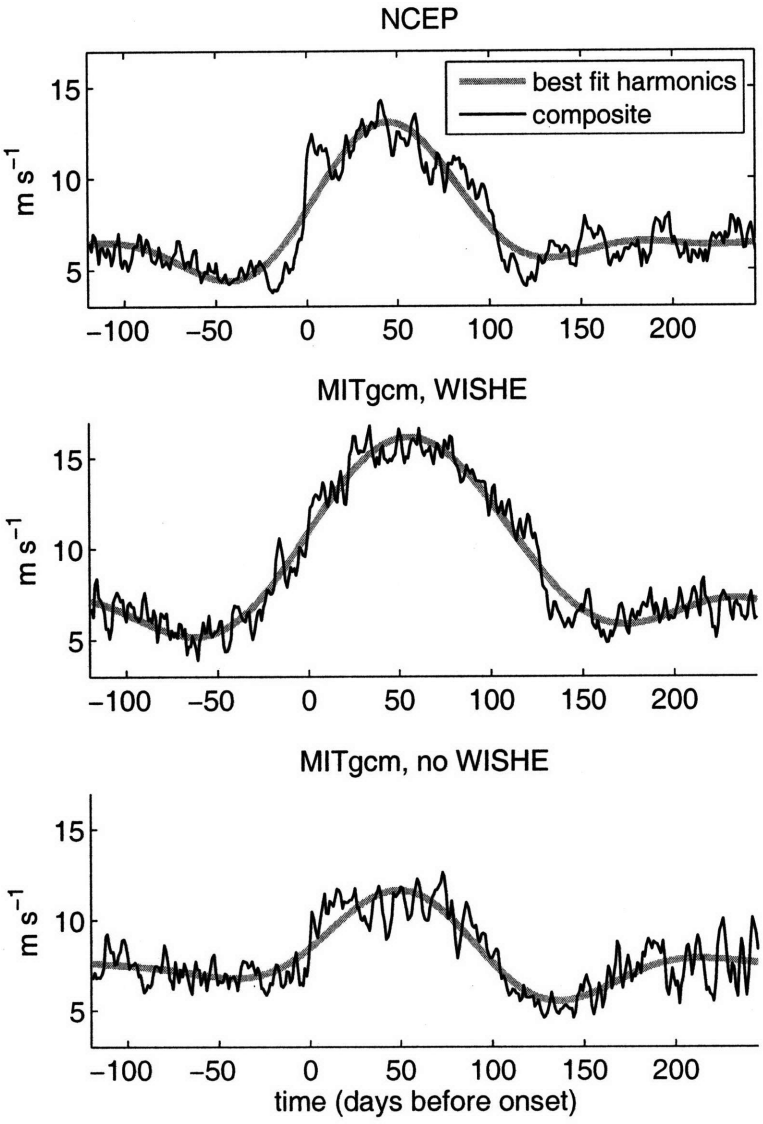

Figure 5-2: The Somali jet index, as defined in the previous chapter, for the NCEP Reanalysis (top), the MITgcm control run (middle), and the MITgcm run without WISHE (bottom), all for the years 1993-1995. Black lines are composite time series relative to the date of jet onset (day 0), and grey lines are the best fit of the first three seasonal harmonics to these composites.

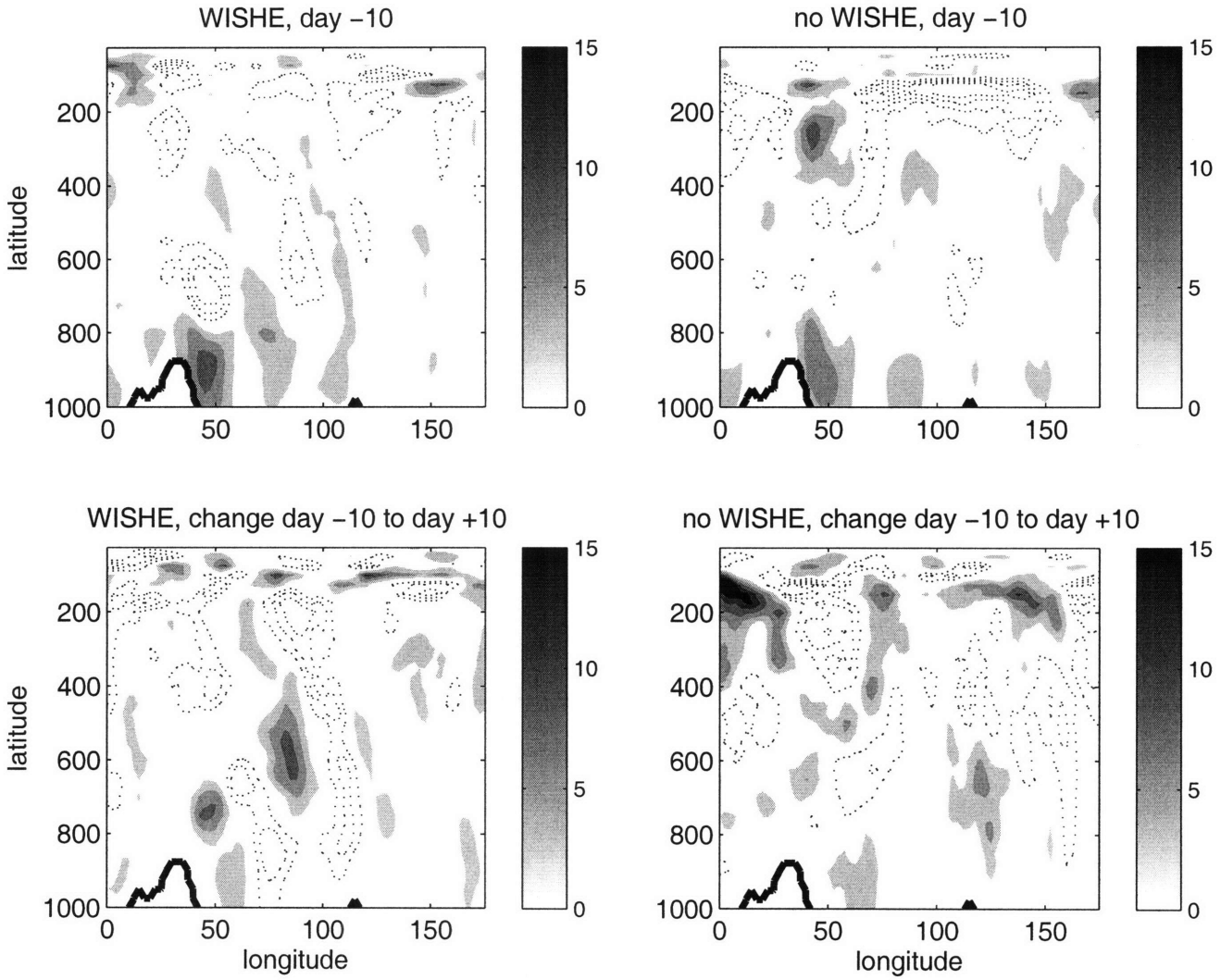

Figure 5-3: Meridional wind at the equator in the MITgcm 10 days before the onset of the Somali jet (top row), and its change over the 20 days centered on the date of jet onset (bottom row). Left column is for the run with WISHE and right for the run without WISHE. In the top panels, shading denotes southerlies and dashed contours northerlies, while in the bottom panel shading denotes winds becoming more southerly and dashed contours more northerly. In all panels the contour interval is 2 m s^{-1} with the zero contour omitted.

variance than the NCEP composite, but this could be due to the shorter averaging period used for the model or to an underestimate in meridional wind variance in the NCEP data.

We compiled composites of the total southerly mass flux across the equator integrated vertically in the troposphere and zonally between 38.75°E and 71.25°E, which gives the total northward mass flux in both the core and periphery of the jet, as defined in the previous chapter. As in the NCEP Reanalysis, this mass flux accounts for about half the total mass flux in the zonal mean Hadley circulation. Consistent with the diagnostics of the jet index, the increase in this mass flux occurs more gradually in the control run than in reanalyzed winds, and achieves a smaller mean summer amplitude (Fig. 5-4). Note that the NCEP time series displayed in this plot is a composite over 27 years, while the composites for the MITgcm were compiled using only the 3 simulated years. The reduction in cross-equatorial mass flux about 130 days after jet onset in the control model occurs fairly abruptly, moreso than in the NCEP data. The mass flux in the no-WISHE run does exhibit a rapid increase concurrent with the onset of the southwesterly jet, but this increase is fairly low amplitude and is superimposed on a more gradual increase that begins several months earlier.

Jet onset in both versions of the model is associated with a change in zonal wind that projects strongly onto a barotropic and first-baroclinic mode. In composites of the change in zonal wind at 60°E, which passes through the center of the peak southwesterly jet in the control model, zonal winds over the Arabian Sea become more westerly between the surface and about 500 hPa, and more easterly from 500 hPa up to the tropopause (Fig. 5-5). Projection of the vertical profiles of the change in zonal wind at 12.5°N and 60°E, where the low-level westerlies peak, shows that the modes used in the two-mode model of Chapter 2 decently approximate the vertical structure (Fig. 5-6). The best fit is obtained with barotropic components of 4 and 3 m s^{-1} and baroclinic components of 9 and 11 m s^{-1} for the WISHE and no WISHE runs, respectively. The barotropic components of these wind changes have about half the magnitude of the barotropic component of the NCEP changes (shown in Fig. 4-15 of the previous chapter). The fact that the composite changes in wind project decently onto these two modes indicates the potential utility of using the two-mode framework to describe the dynamics. As discussed in the context of the two-mode model in Chapter 2, the barotropic westerly tendency that accompanies the strengthening of the baroclinic circulation suggests that zonal momentum is converging into the region in the vertical mean (neglecting any tendency due to zonal gradients of barotropic pressure).

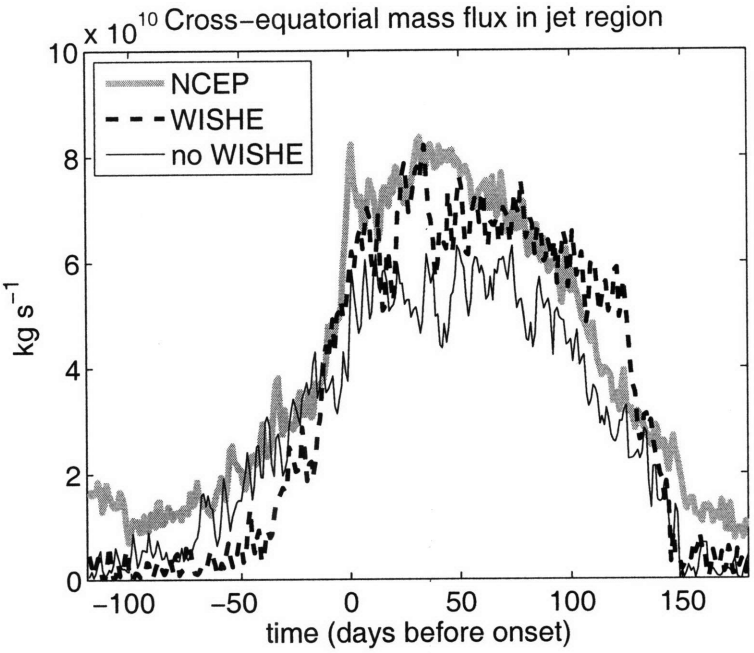

Figure 5-4: Southerly mass flux at the equator, integrated both vertically from the surface to the tropopause and zonally from 38.75°E to 71.25°E, composited relative to the date of jet onset. Grey line is for the NCEP Reanalysis, thick dashed line for the MITgcm control run, and thin solid line for the MITgcm run without WISHE.

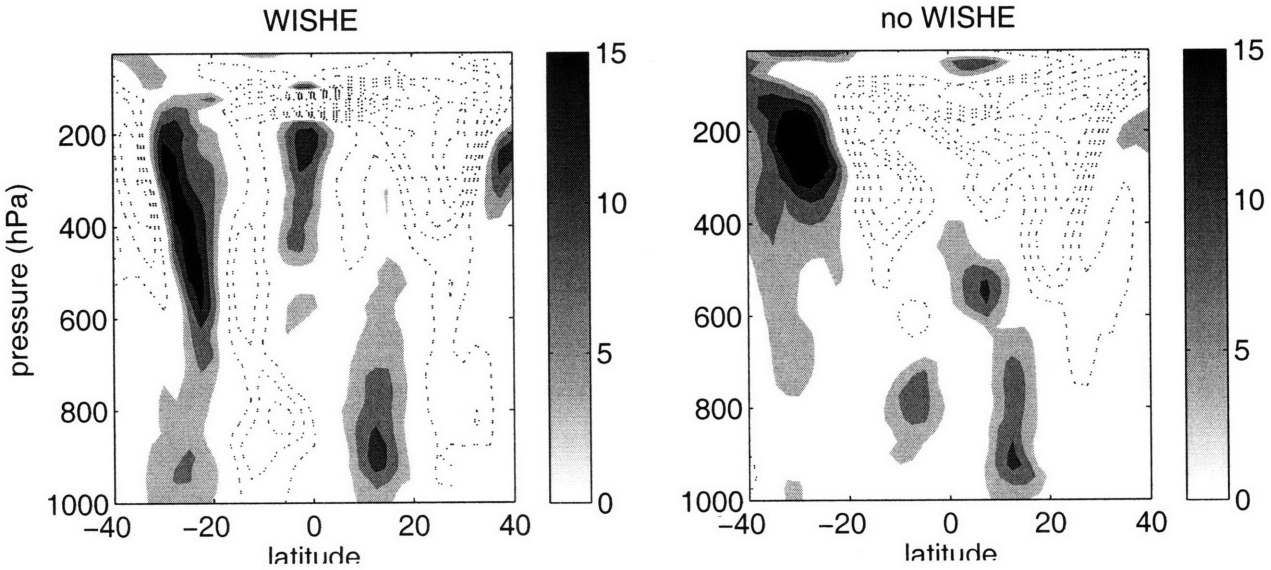

Figure 5-5: Change in zonal wind at 60°E over the 20 day period centered on jet onset, for the MITgcm control run (left) and the run without WISHE (right). Shading denotes winds becoming more westerly and dashed contours winds becoming more easterly, and the contour interval is 4 m s^{-1} with the zero contour omitted.

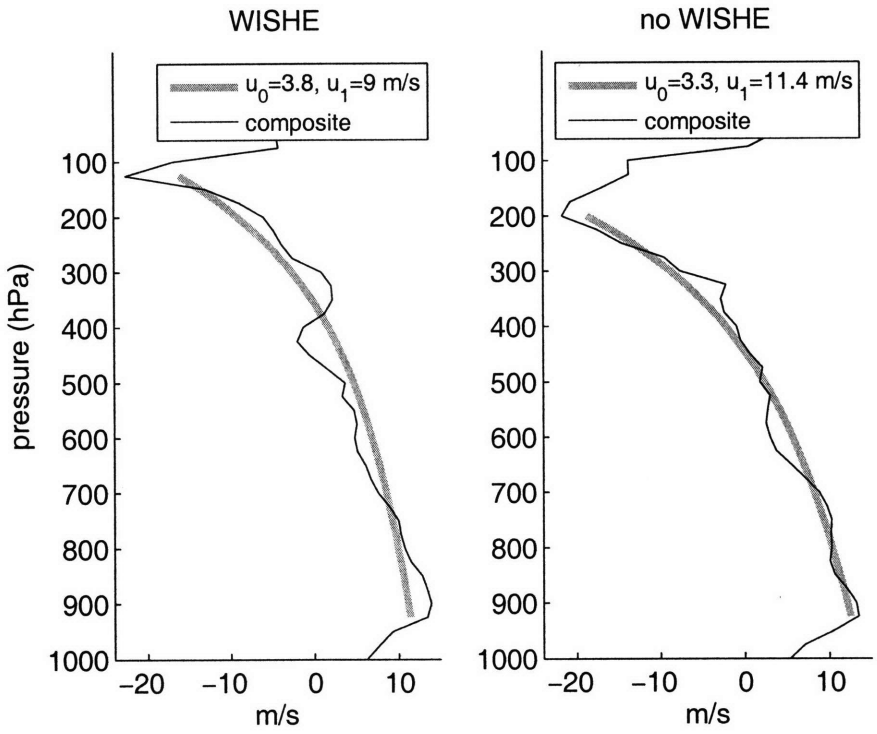

Figure 5-6: Thin black lines show the change in zonal wind at 60°E and 12.5°N over the 20 day period centered on jet onset, for the MITgcm control run (left) and the run without WISHE (right). The thick grey lines show the best fit of the barotropic (u_0) and first baroclinic (u_1) modes to the composite profiles, with the fit coefficients given in the legends.

As might be expected, surface enthalpy fluxes increase considerably over the northern Indian Ocean concurrent with jet onset in the control run, but not in the no-WISHE run. Ten days before jet onset in the control run, the surface enthalpy flux has a zonally elongated peak near 10°N over the Indian Ocean, as well as several strong maxima over the southern hemisphere ocean (Fig. 5-7, top left). The northern and southern hemisphere maxima are connected in the control model by a band of strong enthalpy fluxes stretching across the equator off the east coast of Africa, which is notably absent from the OAFlux observational estimates (see Fig. 4-14 of previous chapter). Consistent with the seasonal mean diagnostics of evaporation presented by M07, ocean surface enthalpy fluxes 10 days before jet onset are about 50 percent larger in the control model than in the OAFlux estimate. Over the twenty day period spanning jet onset, the increase in surface enthalpy flux peaks near 80 W m^{-2} over the Arabian Sea, which is comparable with the composite OAFlux change, but the model also produces an increase over the Bay of Bengal that peaks near 150 W m^{-2} (Fig. 5-7, bottom left), while almost no coherent increase is seen in the OAFlux composite in the Bay of Bengal. The model increase over the Bay of Bengal is consistent with a collocated increase in low-level westerlies that is not seen in the NCEP data. There is thus evidence that the thermally direct baroclinic circulation increases concurrently with meridional gradients of surface enthalpy flux in the model, and that this is accompanied by an increase in westerly barotropic winds. Given that these dynamics resulted in an abrupt onset in the two-mode model used in Chapter 2, it is not clear why onset is not more abrupt in the control run of the MITgcm.

5.3.3 WISHE and the mean monsoon

Although the effect of WISHE on the phenomenon of abrupt onset could not be assessed in this model, WISHE did strongly alter the intensity and structure of the model's mean summer monsoon. We have already shown that WISHE increased the amplitude of low-level monsoon westerlies by about 50 percent and strengthened the cross-equatorial mass flux by at least 20 percent in the MITgcm. This increase in baroclinic monsoon flow is consistent with fact that a stronger summer mean meridional gradient of surface enthalpy fluxes exists in the run with WISHE (Fig. 5-8). Compared to the no-WISHE run, the control run has larger surface enthalpy fluxes stretching from the Arabian Sea to the Bay of Bengal, and smaller fluxes over the equatorial Indian Ocean. This amounts to an increase

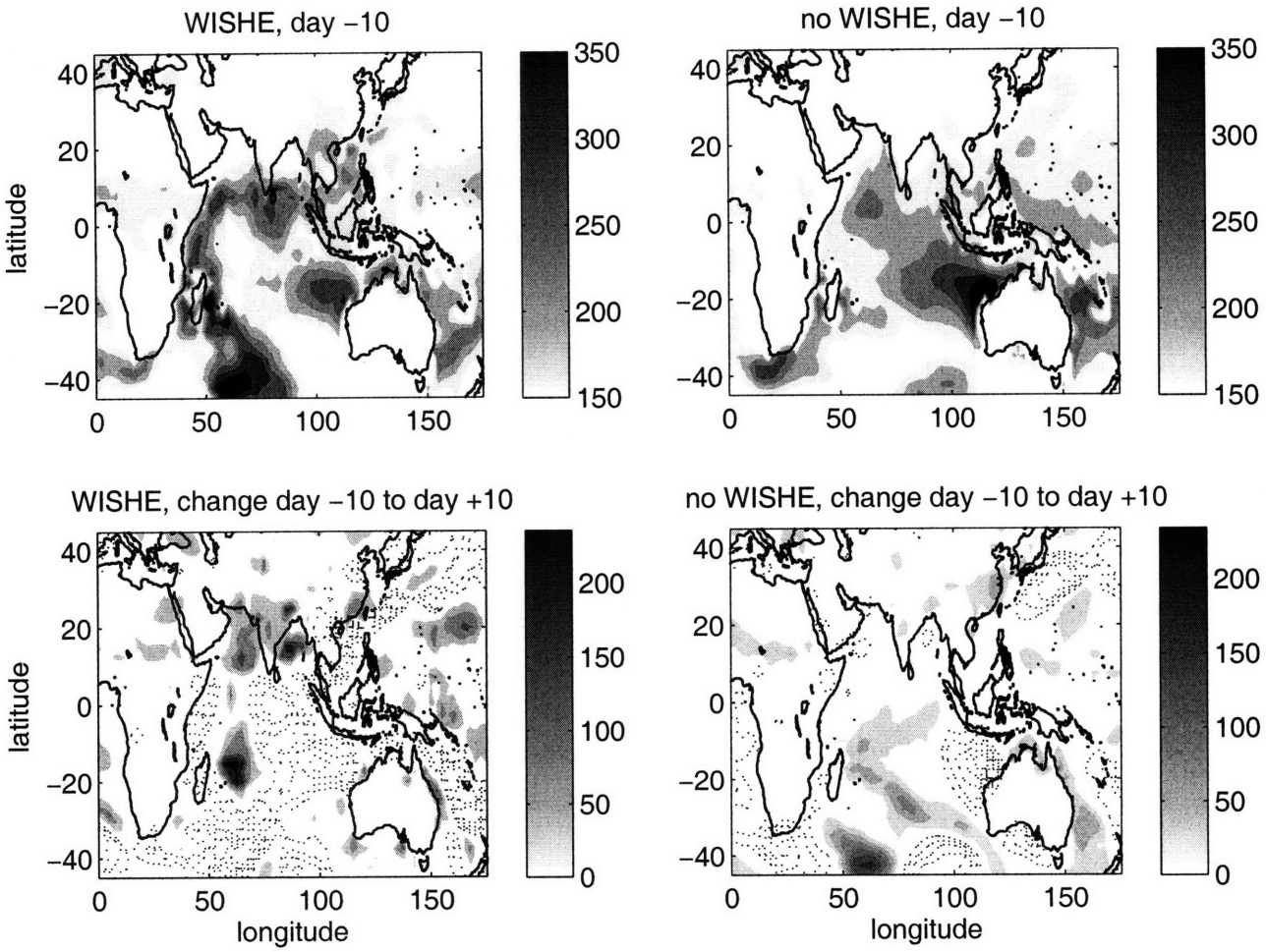

Figure 5-7: Composite surface enthalpy flux in the MITgcm 10 days before jet onset for the control run (top left) and the run without WISHE (top right). In the top panels shading starts at 150 W m^{-2} with a contour interval of 40 W m^{-2}. Bottom panels show the change in surface enthalpy fluxes over the 20 day period centered on jet onset for the run with WISHE (bottom left) and the run without WISHE (bottom right). In the bottom panels shading denotes an increase in surface enthalpy fluxes, dotted contours a decrease, and the contour interval is 40 W m^{-2} with the zero contour omitted.

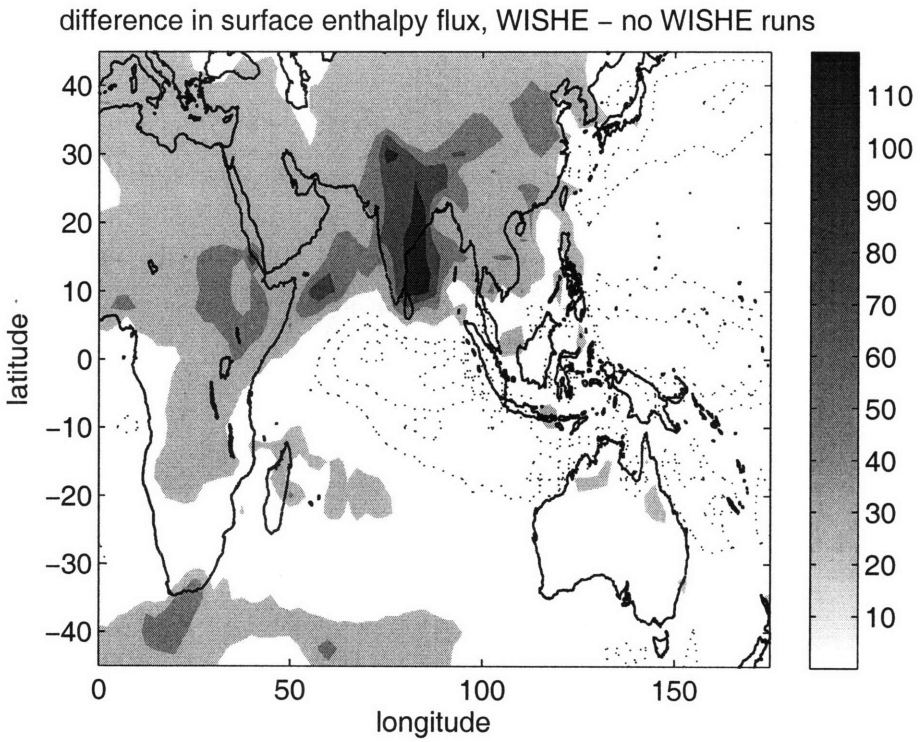

Figure 5-8: June-August mean difference in surface enthalpy flux between the WISHE and no-WISHE runs. Shading denotes fluxes that are larger in the run with WISHE, and dotted lines fluxes that are smaller. Contour interval is 25 W m^{-2} with the zero contour omitted.

in the meridional gradient of surface enthalpy fluxes of more than 100 W m^{-2} over about 10°of latitude. Surface enthalpy fluxes are about 80 W m^{-2} larger over India in the control run than in the no-WISHE run, which is not a direct effect of WISHE because the net downward surface radiation over India differs by the same amount (not shown). This change in radiation seems to occur because enhanced ocean evaporation produces increased atmospheric humidity over India, which then increases the atmospheric thermal emissivity. WISHE may thus be coupled through advection to a moisture-radiation feedback over land. Although this effect is largest over India, surface enthalpy fluxes do increase by about 30 W m^{-2} over much of Africa and Asia.

The model precipitation field shows that WISHE also strongly alters the distribution of precipitation in a manner consistent with the idealized model results of Chapter 3. To illustrate this, we present monthly mean climatologies of precipitation from the control run, the no-WISHE run, and the Global Precipitation Climatology Project (GPCP) Version 2

Combination product. The GPCP product is a weighted average of precipitation estimates from rain gauges and both infrared and microwave satellite irradiances. The use of monthly mean climatologies provides a useful smoothing of intraseasonal variations, partially compensating for the small number of years included in the model climatologies and allowing the seasonal mean meridional structure to be more easily seen. In a limited zonal mean over part of the Asian monsoon domain (50-100°E), a precipitation maximum is consistently positioned 5-15° south of the equator throughout the year in both the control run and observations, and the transition from boreal winter to boreal summer is associated with the migration of a second precipitation maximum from the equator to about 20°N (Fig. 5-9). During boreal summer the peak near 20°N has a higher amplitude than the peak just south of the equator. The control model precipitation is stronger by a few mm day^{-1} and is more bimodal than the observed precipitation outside of boreal summer, with a peak just north of the equator separated from the southern hemisphere peak.

In the run integrated without WISHE, the near-equatorial precipitation peak dominates throughout the year and has more than twice the amplitude of that in the control run or observations. This peak moves fairly smoothly in a seasonal cycle between about 10°S and the equator, and is centered near 2°N in July. A secondary maximum does migrate northward to about 20°N during boreal summer, but this peak has about half the amplitude of the northern hemisphere peak in the control run. Although the peak near 20°N in the no-WISHE run is almost as strong as in observations, it begins its poleward migration about one month later in the year and does not progress quite as far north. A qualitatively similar effect of WISHE was seen in integrations of the two-mode model forced by the combination of a subtropical SST anomaly and an SST distribution with a cross-equatorial gradient. As long as the subtropical SST anomaly was sufficiently weak in that model (about 3 K or smaller), turning off WISHE localized convective activity near the equator and substantially weakened the secondary maximum near 20°N (e.g. Fig. 3-12 of Chapter 3).

Given the two-mode model results from Chapter 3, this would seem to suggest that without WISHE, the thermal forcing associated with the South Asian land mass is not sufficiently strong to produce a cross-equatorial angular momentum conserving (AMC) circulation. In the axisymmetric two-mode model the degree to which the circulation homogenized absolute angular momentum could be assessed using the absolute vorticity, η, near the model tropopause, which approached zero for an AMC circulation. For a 3 K subtropical SST

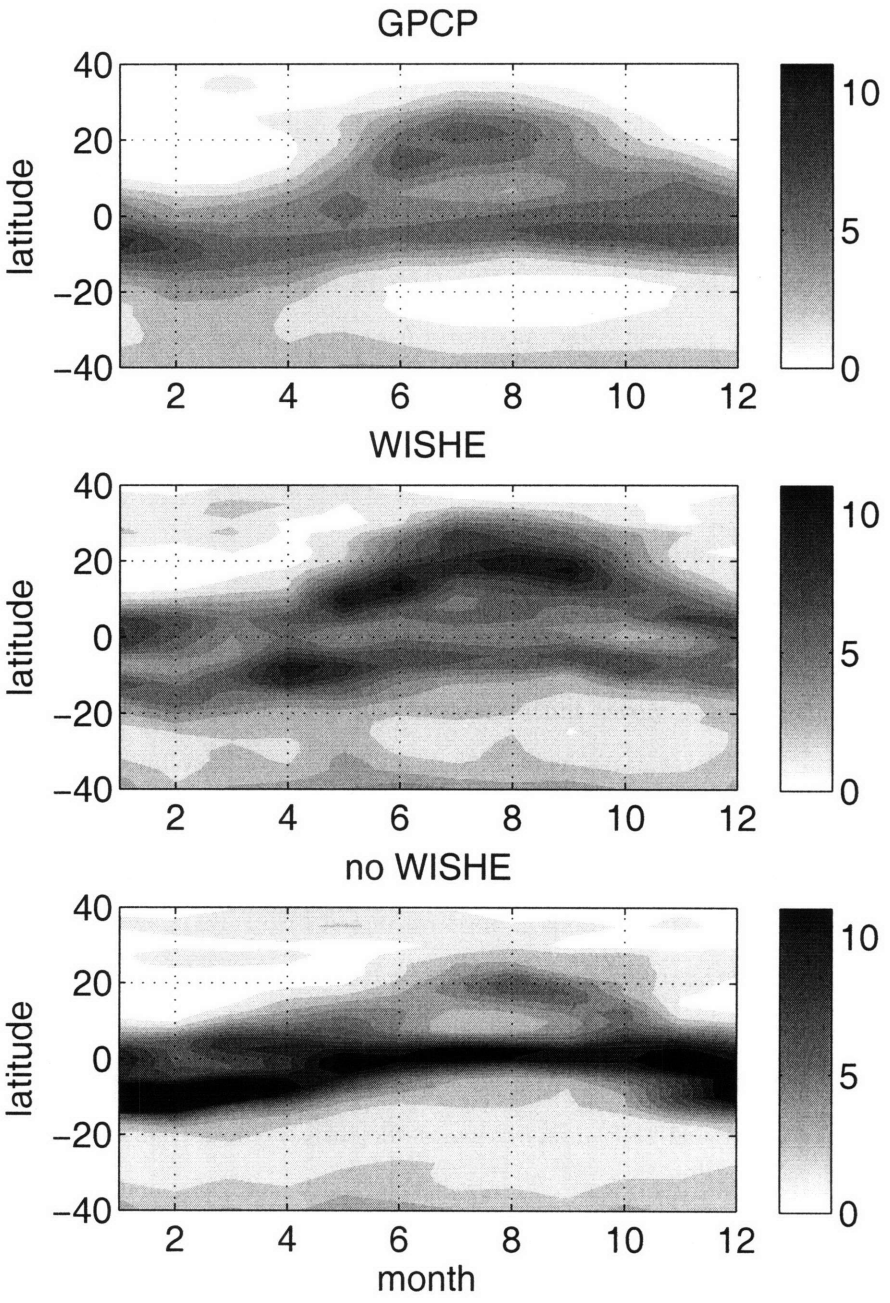

Figure 5-9: Monthly mean climatologies of precipitation, averaged 50-100°E, for the GPCP observational dataset (top), the MITgcm control run (middle), and the MITgcm run without WISHE (bottom). Contour interval is 1 mm day^{-1} in all panels. Contours in the bottom panel exceed the color scale, with the near-equatorial precipitation peaking at 22 mm day^{-1} in boreal winter and 14 mm day^{-1} in boreal summer.

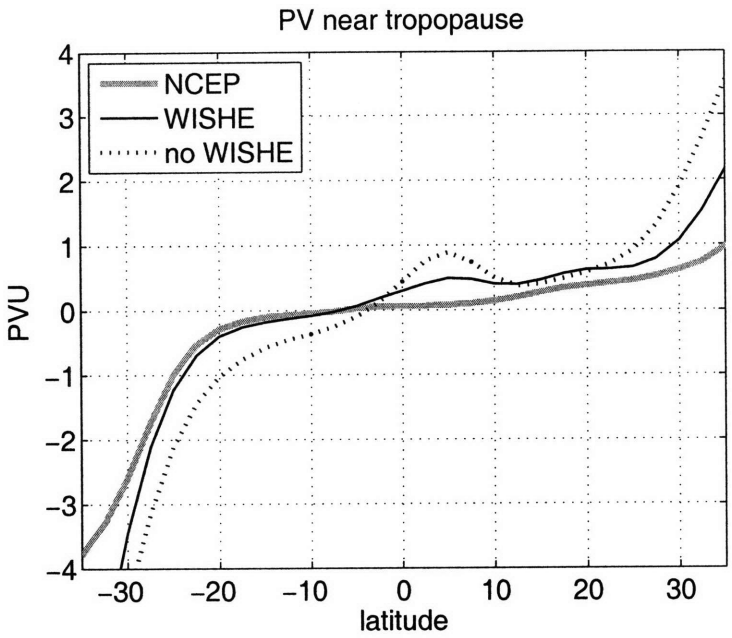

Figure 5-10: Potential vorticity (PV), averaged for June-August and 50-100°E. Grey line shows PV for the NCEP Reanalysis at 350 K. PV for the MITgcm is approximated by $-g(f+\zeta)\partial_p\theta$ at 150 hPa, and is shown by the black solid line for the run with WISHE and the dotted line for the run without WISHE.

anomaly superimposed on a cross-equatorial SST gradient, η approached zero uniformly in the tropics only when WISHE was included in the model. Without WISHE, ascent and a positive region of η occurred just north of the equator, indicating that an AMC circulation did not exist between the equator and the subtropical SST anomaly. As discussed by Plumb (2007), the relevant dynamical constraint on AMC flow in three dimensions is phrased in terms of the tropopause potential vorticity (PV): steady, inviscid upper-level divergence can be maintained only when the upper-level PV is no longer locally cyclonic. We have already seen that in the three-dimensional MITgcm, turning off WISHE produces intense precipitation just north of the equator in the summer mean over the Indian Ocean. Diagnosis of the PV at 150 hPa, which is near the model tropopause, shows that this precipitation peak in the no-WISHE run is accompanied by a positive PV anomaly (Fig. 5-10). The control run does exhibit a small positive anomaly in the same region, but it is weaker than that in the no-WISHE run. To compare with the NCEP Reanalysis, we show the PV at 350 K, which is near the 150 hPa surface within about 10°of the equator. No local positive PV anomaly is seen near the equator on this isentropic surface.

5.4 Concluding remarks

This chapter assessed the role played by WISHE in the seasonal cycle of the South Asian summer monsoon as simulated by a three-dimensional atmospheric GCM with realistic topography and detailed parameterizations of subgrid scale physics. Low-level westerlies and precipitation in the model's summer monsoon were about 20 percent stronger than in observations, although the cross-equatorial mass flux was slightly weaker than in reanalyzed winds. The control model, integrated with WISHE, did not produce an onset of southwesterly wind speeds in the Somali jet that was significantly more abrupt than the evolution of the insolation forcing. However, the spatial structure of changes in zonal wind and cross-equatorial flow accompanying the onset of this jet did resemble that found in reanalyzed winds, even though the onset was less abrupt. Also, the control model simulated the bimodal structure of precipitation in the mean South Asian summer monsoon, with the peak convection occurring near 20° N and a secondary maximum located just south of the equator over the Indian Ocean.

Even though the control model did not produce an abrupt onset of the Somali jet, a version of the model was integrated without WISHE to examine the role of this process in the monsoon's seasonal cycle. This task was motivated by the axisymmetric model results of Chapter 3, which showed that if a subtropical forcing is not sufficiently strong to produce angular momentum conserving flow in the absence of WISHE, WISHE can bring about a transition to AMC flow. Results from the MITgcm are consistent with these idealized model results in that, for the run without WISHE, the peak precipitation remained within a few degrees of the equator during boreal summer, and the precipitation maximum near 20°N was weakened by a factor of two compared to the control model. The Somali jet and zonal winds over the Indian Ocean also weakened considerably in the no-WISHE run. Together with the results of Chapter 3 and the diagnosis of upper-level PV in the MITgcm, this suggests that turning off WISHE breaks the conservation of absolute angular momentum at upper levels between South Asia and the equator. Turning off WISHE in the MITgcm also reduced the net downward radiation at TOA over India, suggesting that WISHE is coupled to radiative processes that also enhance meridional gradients of surface enthalpy fluxes over land. Without the combined effects of WISHE and this coupled radiative feedback, the thermal forcing associated with the South Asian land mass seems to be insufficient for

driving an AMC circulation.

To be clear, the hypothesis that WISHE is responsible for the abrupt onset of the South Asian summer monsoon was not tested in this chapter because the phenomenon of abrupt onset was not simulated by the model. Indeed, the fact that the model included WISHE and did not produce an abrupt onset could be taken as evidence that some other physics not well represented in the model is responsible for the abrupt nature of onset. For example, preliminary spectral analyses of OLR (not shown) indicate that tropical intraseasonal variability in the MITgcm is biased toward lower frequencies in both space and time compared to observations, and lacks a peak corresponding to the eastward propagating Madden Julian Oscillation (MJO). These deficiencies are common to almost all GCMs participating in the most recent assessments of climate simulations (Lin and coauthors, 2006). If the MJO is somehow responsible for the abrupt nature of monsoon onset, then its absence in the MITgcm could produce an onset less abrupt than in observations. Numerous authors have investigated the role of the MJO in the onset of the Australian monsoon with somewhat disparate results (see Wheeler and McBride, 2005, for a review), but comparatively few studies have documented its association with onset of the South Asian monsoon (e.g. Lau et al., 1998; Flatau et al., 2001). Lack of an MJO is only one example of a model deficiency that might result in a too gradual onset of the monsoon. Another possibility is that WISHE is responsible for the abrupt onset seen in observations, but that some other process obscures this phenomenon in the MITgcm. For example, Chapter 2 showed that the WISHE feedback can only produce an abrupt intensification of an axisymmetric Hadley circulation once the thermal forcing exceeds a particular threshold. The use of interactive SST might increase the magnitude of this threshold so that when prescribed SSTs are used in a model the feedback becomes active too early in the year, thereby producing an early onset that is perhaps of lower amplitude due to the weaker poleward gradient of insolation at that time. These ideas are only provided as examples of deficiencies that might operate in this and other GCMs.

Despite the fact that the phenomenon of abrupt onset was not represented in the MITgcm, our results provide some insight into the role WISHE might play in setting the summer mean distribution of winds and precipitation in South Asia. Furthermore, the diagnostics presented here and in the previous chapter may be useful in assessing the fidelity of the dynamical signals associated with monsoon onset in other GCMs.

THIS PAGE INTENTIONALLY LEFT BLANK

Chapter 6

Conclusion

6.1 Summary of chapters

The first two chapters of this thesis examined the effect of wind-induced surface heat exchange (WISHE) on nonlinear axisymmetric Hadley circulations forced by seasonally varying SST. A quasi-equilibrium closure was used to represent the effects of moist convection. In two different axisymmetric aquaplanet models, an SST maximum localized off the equator was used as a proxy for the thermal forcing of an off-equatorial land mass. The effect of WISHE on the resulting circulation in these models was classified in several qualitatively different regimes, depending on the strength of the SST forcing. For the weakest SST forcings, the meridional circulation evolved linearly with the forcing because any wind-evaporation feedback was suppressed due to the fact that drag keeps surface winds small compared to upper-level winds in the Hadley circulation. For slightly stronger forcings, the convergence of zonal momentum into the ascent branch of the circulation overcame the effect of surface drag to create strong surface westerlies, and thus strong surface enthalpy fluxes, near the SST peak. This amounted to a positive feedback between the strength of the circulation and the poleward gradient of surface enthalpy fluxes, and produced a nonlinear increase in meridional flow as a function of the SST forcing. These two regimes, examined in Chapter 2 using both a primitive equation model and a model with two vertical modes, occurred for fairly weak circulations with little homogenization of absolute angular momentum in the upper troposphere.

Chapter 3 used the axisymmetric two-mode model to show that WISHE reduces the critical forcing amplitude needed to produce flow that does homogenize absolute angular

momentum at upper levels. This reduction in the critical forcing amplitude was shown to occur because WISHE narrows the subcloud layer entropy peak and shifts it toward the equator, with a similar effect on the ITCZ. These effects, in turn, were shown to occur because of a mechanism similar to that thought responsible for the frontal collapse of hurricane eyewalls (Emanuel, 1997). For forcings strong enough to produce angular momentum conserving (AMC) flow even in the absence of WISHE, the conservation of angular momentum was shown to provide a strong dynamical constraint. The primary effect of WISHE for such strong forcings was the same narrowing and slight equatorward shift of the ITCZ and subcloud entropy peak that occurred for weaker forcings. All of these results were shown to hold for seasonally varying forcings. In particular, when the strongest SST forcings were varied in a seasonal cycle WISHE shifted the abrupt onset to a time earlier in the seasonal cycle. For weaker seasonal forcings which would not reach a critical threshold for AMC flow in the absence of WISHE, WISHE produced an abrupt onset by either reducing the critical threshold or providing a positive feedback on the strength of non-AMC flow.

The consistency of these ideas with observations of the South Asian summer monsoon was assessed in Chapter 4. A dynamical index of monsoon flow was defined based on the speed of the southwesterly Somali jet, following Krishnamurti et al. (1981), and was used to create composites of changes occurring during the onset of the jet. These composites confirmed that the onset of the jet does occur faster than can be accounted for by a linear response to the insolation forcing, and is accompanied by an increase in both the meridional monsoon flow and convective activity over India and the surrounding ocean. The dynamical changes that occur during jet onset were found to project strongly onto the two modes used in the idealized axisymmetric model of Chapters 2 and 3, and these changes were seen to occur concurrent with a large increase in surface enthalpy fluxes over the Arabian Sea. While this alone is consistent with a wind-evaporation feedback, we quantitatively compared the changes occurring during the onset of the Somali jet with those expected in a convective quasi-equilibrium framework. The increase in surface enthalpy fluxes over the Arabian Sea was shown to be nearly collocated with an increase in boundary layer entropy, which in turn was roughly consistent, under the assumptions of quasi-equilibrium, with the change in geopotential needed to balance the increased southwesterlies in the Somali jet. However, the peak changes in free-tropospheric temperature and upper-level potential vorticity (PV) were found to occur over land near the western edge of the Tibetan Plateau, mostly in a

region of strong subsidence where the free troposphere and subcloud layer were estimated to be thermodynamically decoupled. Investigation of the mechanism responsible for this free-tropospheric temperature change was left for future work.

Finally, Chapter 5 presented integrations of a three-dimensional primitive equation model configured with realistic topography and prescribed weekly SST from observations. The control integration used wind-dependent surface enthalpy fluxes, and produced a South Asian monsoon with zonal winds and precipitation somewhat stronger than observed. The onset of the Somali jet in this control integration was not abrupt, so it was not possible to use this model to test whether WISHE produces the abrupt onset of the South Asian monsoon. However, it was possible to reject the null hypothesis that WISHE has little effect on the mean summer monsoon in the model, because a run integrated with wind-independent surface enthalpy fluxes produced a much weaker monsoon circulation. In that run, the main precipitation peak remained near the equator throughout the year and failed to migrate poleward toward South Asia, and the upper-level PV exhibited a near-equatorial peak indicative of a lack of homogenization of absolute angular momentum. This is consistent with results from the two-mode model forced by an off-equatorial SST anomaly that was strong enough to produce AMC flow only with the effects of WISHE, and thus suggests that the thermal forcing of the South Asian land mass may be supercritical to AMC flow only with WISHE.

6.2 Open questions

These results are only a first step in the examination of the role of WISHE in the Earth's seasonal cycle, especially since the axisymmetric models on which the theoretical ideas in this thesis were based did not include the effects of numerous complications, including zonal asymmetries, interactive SST, land surface hydrology, and moisture-radiation feedbacks. Chapter 5 attempted to determine the role of WISHE in monsoon onset in the presence of these complications without understanding their effect at a fundamental level, but this approach met with mixed success because, while WISHE was shown to be necessary for a producing a reasonably strong summer monsoon in the model, it did not produce an abrupt onset of this monsoon. This highlights two distinct approaches for using numerical models to assess the effect of a physical mechanism: testing the effect of the mechanism in a

three-dimensional GCM with realistic boundary conditions and forcings, and using models of intermediate complexity in idealized process studies to understand certain aspects of the mechanism.

While the first approach may seem to provide some quick answers, it assumes that a GCM can be found that faithfully represents the phenomenon of interest, which in this thesis is the abrupt onset of monsoons as assessed by dynamical criteria. Some of the diagnostics presented in this thesis would need to be applied to various GCMs to determine whether such a GCM exists. Until that is done, we suggest using idealized models of intermediate complexity in future work to explore two processes in particular. The first process is the effect of interactive SST on WISHE. As suggested in Chapter 5, this is intriguing because numerous atmospheric GCMs seem to produce overly strong monsoons (e.g. Kang et al., 2002), and this bias was reduced in one particular model by use of interactive SST (Meehl et al., 2006). Perhaps the use of interactive SST would preferentially damp the action of wind-evaporation feedback on longer time scales, thereby reducing the strength of the mean monsoon while having comparatively little effect on the faster process of monsoon onset. This possibility could be explored not only in numerical models, but analytically by extending the linear WISHE theory of Emanuel (1993) to allow for variations in SST.

The second process we suggest examining in idealized models is the interaction of monsoon onset with propagating intraseasonal convective anomalies. Poleward propagating convective anomalies occurred in the two-mode model for sufficiently low values of the surface gustiness parameter (i.e. 2 m s^{-1} or less), but these were suppressed when the subtropical SST anomaly was large enough to produce AMC flow. In that case, the process of abrupt onset consisted of a discontinuous poleward jump of the ITCZ rather than a continuous poleward migration (e.g. Fig. 3-12)[1]. Bellon and Sobel (2008, in press) obtained poleward propagating convective anomalies in a two-mode model coupled to a dynamical boundary layer, and found that boundary layer physics played an important role in the dynamics of these anomalies. It could thus be useful to examine the response of their model to a seasonally varying forcing, which would also allow for an assessment of the effects of a dynamical boundary layer on the mechanisms discussed in this thesis.

[1]It is not obvious whether observations of South Asian monsoon onset provide more evidence for a continuous migration or a discontinuous jump of the convective maximum (e.g. see events presented in Goswami, 2005). Although the climatological OLR presented in Chapter 1 (Fig. 1-3) exhibited a continuous migration of the convective maximum, this could be due to averaging of a large number of discontinuous jumps.

Further analysis of observations may prove just as valuable as work with numerical models. In particular, we emphasize the suggestion made in Chapter 4 to calculate the change in horizontal advection of subcloud layer entropy occurring during the onset of the Somali jet. This would be best done on the native σ levels of the NCEP Reanalysis, which were not used in the composites presented in Chapter 4. As noted in that chapter, changes in horizontal entropy advection may prove important because the largest change in free-tropospheric temperature was centered over land nearly coincident with the peak horizontal gradient in subcloud layer entropy. Also, analysis of the moist static energy budget showed an abrupt increase in ascent over land without any abrupt change in the vertically integrated atmospheric moist static energy source. While this could be explained by an abrupt change in the gross moist stability, changes in the horizontal advection of moist static energy (which we would naively expect to be dominated by advection in the subcloud layer) could be of equal or even greater importance.

Finally, we suggest using both observations and numerical models to examine whether the radiative effects of atmospheric moisture could provide a positive feedback on the strength of the monsoon circulation. Results from the three-dimensional GCM used in Chapter 5 showed that including WISHE in the model increased surface enthalpy fluxes over the Indian subcontinent, not because of a direct wind-evaporation feedback with the land surface, but seemingly because WISHE indirectly altered the radiative energy balance of the land surface. Enhanced evaporation over the Arabian Sea could lead to more humid air over India through zonal advection by the low-level monsoon westerlies, which could then reduce the thermal radiation lost by the land surface. Alternatively, a wind-evaporation feedback could produce stronger monsoon precipitation, cooling the soil and thus also reducing the thermal radiation lost by the land surface. It should be possible to use observations to estimate changes in the land surface radiative balance during the course of monsoon onset. Additional work could be performed with numerical models, although axisymmetric models with a coastline set at one particular latitude will likely not represent the processes just discussed because of the peninsular geometry of India.

6.3 Concluding remarks

Axisymmetric baroclinic circulations are known to be linearly unstable to wind-evaporation feedback (Emanuel, 1993), and the onset of the South Asian summer monsoon is known to be accompanied by a large increase in evaporation over the Arabian Sea (Weller et al., 1998). It thus seemed reasonable to hypothesize that wind-evaporation feedback is responsible for the abrupt onset of monsoon circulations, at least in the regions of South Asia and Australia where the bulk of monsoon precipitation occurs over ocean. Indeed, Numaguti (1995) showed that the wind-dependence of ocean evaporation in a GCM produced an abrupt poleward shift of the intertropical convergence zone (ITCZ) as the peak of a sea surface temperature (SST) forcing was moved gradually from the equator toward the subtropics. This thesis examined the role played by wind-evaporation feedback in the context of nonlinear axisymmetric Hadley circulations, comparing highly idealized theory and models to both observations and a detailed, three-dimensional primitive equation model.

Results from the first half of the thesis showed that previous theory for the nonlinear response of axisymmetric Hadley circulations to off-equatorial thermal forcings (e.g. Plumb and Hou, 1992) is valid in a moist framework where surface enthalpy fluxes depend on wind speed. WISHE was shown to reduce the critical forcing amplitude needed to obtain a nonlinear response, and results from the three-dimensional GCM discussed in Chapter 5 suggest that the thermal forcing of the South Asian land mass would be subcritical without the effect of WISHE. While there are numerous open questions concerning these model results, the observational composites presented in Chapter 4 are remarkably consistent with a wind-evaporation feedback causing the abrupt increase of ascent, convective activity, and baroclinic zonal wind seen over ocean during the onset of the Somali jet. Future work will hopefully determine how the concurrent, lower amplitude changes seen over land are related.

Appendix A

The relevance of zonal mean diagnostics to monsoon onset

In the zonal mean, the peak tropical precipitation and ascent is known to shift rather abruptly from one side of the equator to the other some time before each solstice (e.g. Xian and Miller, 2007, in press). This can be seen in the climatological zonal mean OLR from NOAA satellites, which has tropical minima centered between 5° and 10° off the equator throughout the year, even during the equinoxes when the peak solar insolation falls on the equator (Fig. A-1, top panel). In April the OLR minimum south of the equator fades and a new OLR minimum forms north of the equator, resulting in an abrupt meridional shift of the tropical OLR minimum (denoted by the black line in Fig. A-1). The reverse shift from north to south of the equator occurs in early December.

These abrupt shifts in the latitude of the tropical OLR minimum actually result from the superposition of a bimodal precipitation distribution in the Pacific with a relatively smooth seasonal cycle at all other longitudes. A limited zonal mean across the Pacific (135-275°E) shows a pattern similar to that seen in the zonal mean, with OLR minima centered 5-10° off the equator throughout the year (Fig. A-1, middle panel). In this Pacific mean, the Northern and Southern Hemisphere minima are both present throughout the year, although their relative amplitudes vary in a seasonal cycle. As shown in Chapter 1 (Fig. 1-1), the bulk of convective activity in the tropical Pacific occurs in the East Pacific intertropical convergence zone (ITCZ), the South Pacific Convergence Zone (SPCZ), and near the Philippines, all of which are located 5-10° off the equator. The Northern

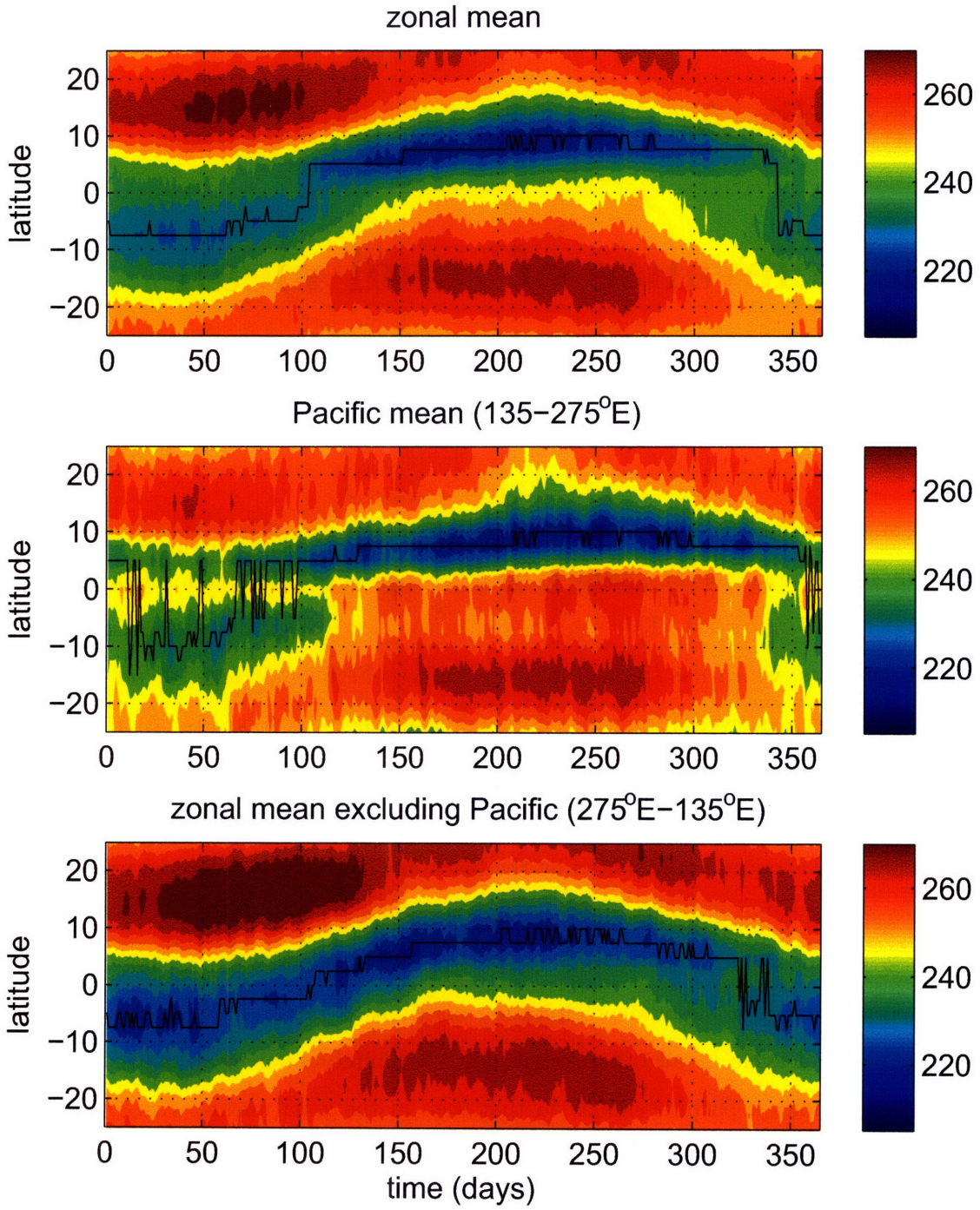

Figure A-1: Climatological daily NOAA OLR for a global zonal mean (top), a limited zonal mean across the Pacific Ocean (middle), and a limited zonal mean for all latitudes outside the Pacific (bottom). Contour interval in all panels is 5 W m^{-2}, and the solid black line passes through the minimum tropical OLR.

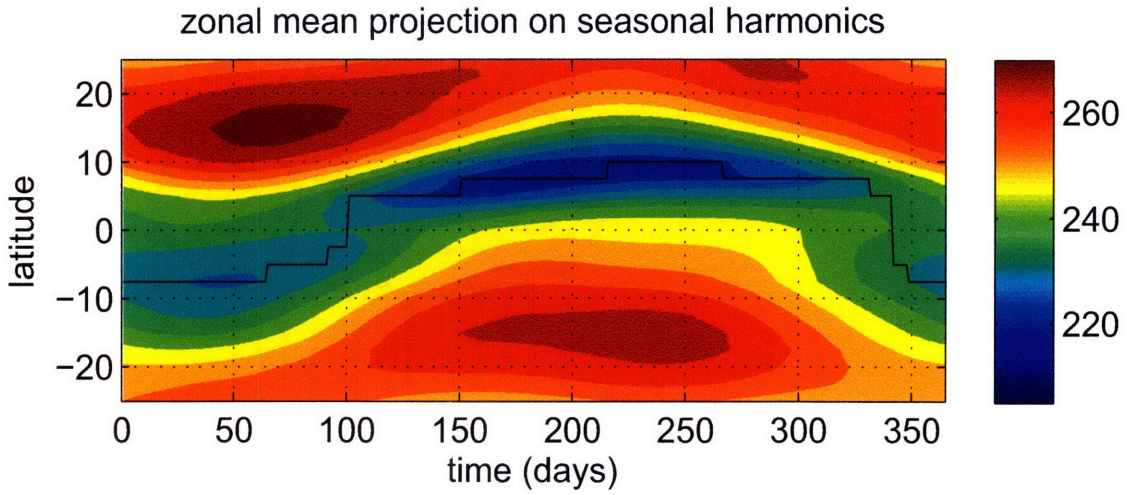

Figure A-2: As in the previous figure, but for the projection of the zonal mean OLR onto the first three seasonal harmonics.

Hemisphere minimum in the Pacific mean is more intense than the Southern Hemisphere minimum largely because the signals of the Philippines minimum and the East Pacific ITCZ add, while the SPCZ signal is partly cancelled by the large OLR occurring over the stratocumulus region off the west coast of South America.

An average over all latitudes outside the Pacific (i.e. a zonal mean excluding 135-275°E) shows an OLR minimum that migrates in a fairly smooth seasonal cycle from about 8°S in boreal winter to 10°N in boreal summer (Fig. A-1, bottom panel). There is some hint of an abrupt shift of the minimum across the equator in late November, but there is little evidence for a similar shift in boreal spring or summer (the small abrupt shifts in the black line are mostly due to the 2.5° discretization of the OLR data).

The abrupt shift in the latitude of the zonal mean OLR minimum thus does not seem to represent an abrupt onset of any monsoon circulation, but simply a seasonal cycle in the relative amplitude of the SPCZ and the East Pacific ITCZ, with some additional contribution from convective activity north of the equator near the Philippines. The cross-equatorial shift of the zonal mean OLR minimum cannot even be called abrupt by the definition used in this thesis, because it still occurs after subtracting any signal from the zonal mean OLR that projects onto frequencies higher than the first three seasonal harmonics (Fig. A-2).

THIS PAGE INTENTIONALLY LEFT BLANK

Appendix B

Equilibration time scale of axisymmetric models

The nonlinear dependence of circulation strength on the forcing in axisymmetric theory results from advection of absolute angular momentum in the free troposphere, so the relevance of this nonlinearity in a time-dependent scenario would seem to depend on the relative magnitudes of the momentum advection time scale and the forcing time scale. Plumb and Hou (1992) found that it took as long as 400 days for their dry, axisymmetric model to reach a steady state, and suggested that this resulted from the roughly 100-day time scales for viscous dissipation and meridional overturning in their model. In this section we use simple scaling arguments to estimate more explicitly the factors that set the time scale for advection of angular momentum in axisymmetric models.

The circulation in the interior of an inviscid atmosphere will conserve absolute angular momentum M:

$$M = \Omega_e a^2 \cos^2 \phi + ua \cos \phi \tag{B.1}$$

where Ω_e is the planetary rotation rate, a the planetary radius, u zonal velocity, and ϕ latitude. In an atmosphere near a resting state, advection will be almost entirely meridional until M surfaces deviate considerably from the vertical. A scale estimate for the meridional wind v can be obtained from the thermodynamic equation under the assumption that the dominant balance is between the diabatic heating Q and vertical advection of potential

temperature θ:

$$\omega S \sim \frac{Q}{c_p} \tag{B.2}$$

where ω is vertical velocity in pressure coordinates, $S \equiv \partial\theta/\partial p$, and c_p is the specific heat at constant pressure. The meridional circulation will adjust quite rapidly to satisfy (B.2): Eliassen (1951) showed that the thermally forced meridional circulation in an axisymmetric vortex equilibrates on a time scale near that of the local inertial period. The bulk of the free tropospheric meridional flow will occur over some vertical distance Δp and some horizontal distance $\Delta y = y_2 - y_1$ (we use Cartesian coordinates for simplicity). Then by continuity in a zonally symmetric fluid,

$$v = -\int_{y_1}^{y_2} \frac{\partial\omega}{\partial p} dy \sim \frac{Q\Delta y}{Sc_p\Delta p} \tag{B.3}$$

The time scale τ_M for meridional advection is then

$$\tau_M \sim \frac{Sc_p\Delta p}{Q} \tag{B.4}$$

Estimates of τ_M for several models are presented in Table B.1. The fact that the integrations conducted by Plumb and Hou (1992) took hundreds of days to equilibrate is consistent with the parameters of their model: Δp = 400 hPa and values of S and Q appropriate for relaxation over a 10-day time scale to a temperature profile that was isothermal in the vertical and had maximum horizontal anomalies of about 10 K. The dry model of Fang and Tung (1999) used a stratification characteristic of a moist adiabat, but prescribed temperature relaxation over a 20-day time scale to produce typical Newtonian cooling rates of 0.3 K/day (inferred from their figures). It should be noted that τ_M is the time scale for M advection, and that the M field will likely take several times this long to

Table B.1: Estimated equilibration time scales

Model	Temperature profile	Stratification (S)	Heating rate	τ_M
Plumb and Hou (1992)	Isothermal	-2 × 10^{-3} K Pa^{-1}	0.5 K day^{-1}	165 days
Fang and Tung (1999)	Γ = 6 K km^{-1}	-5 × 10^{-4} K Pa^{-1}	0.3 K day^{-1}	75 days
Zheng (1998)	Moist adiabat	-5 × 10^{-4} K Pa^{-1}	1 K day^{-1}	25 days
Near-neutral stratification	$\Gamma = 0.9\ g/c_p$	-2 × 10^{-4} K Pa^{-1}	0.5 K day^{-1}	15 days

fully equilibrate. Thus, although τ_M for the Fang and Tung (1999) model is only slightly larger than the 58 day time scale of their applied thermal forcing, the M field in their model cannot be expected to achieve equilibrium when subjected to an oscillatory forcing of that frequency.

In contrast, a value of $\tau_M = 25$ days is obtained if one uses the same value of Δp but with a stratification typical of a moist adiabat and a radiative cooling rate of 1 K day^{-1}, typical values for the tropical troposphere. Such an average radiative cooling rate is the appropriate value for Q if the intensity of meridional flow is required to be consistent with a balance between radiative cooling and adiabatic heating in the subsiding branch of the circulation (e.g. Nilsson and Emanuel, 1999; Emanuel et al., 1994). The value of τ_M may be further reduced by the fact that free-tropospheric Hadley flow typically occurs within about 200 hPa of the tropopause (Peixoto and Oort, 1992). In any case, the time scale of Earth's insolation forcing is at least two to three times greater than τ_M for parameters relevant to a moist tropical atmosphere, which explains why Zheng (1998) achieved large M deformation on seasonal time scales in his moist model.

THIS PAGE INTENTIONALLY LEFT BLANK

Appendix C

Angular momentum conserving temperature in the two-mode model

The distribution of free-tropospheric saturation entropy, s^*, needed to balance winds that conserve absolute angular momentum near the tropopause has been shown by Emanuel (1995) to be a critical distribution for the onset of thermally direct circulations. When the curvature of the subcloud layer entropy exceeds that of this critical distribution, a meridional circulation must exist. However, this theory cannot be rephrased on a β-plane and directly applied to the two-mode model, because this model only conserves absolute angular momentum at one particular level slightly below its specified tropopause, as discussed in the text. Burns et al. (2006) showed that the m-conserving baroclinic zonal wind can be obtained simply by integrating the expression for m conservation at this level. This is done by using the fact that $u_0 = -u_1$ to first order in their asymptotic expansion, so that (3.6) can be rewritten, for nonzero v_1:

$$(A-1)\frac{\partial u_1}{\partial y} = \beta y \tag{C.1}$$

As also noted by Burns et al. (2006), the free-tropospheric temperature can be obtained by assuming geostrophic balance:

$$\beta y u_1 = \Delta T \frac{\partial s^*}{\partial y} \tag{C.2}$$

If (C.1) is integrated from the latitude of maximum s^*, denoted y_m, and the result is then used to integrate (C.2) from this same latitude, the result is

$$s^* = s^*_m - \frac{\beta^2}{8\Delta T(A-1)}(y_m^2 - y^2)^2 \tag{C.3}$$

Here s^*_m is the maximum saturation entropy in the free troposphere, and s^* is the saturation entropy at the latitude y. Using the definition $s = c_p ln\theta_e$ and the assumption of convective quasi-equilibrium, this provides an expression for the critical distribution of subcloud layer equivalent potential temperature θ_{eb} in the two-mode model:

$$\theta_{eb} = \theta_{em} \exp\left[-\xi(y_m^2 - y^2)^2\right] \tag{C.4}$$

with the constant ξ defined

$$\xi = \frac{\beta^2}{8c_p\Delta T(A-1)} \tag{C.5}$$

Here θ_{em} is the peak equivalent potential temperature of the subcloud layer (at latitude y_m).

Bibliography

Ackerman, S. A. and S. K. Cox, 1987: Radiative energy budget estimates for the 1979 southwest summer monsoon. *J. Atmos. Sci.*, **44**, 3052–3078.

Adcroft, A., J. Campin, C. Hill, and J. Marshall, 2004: Implementation of an atmosphere-ocean general circulation model on the expanded spherical cube. *Mon. Wea. Rev.*, **132**, 2845–2863.

Adcroft, A. J., C. N. Hill, and J. C. Marshall, 1999: A new treatment of the Coriolis terms in C-grid models at both high and low resolutions. *Mon. Wea. Rev.*, **127**, 1928–1936.

Ahrens, C. D., 2000: *Meteorology Today.* Brooks/Cole, Thomson Learning, 528 pp.

Arakawa, A. and W. Schubert, 1974: Interaction of a cumulus cloud ensemble with the large-scale environment, Part I. *J. Atmos. Sci.*, **31**, 674–701.

Bellon, G. and A. H. Sobel, 2008, in press: Poleward-propagating intraseasonal monsoon disturbances in an intermediate-complexity axisymmetric model. *J. Atmos. Sci.*

Bony, S. and K. A. Emanuel, 2005: On the role of moist processes in tropical intraseasonal variability: Cloud-radiation and moisture-convection feedbacks. *J. Atmos. Sci.*, **62**, 2770–2789.

Boyer, T., S. Levitus, H. Garcia, R. A. Locarnini, C. Stephens, and J. Antonov, 2005: Objective analyses of annual, seasonal, and monthly temperature and salinity for the World Ocean on a 0.25° grid. *Int. J. Climatol.*, **25**, 931–945.

Burns, S., A. Sobel, and L. Polvani, 2006: Asymptotic solutions of the axisymmetric moist Hadley circulation in a model with two vertical modes. *Theor. Comput. Fluid Dyn.*, **20**, 443–467.

Chang, C.-P., Z. Wang, J. McBride, and C.-H. Liu, 2005: Annual cycle of Southeast Asia – Maritime Continent rainfall and the asymmetric monsoon transition. *J. Climate*, **18**, 287–301.

da Silva, A. M., C. Young, and S. Levitus, 1994: Atlas of surface marine data, vol. 3: Anomalies of heat and momentum fluxes. Tech. rep., NOAA National Environmental Satellite, Data, and Information Service, 416 pp.

Dima, I. M. and J. M. Wallace, 2003: On the seasonality of the Hadley cell. *J. Atmos. Sci.*, **60**, 1522–1527.

Durre, I., S. V. Russell, and D. B. Wuertz, 2006: Overview of the Integrated Global Radiosonde Archive. *J. Climate*, **19**, 53–68.

Eliassen, A., 1951: Slow thermally or frictionally controlled meridional circulation in a circular vortex. *Astrophysica Norvegica*, **5**, 19–60.

Emanuel, K., 1993: The effect of convective response time on WISHE modes. *J. Atmos. Sci.*, **50**, 1763–1775.

Emanuel, K. A., 1987: Air-sea interaction model of intraseasonal oscillations in the Tropics. *J. Atmos. Sci.*, **44**, 2324–2340.

Emanuel, K. A., 1995: On thermally direct circulations in moist atmospheres. *J. Atmos. Sci.*, **52**, 1529–1536.

Emanuel, K. A., 1997: Some aspects of hurricane inner-core dynamics and energetics. *J. Atmos. Sci.*, **54**, 1014–1026.

Emanuel, K. A., J. D. Neelin, and C. S. Bretherton, 1994: On large-scale circulations in convecting atmospheres. *Q. J. R. Meteorol. Soc.*, **120**, 1111–1143.

Emanuel, K. A. and M. Zivkovic-Rothman, 1999: Development and evaluation of a convection scheme for use in climate models. *J. Atmos. Sci.*, **56**, 1766–1782.

Fang, M. and K. K. Tung, 1999: Time-dependent nonlinear Hadley circulation. *J. Atmos. Sci.*, **56**, 1797–1807.

Fasullo, J. and P. Webster, 2003: A hydrological definition of Indian Monsoon onset and withdrawal. *J. Climate*, **16**, 3200–3211.

Ferranti, L., J. Slingo, T. Palmer, and B. Hoskins, 1999: The effect of land-surface feedbacks on the monsoon circulation. *Q. J. R. Meteorol. Soc.*, **125**, 1527–1550.

Findlater, J., 1969: A major low-level air current near the Indian Ocean during the northern summer. *Q. J. R. Meteorol. Soc.*, **95**, 362–380.

Findlater, J., 1971: Mean monthly air flow at low levels over the western Indian Ocean. *Geophys. Mem.*, HMSO, London, 53.

Findlater, J., 1972: Aerial explorations of the low-level cross-equatorial current over eastern Africa. *Q. J. R. Meteorol. Soc.*, **98**, 274–289.

Flatau, M. K., P. J. Flatau, and D. Rudnick, 2001: The dynamics of double monsoon onsets. *J. Climate*, **14**, 4130–4146.

Flohn, H., 1974: Contribution to a comparative meteorology of mountain areas. *Arctic and Alpine Environments*, J. D. Ives and R. G. Barry, Eds., Methuen, London, 55–71.

Fouquart, Y. and B. Bonnel, 1980: Computation of solar heating of the Earth's atmosphere: A new parameterization. *Beitr. Phys. Atmos.*, **53**, 35–62.

Gadgil, S. and K. R. Kumar, 2006: The Asian monsoon – agriculture and economy. *The Asian monsoon*, B. Wang, Ed., Springer-Praxis Publishing, Berlin, 651–683.

Gadgil, S., M. Rajeevan, and R. Nanjundiah, 2005: Monsoon prediction – why yet another failure? *Current Science*, **88**, 1389–1400.

Gadgil, S. and S. Sajani, 1998: Monsoon precipitation in the AMIP runs. *Climate Dynamics*, **14**, 659–689.

Goswami, B. N., 2005: South Asian summer monsoon. *Intraseasonal Variability in the Atmosphere-Ocean Climate System*, W. Lau and D. Waliser, Eds., Praxis, Springer, Berlin Heidelberg, 125–173.

Goswami, B. N. and D. Sengupta, 2003: A note on the deficiency of NCEP/NCAR reanalysis surface winds over the equatorial Indian Ocean. *J. Geophys. Res.*, **108**, 3124–+, doi: 10.1029/2002JC001497.

Grabowski, W. W., 2001: Coupling Cloud Processes with the Large-Scale Dynamics Using the Cloud-Resolving Convection Parameterization (CRCP). *J. Atmos. Sci.*, **58**, 978–997.

Grabowski, W. W. and M. W. Moncrieff, 2004: Moisture-convection feedback in the tropics. *Q. J. R. Meteorol. Soc.*, **130**, 3081–3104.

Hahn, D. G. and S. Manabe, 1975: The role of mountains in the South Asian monsoon circulation. *Journal of Atmospheric Sciences*, **32**, 1515–1541.

Halpern, D., M. Freilich, and R. Weller, 1999: ECMWF and ERS-1 Surface Winds over the Arabian Sea during July 1995. *J. Phys. Oceanogr.*, **29**, 1619–1623.

Halpern, D. and P. M. Woiceshyn, 1999: Onset of the Somali Jet in the Arabian Sea during June 1997. *J. Geophys. Res.*, **104**, 18 041–18 046.

Halpern, D. and P. M. Woiceshyn, 2001: Somali Jet in the Arabian Sea, El Niño, and India Rainfall. *J. Climate*, **14**, 434–441.

Hart, J., G. Rao, H. V. D. Boogaard, J. Young, and J. Findlater, 1978: Aerial observations of the East African low-level jet stream. *Mon. Wea. Rev.*, **106**, 1714–1724.

Held, I. M. and A. Y. Hou, 1980: Nonlinear axially symmetric circulations in a nearly inviscid atmosphere. *J. Atmos. Sci.*, **37**, 515–533.

Helfand, H. M. and J. C. Labraga, 1988: Design of a nonsingular level 2.5 second-order closure model for the prediction of atmospheric turbulence. *J. Atmos. Sci.*, **45**, 113–132.

Helfand, H. M. and S. D. Schubert, 1995: Climatology of the simulated Great Plains low-level jet and its contribution to the continental moisture budget of the United States. *J. Climate*, **8**, 784–806.

Hendon, H., N. Davidson, and B. Gunn, 1989: Australian Summer Monsoon onset during AMEX 1987. *Mon. Wea. Rev.*, **117**, 370–390.

Holton, J. R., 2004: *An Introduction to Dynamic Meteorology.* Elsevier Academic Press, 535 pp.

Hoskins, B. J. and M. J. Rodwell, 1995: A model of the Asian summer monsoon. Part I: The global scale. *J. Atmos. Sci.*, **52**, 1329–1340.

Hung, C. and M. Yanai, 2004: Factors contributing to the onset of the Australian summer monsoon. *Q. J. R. Meteorol. Soc.*, **130**, 739–758.

Kalnay, E., et al., 1996: The NCEP/NCAR 40-Year Reanalysis Project. *Bull. Amer. Met. Soc.*, **77**, 437–472.

Kang, I.-S., et al., 2002: Intercomparison of the climatological variations of Asian summer monsoon precipitation simulated by 10 GCMs. *Climate Dynamics*, **19**, 383–395, doi: 10.1007/s00382-002-0245-9.

Kawamura, R., Y. Fukuta, H. Ueda, T. Matsuura, and S. Iizuka, 2002: A mechanism of the onset of the Australian summer monsoon. *J. Geophys. Res*, **107**.

Khairoutdinov, M., D. Randall, and C. Demott, 2005: Simulations of the atmospheric general circulation using a cloud-resolving model as a superparameterization of physical processes. *J. Atmos. Sci.*, **62**, 2136–2154.

Krishnakumar, V. and K.-M. Lau, 1997: Symmetric instability of monsoon flows. *Tellus A*, **49**, 228–245.

Krishnakumar, V. and K.-M. Lau, 1998: Possible role of symmetric instability in the onset and abrupt transition of the Asian Monsoon. *J. Meteorol. Soc. Jpn*, **76**, 363–383.

Krishnamurti, T. N., P. Ardanuy, Y. Ramanathan, and R. Pasch, 1981: On the onset vortex of the summer monsoon. *Mon. Wea. Rev.*, **109**, 344–363.

Krishnamurti, T. N. and H. N. Bhalme, 1976: Oscillations of a Monsoon System. Part I. Observational Aspects. *J. Atmos. Sci.*, **33**, 1937–1954.

Krishnamurti, T. N., J. Molinari, and H. L. Pan, 1976: Numerical Simulation of the Somali Jet. *J. Atmos. Sci.*, **33**, 2350–2362.

Krishnamurti, T. N. and V. Wong, 1979: A Planetary Boundary-Layer Model for the Somali Jet. *J. Atmos. Sci.*, **36**, 1895–1907.

Krishnamurti, T. N., V. Wong, H.-L. Pan, R. Pasch, J. Molinari, and P. Ardanuy, 1983: A Three-Dimensional Planetary Boundary Layer Model for the Somali Jet. *J. Atmos. Sci.*, **40**, 894–908.

Lau, K.-M., H.-T. Wu, and S. Yang, 1998: Hydrologic processes associated with the first transition of the Asian summer monsoon: A pilot satellite study. *Bull. Amer. Met. Soc.*, **79**, 1871–1882.

Lawrence, D. M. and P. J. Webster, 2002: The Boreal Summer Intraseasonal Oscillation: Relationship between Northward and Eastward Movement of Convection. *Journal of Atmospheric Sciences*, **59**, 1593–1606.

Lestari, R. and T. Iwasaki, 2006: A GCM study on the roles of the seasonal marches of the SST and land-sea thermal contrast in the onset of the Asian Summer Monsoon. *J. Meteor. Soc. Japan*, **84**, 69–83.

Li, C. and M. Yanai, 1996: The onset and interannual variability of the Asian summer monsoon in relation to land-sea thermal contrast. *J. Climate*, **9**, 358–375.

Liebmann, B. and C. Smith, 1996: Description of a complete (interpolated) outgoing longwave radiation dataset. *Bull. Amer. Meteor. Soc*, **77**, 1275–1277.

Lin, J.-L. and coauthors, 2006: Tropical intraseasonal variability in 14 IPCC AR4 climate models. Part I: Convective signals. *J. Climate*, **19**, 2665–2690.

Lindzen, R. S. and A. Y. Hou, 1988: Hadley circulation for zonally averaged heating centered off the Equator. *J. Atmos. Sci.*, **45**, 2416–2427.

Liou, K., 2002: *An Introduction to Atmospheric Radiation.* Academic Press, San Diego, California, 583 pp.

Luo, Z. and G. L. Stephens, 2006: An enhanced convection-wind-evaporation feedback in a superparameterization GCM (SP-GCM) depiction of the Asian summer monsoon. *Geophys. Res. Lett.*, **33**, L06 707, doi:10.1029/2005GL025060.

Madden, R. A. and P. R. Julian, 1972: Description of global-scale circulation cells in the tropics with a 40-50 day period. *J. Atmos. Sci.*, **29**, 1109–1123.

Mapes, B. E., P. Liu, and N. Buenning, 2005: Indian Monsoon Onset and the Americas Mid-summer Drought: Out-of-Equilibrium Responses to Smooth Seasonal Forcing. *J. Clim.*, **18**, 1109–1115.

Marengo, J., B. Liebmann, V. Kousky, N. Filizola, and I. Wainer, 2001: Onset and end of the rainy season in the Brazilian Amazon Basin. *J. Climate*, **14**, 833–852.

Marshall, J., A. Adcroft, J.-M. Campin, and C. Hill, 2004: Atmosphere-ocean modeling exploiting fluid isomorphisms. *Mon. Wea. Rev.*, **132**, 2882–2894.

Marshall, J., A. Adcroft, C. Hill, L. Perelman, and C. Heisey, 1997: A finite-volume, incompressible Navier Stokes model for studies of the ocean on parallel computers. *J. Geophys. Res.*, **102**, 5753–5766.

Martin, G. M., 1999: The simulation of the Asian summer monsoon, and its sensitivity to horizontal resolution, in the UK Meteorological Office Unified Model. *Q. J. R. Meteorol. Soc.*, **125**, 1499–1525.

Meehl, G., 1994: Influence of the land surface in the Asian Summer Monsoon: External conditions versus internal feedbacks. *J. Climate*, **7**, 1033–1049.

Meehl, G. A., J. M. Arblaster, D. M. Lawrence, A. Seth, E. K. Schneider, B. P. Kirtman, and D. Min, 2006: Monsoon Regimes in the CCSM3. *J. Climate*, **19**, 2482–2495.

Molnar, P. and K. A. Emanuel, 1999: Temperature profiles in radiative-convective equilibrium above surfaces at different heights. *J. Geophys. Res.*, **104**, 24 265–24 272, doi: 10.1029/1999JD900485.

Molod, A., J.-M. Campin, C. Hill, and J. Marshall, 2007: Description of the MITgcm atmospheric physics (Fizhi): Algorithm and simulated climate. Tech. rep., MIT Joint Program on the Science and Policy of Global Change.

Moorthi, S. and M. Suarez, 1992: Relaxed Arakawa-Schubert: A parameterization of moist convection for general circulation models. *Mon. Wea. Rev.*, **120**, 978–1002.

Morcrette, J.-J., 1991: Radiation and cloud radiative properties in the European Centre for Medium-Range Weather Forecasts forecasting system. *J. Geophys. Res.*, **96**, 9121–9132.

Murakami, T., L.-X. Chen, and A. Xie, 1986: Relationship among seasonal cycles, low-frequency oscillations, and transient disturbances as revealed from outgoing long-wave radiation data. *Mon. Wea. Rev.*, **114**, 1456–1465.

Neale, R. B. and B. J. Hoskins, 2000: A standard test for AGCMs including their physical parameterizations. I: The proposal. *Atmos. Sci. Lett.*, **1**, 101–107.

Neelin, J. and I. Held, 1987: Modeling tropical convergence based on the moist static energy budget. *Mon. Wea. Rev.*, **115**, 3–12.

Neelin, J., I. Held, and K. Cook, 1987: Evaporation-wind feedback and low-frequency variability in the tropical atmosphere. *J. Atmos. Sci.*, **44**, 2341–2348.

Neelin, J. D. and N. Zeng, 2000: A quasi-equilibrium tropical circulation model: Formulation. *J. Atmos. Sci.*, **57**, 1741–1766.

Nilsson, J. and K. A. Emanuel, 1999: Equilibrium atmospheres of a two-column radiative-convective model. *Q. J. R. Meteorol. Soc.*, **125**, 2239–2264.

Numaguti, A., 1993: Dynamics and energy balance of the Hadley circulation and the tropical precipitation zones: Significance of the distribution of evaporation. *J. Atmos. Sci.*, **50**, 1874–1887.

Numaguti, A., 1995: Dynamics and energy balance of the Hadley circulation and the tropical precipitation zones. Part II: Sensitivity to meridional SST distribution. *J. Atmos. Sci.*, **52**, 1128–1141.

Pauluis, O., 2004: Boundary layer dynamics and cross-equatorial Hadley circulation. *J. Atmos. Sci.*, **61**, 1161–1173.

Pauluis, O. and K. Emanuel, 2004: Numerical instability resulting from infrequent calculation of radiative heating. *Mon. Wea. Rev.*, **132**, . 673–686.

Pauluis, O., D. Frierson, and A. Majda, 2007: Propagation, reflection and transmission of precipitation fronts in the tropical atmosphere. *Submitted to Quart. J. Roy. Meteor. Soc.*

Peixoto, J. P. and A. H. Oort, 1992: *Physics of Climate.* American Institute of Physics, New York, 520 pp.

Plumb, R. A., 2007: Dynamical constraints on monsoon circulations. *The Global Circulation of the Atmosphere*, T. Schneider and A. H. Sobel, Eds., Princeton University Press, Princeton, New Jersey, 252–266.

Plumb, R. A. and A. Y. Hou, 1992: The response of a zonally symmetric atmosphere to subtropoical thermal forcing: threshold behavior. *J. Atmos. Sci.*, **49**, 1790–1799.

Prive, N. C. and R. A. Plumb, 2007: Monsoon dynamics with interactive forcing. Part II: Impact of eddies and asymmetric geometries. *J. Atmos. Sci.*, **64**, 1431–1442.

Raymond, D. J., 1995: Regulation of moist convection over the West Pacific warm pool. *J. Atmos. Sci.*, **52**, 3945–3959.

Reynolds, R. W. and T. M. Smith, 1994: Improved global sea surface temperature analyses using optimum interpolation. *J. Climate*, **7**, 929–948.

Rodwell, M. J. and B. J. Hoskins, 1995: A Model of the Asian Summer Monsoon.Part II: Cross-Equatorial Flow and PV Behavior. *J. Atmos. Sci.*, **52**, 1341–1356.

Schneider, E. K., 1977: Axially symmetric steady-state models of the basic state for instability and climate studies. Part II. Nonlinear calculations. *J. Atmos. Sci.*, **34**, 280–296.

Schneider, T. and S. Bordoni, 2007, in press: Eddy-mediated regime transitions in the seasonal cycle of a Hadley circulation and implications for monsoon dynamics. *J. Atmos. Sci.*

Schubert, S. D., R. B. Rood, and J. Pfaendtner, 1993: An assimilated dataset for earth science applications. *Bull. Amer. Met. Soc.*, **74**, 2331–2342.

Sikka, D. R. and S. Gadgil, 1980: On the maximum cloud zone and the ITCZ over India longitude during the southwest monsoon. *Mon. Wea. Rev.*, **108**, 1840–1853.

Sobel, A. and J. Neelin, 2006: The boundary layer contribution to intertropical convergence zones in the quasi-equilibrium tropical circulation model framework. *Theor. Comput. Fluid Dyn.*, **20**, 323–350.

Stull, R. B., 1988: *An Introduction to Boundary Layer Meteorology.* Kluwer Academic Publishers, Dordrecht, 666 pp.

Sud, Y. C. and A. Molod, 1988: The roles of dry convection and cloud radiation feedback processes and the influence of recent improvements in the parameterization of convection in the GLA GCM. *Mon. Wea. Rev.*, **116**, 2366–2387.

Sultan, B. and S. Janicot, 2000: Abrupt shift of the ITCZ over West Africa and intraseasonal variability. *Geophys. Res. Lett*, **27**, 3353–3356.

Tomas, R. A., J. R. Holton, and P. J. Webster, 1999: The influence of cross-equatorial pressure gradients on the location of near-equatorial convection. *Q. J. R. Meteorol. Soc.*, **125**, 1107–1127.

Walker, C. C. and T. Schneider, 2005: Response of idealized Hadley circulations to seasonally varying heating. *Geophys. Res. Lett.*, **32**.

Walker, C. C. and T. Schneider, 2006: Eddy influences on Hadley circulations: simulations with an idealized GCM. *J. Atmos. Sci.*, **63**, 3333–3350.

Wang, B. and H. Rui, 1990: Synoptic climatology of transient tropical intraseasonal convective anomalies. *Meteorol. Atmos. Phys.*, **44**, 43–61.

Webster, P. J. and J. Fasullo, 2003: Monsoon: Dynamical theory. *Encyclopedia of Atmospheric Sciences*, Academic Press, 1370–1385.

Webster, P. J. and C. Hoyos, 2004: Prediction of monsoon rainfall and river discharge on 15 30-day time scales. *Bull. Amer. Met. Soc.*, **85**, 1745–1765.

Webster, P. J., V. O. Magana, T. N. Palmer, J. Shukla, R. A. Tomas, M. Yanai, and T. Yasunari, 1998: Monsoons: processes, predictability, and the prospects for prediction. *J. Geophys. Res.*, **103**, 14 451–14 510.

Weickmann, K. M. and R. M. Chervin, 1988: The Observed and Simulated Atmospheric Seasonal Cycle. Part I: Global Wind Field Modes. *J. Climate*, **1**, 265–289.

Weller, R. A., M. F. Baumgartner, S. A. Josey, A. S. Fischer, and J. C. Kindle, 1998: Atmospheric forcing in the Arabian Sea during 1994-1995: Observations and comparisons with climatology and models. *Deep Sea Res.*, **45**, 1961–1999.

Wheeler, M. and G. N. Kiladis, 1999: Convectively coupled equatorial waves: Analysis of clouds and temperature in the wavenumber-frequency domain. *J. Atmos. Sci.*, **56**, 374–399.

Wheeler, M. C. and J. L. McBride, 2005: Australian-Indonesian monsoon. *Intraseasonal Variability in the Atmosphere-Ocean Climate System*, W. Lau and D. Waliser, Eds., Praxis, Springer, Berlin Heidelberg, 125–173.

Williams, A. G., 2001: A physically based parametrization for surface flux enhancement by gustiness effects in dry and precipitating convection. *Q. J. R. Meteorol. Soc.*, **127**, 469–491.

Wirth, V. and T. J. Dunkerton, 2006: A unified perspective on the dynamics of axisymmetric hurricanes and monsoons. *J. Atmos. Sci.*, **63**, 2529–2547.

Xian, P. and R. L. Miller, 2007, in press: Abrupt seasonal migration of the ITCZ into the summer hemisphere. *J. Atmos. Sci.*

Xie, S.-P. and N. Saiki, 1999: Abrupt onset and slow seasonal evolution of summer monsoon in an idealized GCM simulation. *J. Meteor. Soc. Japan*, **77**, 949–968.

Yano, J.-I. and K. Emanuel, 1991: An improved model of the equatorial troposphere and its coupling with the stratosphere. *J. Atmos. Sci.*, **48**, 377–389.

Yasunari, T., 1979: Cloudiness fluctuation associated with the northern hemisphere summer monsoon. *J. Meteor. Soc. Japan*, **57**, 227–242.

Yu, L., X. Jin, and R. Weller, 2007: Annual, seasonal, and interannual variability of air-sea heat fluxes in the Indian Ocean. *J. Climate*, **20**, 3190–3209.

Yu, L. and R. Weller, 2007: Objectively analyzed air-sea heat fluxes for the global ice-free oceans (1981-2005). *Bull. Amer. Meteor. Soc.*, **88**, 527–539.

Yu, L., R. A. Weller, and B. Sun, 2004: Improving Latent and Sensible Heat Flux Estimates for the Atlantic Ocean (1988-99) by a Synthesis Approach. *J. Climate*, **17**, 373–393.

Zhang, Y., T. Li, B. Wang, and G. Wu, 2002: Onset of the summer monsoon over the Indochina Peninsula: Climatology and interannual variations. *J. Climate*, **15**, 3206–3221.

Zheng, X., 1998: The response of a moist zonally symmetric atmosphere to subtropical surface temperature perturbation. *Q. J. R. Meteorol. Soc.*, **124**, 1209–1226.

Zhou, J. and K. Lau, 1998: Does a monsoon climate exist over South America? *J. Climate*, **11**, 1020–1040.